

Neurocalcin delta (NCALD) knockout impairs adult neurogenesis whereas half reduction is a safe therapeutic option for spinal muscular atrophy



Inaugural-Dissertation
zur
Erlangung des Doktorgrades
der Mathematisch-
Naturwissenschaftlichen Fakultät
der Universität zu Köln

vorgelegt von
Aaradhita Upadhyay
Aus Raipur, Indien

Köln
2019

The Doctoral Thesis “Neurocalcin delta (NCALD) knockout impairs adult neurogenesis whereas half reduction is a safe therapeutic option for spinal muscular atrophy” was performed at the Institute of Human Genetics, Institute of Genetics and Centre for Molecular Medicine Cologne (CMMC) of the University of Cologne from January 2015 to October 2018.

Berichterstatter: Prof. Dr. rer. nat. Brunhilde Wirth

Prof. Dr. rer. nat. Matthias Hammerschmidt

Tag der mündlichen Prüfung: 30.11.2018

Dedicated to my mother and nani,

Contents

Abbreviations	6
Summary	8
Zusammenfassung.....	10
1 Introduction.....	12
1.1 Spinal Muscular Atrophy and therapeutic strategies.....	12
1.2 SMA modifiers independent of SMN.....	15
1.2.1 Plastin 3	15
1.2.2 Neurocalcin delta (Ncald).....	16
1.2.3 Calcineurin-like EF-hand protein 1 (Chp1)	17
1.3 Neurocalcin delta, a neuronal calcium sensor	18
1.3.1 NCS family.....	18
1.3.2 Neurocalcin delta	19
1.3.3 NCALD abundancy and functions	19
1.3.4 NCALD implications in various neurological diseases	20
1.3.4.1 Neurodegenerative diseases	21
1.3.4.2 Neurodevelopmental diseases.....	21
1.3.5 NCALD in other diseases.....	22
1.4 Modifying role of NCALD reduction in SMA	22
1.4.1 Adult neurogenesis.....	24
2 Aim of the study	26
3 Results	28
3.1 NCALD protein, abundancy and pattern in wildtype mice.....	28
3.1.1 NCALD protein levels rise dramatically during early postnatal stages.....	28
3.1.2 NCALD is abundant in hippocampus and synaptic punctas	29
3.2 Characterization of Ncald knockout mouse	31
3.2.1 Ncald knockout causes significant reduction of body weight.....	31
3.2.2 Adult Ncald knockout brain exhibit gross morphological alterations and reduced dentate gyrus	32
3.2.3 Ncald knockout brain do not show progressive neurodegeneration.....	33
3.2.4 Ncald knockout brain show mild morphological defects even before adulthood	36
3.2.5 Ncald knockout impairs adult neurogenesis	37
3.2.6 Ncald knockout does not cause any migrational defects in the cortex	39
3.2.7 Myelination is disturbed in Ncald knockout brain	40
3.3 NCALD physiological interactions and function in mouse brain	41
3.3.1 NCALD is absent in oligodendrocytes.....	41

3.3.2	NCALD interacts with MAP3K10.....	42
3.3.3	pJNK is upregulated in Ncald knockout brain.....	43
3.3.4	Transient inhibition of JNK could not rescue the impairment in adult neurogenesis.....	44
3.3.5	pJNK is not altered in Ncald knockout spinal cord	47
3.3.6	RNA sequencing and transcriptomics of Ncald ^{KO/KO} samples	47
3.4	Characterization of Ncald ^{KO/WT} animals	49
3.4.1	Ncald ^{KO/WT} animals did not exhibit any severe physiological defects.....	49
3.4.2	Ncald ^{KO/WT} and Ncald ^{KO/KO} motor neurons show elongated axons and increased branching	51
3.4.3	Ncald ^{KO/WT} and Ncald ^{KO/KO} animals perform well in the motoric test.....	52
4	Discussion.....	54
4.1	NCALD in postnatal brain development and maturation.....	54
4.1.1	Axonal and dendritic projections	54
4.1.2	Synaptogenesis and neurotransmission.....	54
4.1.3	Myelination	55
4.2	Relevance of NCALD in presubiculum	56
4.3	Adult neurogenesis, JNK activation and NCALD	57
4.4	NCALD reduction in SMA.....	60
4.5	NCALD in neurodevelopmental disorders.....	61
4.6	Interesting candidates and pathways in Ncald ^{KO/KO} transcriptome analysis	62
4.7	Future outlook.....	63
5	Materials and methods	66
5.1	Materials.....	66
5.1.1	Laboratory equipment.....	66
5.1.2	Mouse work equipment	68
5.1.3	Chemical	68
5.2	Reagents	69
5.2.1	Reagents for molecular biology.....	69
5.2.2	Cell Culture reagents and media	70
5.2.3	Reagents for molecular biology.....	71
5.2.4	Antibodies.....	72
5.2.4.1	Primary antibodies and staining reagents.....	72
5.2.4.2	Secondary antibodies and staining reagents	72
5.2.5	Solutions and media	73
5.2.5.1	Cell culture media.....	73
5.2.5.2	Solutions to work with DNA	75
5.2.5.3	Solutions to work with Proteins	75

5.2.5.4	Solutions for histology and immunohistology.....	77
5.2.6	Primers and oligoneclueotides.....	78
5.2.7	Plasmid	79
5.2.8	Software packages and internet database.....	79
5.2.9	Mice.....	80
5.3	Methods	80
5.3.1	Working with nucleic acids.....	80
5.3.1.1	RNA isolation	80
5.3.1.2	Isolation of DNA.....	81
5.3.1.3	Polymerase Chain Reaction (PCR)	81
5.3.1.4	Agarose gel electrophoresis	83
5.3.2	Working with proteins.....	83
5.3.2.1	Isolation of proteins from tissues.....	83
5.3.2.2	Bradford assay.....	84
5.3.2.3	SDS polyacrylamide gel electrophoresis (SDS-PAGE)	84
5.3.2.4	Western blot.....	85
5.3.2.5	Immunochemical detection of proteins.....	85
5.3.2.6	Co-immunoprecipitation	86
5.3.2.7	Mass spectrometry and data analysis	86
5.3.3	Working with mice and mouse tissues.....	87
5.3.3.1	Mouse strain.....	87
5.3.3.2	Ncald ^{ko/ko} mice	88
5.3.3.3	Generation of primary motor neurons.....	88
5.3.3.4	Generation of primary hippocampal neurons.....	89
5.3.3.5	Transfection of primary hippocampal neurons.....	90
5.3.3.6	Immunofluorescent staining of primary neurons	90
5.3.3.8	Transcardial perfusion fixation.....	91
5.3.3.9	Serial sectioning and Nissl staining of brain sections.....	92
5.3.3.10	Immunohistochemical staining of brain sections.....	92
5.3.3.11	Microscopic image acquisition and analysis.....	93
5.3.3.11.1	Hippocampal culture colocalization analysis.....	93
5.3.3.11.2	Analysis of sub granular zone nissl staining	93
5.3.3.11.3	Sholl Analysis	93
5.3.3.11.4	Cell density analysis.....	94
5.3.3.11.5	Intensity analysis	94
5.3.3.11.6	Motor neuron morphological analysis	94

5.3.3.12	Rotarod	94
5.3.3.13	Transcriptome analysis.....	95
5.3.3.14	Statistical analysis.....	95
6	References.....	97
7	Appendix.....	I
8	Publications	XXIV
	Acknowledgements	XXV
	Eidesstattliche Erklärung	XXVII

List of Tables

Table 1: Primers for genotyping.....	79
Table 2: A standard 20 µl PCR composition.....	82
Table 3: A standard thermocycler PCR program.....	82
Table 4: Primary and secondary antibodies used for protein detection.....	86
Appendix Table 5 List of potential binding partners of NCALD (comparison between wildtype IPs and control IPs).....	Error! Bookmark not defined.
Appendix Table 6 List of potential binding partners of NCALD (comparison between wildtype IPs and control IPs).....	VI
Appendix Table 7 List of genes with significant differential expression upon <i>Ncald</i> deletion and strongly correlated with <i>Ncald</i> gene expression (Hippocampus).....	XI
Appendix Table 8 List of genes with significant differential expression upon <i>Ncald</i> deletion and strongly correlated with <i>Ncald</i> gene expression (Cortex).....	XII
Appendix Table 9 List of genes with significant differential expression upon <i>Ncald</i> deletion and strongly correlated with <i>Ncald</i> gene expression (Spinal Cord).....	XXI

List of figures

Figure 1 A schematic overview of the transcriptional regulation of <i>SMN1</i> and <i>SMN2</i> gene.....	12
Figure 2 Nusinersen therapy.	14
Figure 3 Proposed model depicting the role of NCALD in the endocytosis in normal, SMA and asymptomatic individuals.....	17
Figure 4 Structure of a neuronal calcium sensor.	18
Figure 5 NCALD reduction induces neuronal differentiation and increases axonal length.	23
Figure 6 NCALD Knockout mice design.....	24
Figure 7 Western blot.....	29
Figure 8 Distribution and localization of NCALD.....	30
Figure 9 <i>Ncald</i> knockout animals show significant reduction in body and brain weight.....	32
Figure 10 <i>Ncald</i> ^{KO/KO} brain exhibit gross morphological defects.	33
Figure 11 <i>Ncald</i> ^{KO/KO} brain shows no sign of neurodegeneration.....	35
Figure 12 Young (P14 and P30) <i>Ncald</i> ^{KO/KO} brain exhibit mild morphological defects.	36
Figure 13 <i>Ncald</i> ^{KO/KO} hippocampus do not show any defects in general cell proliferation.	37
Figure 14 <i>Ncald</i> ^{KO/KO} brain endure impaired adult neurogenesis.	39
Figure 15 Cortical layers in <i>Ncald</i> ^{KO/KO} brain do not show migration defects.....	40
Figure 16 <i>Ncald</i> ^{KO/KO} brain display reduced myelination.....	41
Figure 17 NCALD is absent in oligodendrocytes.....	42
Figure 18 NCALD interacts with MAP3K10.....	43
Figure 19 <i>Ncald</i> ^{KO/KO} brain show increase pJNK levels.	44
Figure 20 Time line of JNK inhibitor and parallel vehicle treatment.....	45
Figure 21 Transient inhibition of JNK does not ameliorate adult neurogenesis in <i>Ncald</i> ^{KO/KO}	46
Figure 22 <i>Ncald</i> ^{KO/KO} spinal cord do not show increased pJNK levels.	47
Figure 23 Principle component analysis of transcriptome data from different tissue samples.....	48
Figure 24 <i>Ncald</i> ^{KO/WT} animals do not show any severe morphological defects.....	50
Figure 25 DCX+ adult born neuron density is not significantly altered in <i>Ncald</i> ^{KO/WT} animals.	51
Figure 26 <i>Ncald</i> ^{KO/KO} and <i>Ncald</i> ^{KO/WT} motor neurons have elongated axons.	52
Figure 27 <i>Ncald</i> ^{KO/KO} and <i>Ncald</i> ^{KO/WT} animals do not show any changes in motor abilities.	53
Figure 28 <i>Ncald</i> expression pattern in different clusters of dentate gyrus cells.....	59

Abbreviations

A	adenine
AChR	acetylcholine receptor
APS	ammonium persulfate
ASO	antisense oligonucleotide
BBB	blood-brain barrier
bp	base pairs
BSA	bovine serum albumin
C	cytosine
CNS	central nervous system
cDNA	coding DNA
DMEM	Dulbecco's modified Eagle medium
DMSO	dimethyl sulfoxide
DNA	deoxyribonucleic acid
Dox	Doxycycline
E	embryonic day
EDTA	ethylene diamine tetraacetic acid
e.g.	exempli gratia
EGTA	ethylene glycol tetraacetic acid
ESC	embryonic stem cells
et al.	et alii
FCS	fetal calf serum
FDA	Food & Drug Administration
FL	full length
fwd	forward
g	gravitational force
G	guanine
GFP	green fluorescent protein
h	hours
HDAC	histone deacetylase
kb	kilobases
kDa	kilodalton
ko	knock-out
L	liter
m	mili
μ	micro
M	molar
min	minutes
MN	motor neuron
mRNA	messenger RNA
n	number

NCS	neuronal calcium sensor
NMJ	neuromuscular junction
n.s.	not significant
o.n.	overnight
<i>P</i>	probability
PAA	polyacrylamide
PBS	phosphate buffered saline
PCR	polymerase chain reaction
PFA	paraformaldehyde
pH	power of hydrogen
pmol	picomol
PND	postnatal day
RNA	ribonucleic acid
rev	reverse
SD	standard deviation
SDS	sodium dodecyl sulfate
sec	seconds
SEM	standard error of means
siRNA	small interfering RNA
SMA	spinal muscular atrophy
snRNP	small nuclear ribonucleoprotein
T	tyrosine
TVA	Transversus abdominis
TEMED	N,N,N',N'-tetramethylethylenediamine
wt	wildtype

Summary

Spinal muscular atrophy (SMA) is the second most common recessive monogenic disease characterized by loss of motor neurons and impaired neuromuscular junctions which leads to proximal muscles atrophy. SMA is primarily caused by mutation/loss of survival of motor neuron 1 (*SMN1*) gene encoding the SMN protein. Interestingly, humans carry additionally *SMN2*, a copy gene of *SMN1* which is relatively new in evolutionary scale of genes and the SMA disease severity is inversely correlated with the copy number of the *SMN2* gene. In the recent year, SMA therapeutics achieved a landmark with FDA and EMA approval of the splice modifier molecule named Nusinersen, which is an SMN dependent therapy as it elevates the SMN protein level derived from the *SMN2* transcript. However, SMN dependent therapies have not been sufficient to fully cure the SMA, especially in most severe SMA type I patients which may carry even a single allele of *SMN2*. Therefore, a combinatorial therapy which includes SMN independent strategies would be remarkably beneficial. Certain modifier genes, which upon differential expression can protect against SMA are most relevant and potential candidates to be studied in context of combinatorial therapies. Recently, reduction of a neuronal calcium sensor, Neurocalcin delta (NCALD) significantly ameliorated major SMA symptoms: reduced motor neuron axon length, neuromuscular junction size, muscle fibre size, impaired endocytosis and motor functions in various SMA model systems. Considering these results, reduction of NCALD was proposed for SMA combinatorial therapeutics. However, depending upon the physiological functions of NCALD in various cellular processes, reduction of NCALD may potentially incur certain side effects. NCALD is a member of the brain-enriched neuronal calcium sensor sub-family Visinin like proteins (VILIPs). However, till date only few NCALD functions have been explored based on the functions of its close homologues VILIP1, hippocalcin and guanylate cyclase activating protein (GCAP). Therefore, in this study we first investigated non redundant physiological functions of NCALD by characterizing *Ncald* knockout (*Ncald*^{KO/KO}) mice; then referring to the phenotypes of *Ncald*^{KO/KO} mice we further analysed heterozygous (*Ncald*^{KO/WT}) mice to verify any potential physiological defects that may arise at 50% NCALD reduction which has been proposed as a potential SMA therapeutic option.

Significant changes were observed in the gross brain morphology of adult *Ncald*^{KO/KO} mice (4 month-old) with bigger ventricles, thinner cortex and smaller hippocampus including significantly reduced length of dentate gyrus sub granular zone. These morphological defects could arise either due to progressive neurodegeneration or impaired brain development/maturation. Therefore, we investigated major hallmarks of progressive neurodegeneration like loss of mature neurons, astrogliosis, reduced dendritic branching or exacerbation of the

gross morphological changes with aging. However, we did not find any evidence of progressive neurodegeneration. On other hand, we found very low NCALD levels in embryonic brain (E16) as well as at birth (P1), however a significant increase was observed at P10, which implies relevance of NCALD during postnatal brain development/ maturation. Therefore, we further investigated generation of doublecortin (DCX) positive new-born granule cells in the dentate gyrus (DG) as well as myelination, two major processes of postnatal brain maturation. We did not observe any changes in DCX positive neurons at P14 and only a tendency of reduction at P30 in *Ncald*^{KO/KO} brain compared to controls. However, 4-month old adult *Ncald*^{KO/KO} animals exhibit significantly reduced amount of DCX cells in DG. Loss of DCX positive cells in adult brain is widely accepted as a loss of adult neurogenesis. Furthermore, we investigated the mechanism behind the observed defects in *Ncald*^{KO/KO} brain by investigating the NCALD interactome using mass spectrometry analysis and as co-immunoprecipitation. We identified a novel NCALD interacting partner named mitogen-activated protein kinase kinase kinase 10 (MAP3K10). MAP3K10 is an upstream kinase in c-Jun N-terminal kinase (JNK) pathway. Therefore we analysed the JNK activation in *Ncald*^{KO/KO} brain and found significantly upregulated pJNK levels compared to controls. Contrary to these observations, adult *Ncald*^{KO/WT} brain analysis showed neither JNK activation nor loss DCX positive cells, thereby ruling out the potential side effects of NCALD reduction in adult neurogenesis. Conclusively, this is the first study to report the effect of NCALD deletion on DCX positive neuron generation, which is a widely accepted as adult neurogenesis marker and to identify MAP3K10 as a novel interacting partner of NCALD; additionally it reports on the safety of using NCALD reduction for SMA combinatorial therapy.

Zusammenfassung

Spinale Muskelatrophie (SMA) ist die zweithäufigste rezessive monogene Erkrankung, die durch den Verlust von Motoneuronen und beeinträchtigten neuromuskulären Verbindungen gekennzeichnet ist, was zu einer proximalen Muskelatrophie führt. SMA wird hauptsächlich durch Mutation / Verlust des Überlebens des Motoneuron 1 (SMN1) -Gens, das das SMN-Protein kodiert, verursacht. Interessanterweise tragen Menschen zusätzlich SMN2, ein Kopiegen von SMN1, das im evolutionären Maßstab von Genen relativ neu ist. Der Schweregrad der SMA-Krankheit korreliert negativ mit der Kopienzahl des SMN2-Gens. Im vergangenen Jahr erreichte SMA Therapeutics mit dem Spleißmodifikatormolekül Nusinersen, das eine SMN-abhängige Therapie durch die Erhöhung des SMN-Proteinspiegels aus dem SMN2-Transkript darstellt, die FDA- und EMA-Zulassung. SMN-abhängige Therapien waren jedoch nicht ausreichend, um die SMA vollständig zu heilen, insbesondere bei den meisten schweren SMA-Typ-I-Patienten, die sogar ein einzelnes Allel von SMN2 tragen können. Daher wäre eine kombinatorische Therapie, die SMN-unabhängige Strategien beinhaltet, sehr vorteilhaft. Bestimmte Modifikationsgene, die bei unterschiedlicher Expression gegen SMA schützen können, sind die relevantesten und potentiellsten Kandidaten, die im Zusammenhang mit kombinatorischen Therapien untersucht werden sollen. Kürzlich verbesserte die Reduktion eines neuronalen Calciumsensors, Neurocalcin delta (NCALD), bedeutende SMA-Symptome: reduzierte Axone des motorischen Neurons, neuromuskuläre Übergangsgröße, Muskelfasergröße, gestörte Endozytose und motorische Funktionen in verschiedenen SMA-Modellsystemen. Unter Berücksichtigung dieser Ergebnisse wurde eine Reduktion von NCALD für kombinatorische SMA-Therapeutika vorgeschlagen. In Abhängigkeit von den physiologischen Funktionen von NCALD in verschiedenen zellulären Prozessen kann die Reduktion von NCALD jedoch möglicherweise bestimmte Nebenwirkungen hervorrufen. NCALD ist ein Mitglied der Gehirn-angereicherten neuronalen Kalzium-Sensor-Unterfamilie Visinin like Proteins (VILIPs). Bislang wurden jedoch nur wenige NCALD-Funktionen basierend auf den Funktionen seiner nahen Homologen VILIP1, Hippocalcin und Guanylatcyclase-aktivierendes Protein (GCAP) untersucht. Daher untersuchten wir in dieser Studie zuerst nicht-redundante physiologische Funktionen von NCALD durch Charakterisierung von Ncald-Knockout (*Ncald*^{KO/KO}) Mäusen; Unter Bezugnahme auf die Phänotypen von Mäusen analysierten wir weiter heterozygote (*Ncald*^{KO/WT}) Mäuse, um mögliche physiologische Defekte zu bestätigen, die bei 50% NCALD-Reduktion auftreten können, was als mögliche SMA-Therapieoption vorgeschlagen wurde.

Signifikante Veränderungen wurden in der Grobhirnmorphologie von adulten *Ncald*^{KO/KO} Mäusen (4 Monate alt) mit größeren Ventrikeln, dünnerem Kortex und kleinerem

Hippocampus, einschließlich einer signifikant reduzierten Länge der subgranularen Zone des dentalen Gyrus, beobachtet. Diese morphologischen Defekte können entweder durch fortschreitende Neurodegeneration oder gestörte Entwicklung / Reifung des Gehirns entstehen. Daher untersuchten wir wichtige Merkmale der progressiven Neurodegeneration wie Verlust von reifen Neuronen, Astrogliose, reduzierte dendritische Verzweigung oder Exazerbation der makroskopischen Veränderungen mit dem Altern. Wir haben jedoch keinen Hinweis auf progressive Neurodegeneration gefunden. Auf der anderen Seite fanden wir sehr niedrige NCALD-Spiegel im embryonalen Gehirn (E16) sowie bei der Geburt (P1), jedoch wurde ein signifikanter Anstieg bei P10 beobachtet, was die Relevanz von NCALD während der postnatalen Gehirnentwicklung / -reifung impliziert. Daher untersuchten wir die Bildung von Doppelkörtin (DCX) positiven, neu geborenen Körnerzellen im Gyrus dentatus (DG) sowie die Myelinisierung, zwei Hauptprozesse der postnatalen Gehirnreifung. Wir beobachteten keine Veränderungen in DCX-positiven Neuronen bei P14 und nur eine Reduktionsneigung bei P30 in *Ncald*^{KO/KO}-Gehirn im Vergleich zu Kontrollen. 4 Monate alte adulte *Ncald*^{KO/KO}-Tiere zeigen jedoch eine signifikant reduzierte Menge an DCX-Zellen in DG. Der Verlust von DCX-positiven Zellen im adulten Gehirn wird weitgehend als Verlust der adulten Neurogenese angesehen. Darüber hinaus untersuchten wir den Mechanismus hinter den beobachteten Defekten im *Ncald*^{KO/KO} Gehirn durch Untersuchung des NCALD-Interaktoms mittels Massenspektrometrieanalyse und als Co-Immunopräzipitation. Wir identifizierten einen neuen NCALD-Interaktionspartner namens Mitogen-aktivierte Protein Kinase Kinase Kinase 10 (MAP3K10). MAP3K10 ist eine stromaufwärts gelegene Kinase im c-Jun N-terminalen Kinase (JNK) Signalweg. Daher analysierten wir die JNK Aktivierung in *Ncald*^{KO/KO} Gehirn und fanden signifikant erhöhte pJNK Werte im Vergleich zu Kontrollen. Im Gegensatz zu diesen Beobachtungen zeigte adulte *Ncald*^{KO/WT}-Gehirnanalyse weder eine JNK-Aktivierung noch einen Verlust von DCX-positiven Zellen, wodurch die möglichen Nebenwirkungen der NCALD-Reduktion in der adulten Neurogenese ausgeschlossen wurden. Zusammenfassend ist dies die erste Studie, die den Effekt der NCALD-Deletion auf die DCX-positive Neurogenese, die als adulter Neurogenesemarker weithin akzeptiert ist, und MAP3K10 als einen neuartigen Interaktionspartner von NCALD identifiziert; Darüber hinaus bestätigt die Studie die Sicherheit der Verwendung von NCALD Reduktion für SMA kombinatorische Therapie.

1 Introduction

1.1 Spinal Muscular Atrophy and therapeutic strategies

Although Spinal Muscular Atrophy (SMA) has been known for more than a century (Hoffmann, 1893) SMA therapeutics still lacks a complete cure for SMA (Talbot and Tizzano, 2017). SMA is caused by loss of the telomeric copy of Survival motor neuron 1 (*SMN1*) which lies at the chromosomal region 5q13 (Brzustowicz et al., 1990; Rodrigues et al., 1995). However, the severity of the SMA depends on the copy number of the centromeric gene *SMN2* (Lefebvre et al., 1997; Feldkotter et al., 2002). The *SMN2* gene sequence differs by only 5 nucleotides from the *SMN1*, without impacting the amino acid sequence. However, one of these nucleotide mutations (a C –T transition) is found at the Exonic Splicing Enhancer (ESE) site in exon 7 (Lorson et al., 1999); this transition leads to loss of the ESE and instead establishes an exonic splicing silencer (ESS) (Kashima and Manley, 2003). In *SMN1* ESE binds to positive splicing factors namely, splicing factor 2 (SF2) and alternative splicing factor (ASF), thereby leading to production of intact SMN protein (Cartegni and Krainer, 2002). Whereas in *SMN2* the ESS formed due to C-T transition, binds to a known splicing repressor protein hnRNPA1 which along with an additional intronic splicing silencer (ISS-N1) at intron 7 causes the skipping of exon 7 in 90% of transcripts (Singh et al., 2006). Thus, 90% unstable SMN protein and only 10% of stable SMN protein is translated via *SMN2* gene (Lefebvre et al., 1998). Hence in SMA cases, although *SMN2* gene is functional it cannot completely rescue the loss of *SMN1* (Kashima and Manley, 2003).

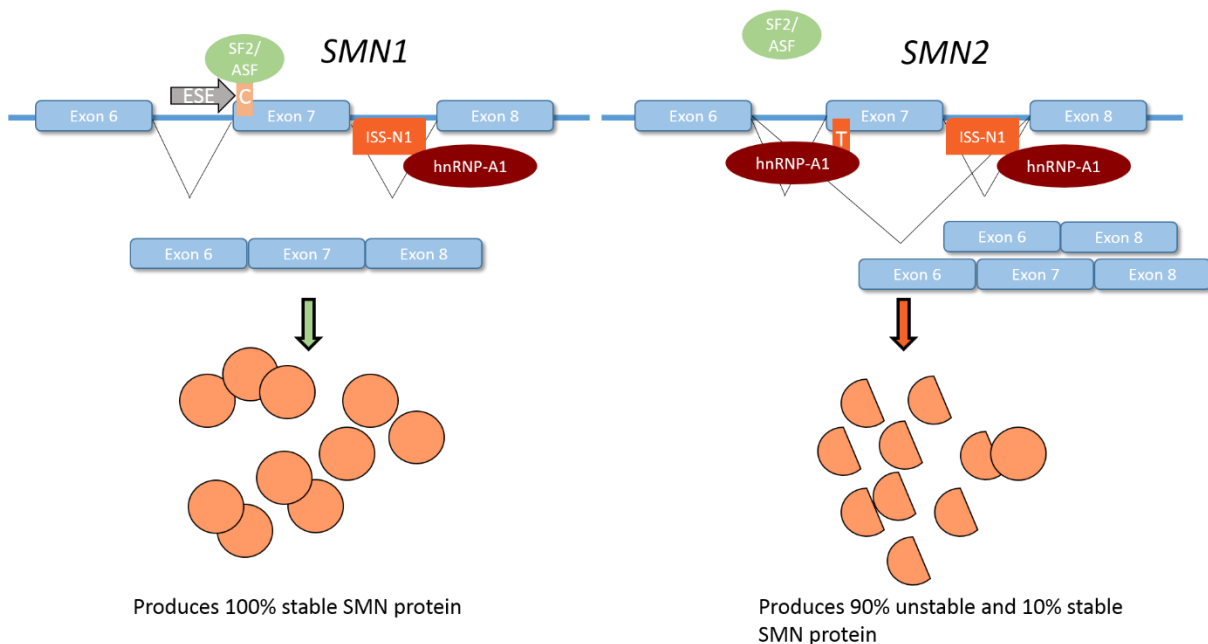


Figure 1 A schematic overview of the transcriptional regulation of *SMN1* and *SMN2* gene.

SMN1 and *SMN2* gene encode the SMN protein. *SMN2* is a copy gene of *SMN1*, which differs by only 5 nucleotides without any change in the amino acid sequence. However one of the mutations, a C-T transition in the exon 7 disrupts an ESE site and instead forms an ESS site recruiting splicing repressor hnRNP1. Combination of the newly generated ESS site and another physiological intronic splicing silencer site ISS-N1 on intron 7 leads to exclusion of exon 7 in most *SMN2* mRNA transcripts, thereby producing 90% of unstable protein and only 10% stable SMN protein.

The SMN is a 294 aa long, ~32 kDa protein (Lefebvre et al., 1995). In its cytoplasmic form, SMN interacts with itself (forming oligomers), Smn Interacting Protein 1 (SIP1) and Sm proteins (snRNP complex members) imposing an effect on the spliceosomal assembly (Fischer et al., 1997). On the other hand the nuclear SMN is usually stored in circular structures called 'gems' (Liu and Dreyfuss, 1996). Interestingly, deficiency of SMN in motor neurons leads to reduction of β -actin protein and mRNA in axons and their growth cones as well as can cause axon path finding defects (McWhorter et al., 2003; Rossoll et al., 2003). Moreover, accumulation of SMN in the growth cone of neuronal cells, suggests its role in the neuronal growth, synaptic vesicle recycling and maturation of the neuromuscular junctions (NMJs) (Fan and Simard, 2002). NMJs are the synapses formed between a motor neuron and skeletal muscle, which mature in the early postnatal period and needs to be maintained lifelong for proper functioning of muscles (Shi et al., 2012).

SMA is an autosomal recessive genetic disease characterized by muscular weakness, denervation and atrophy along with the degeneration of the motor neurons in the anterior horn of spinal cord. Depending upon the onset and severity of the symptoms, SMA has been divided by International SMA Consortium into four different types: SMA type I (most severe), SMA type II, SMA type III and SMA type IV (Finkel et al., 2018; Mercuri et al., 2018b).

Strategies to treat SMA involve various types of transcriptional regulation to eventually increase the SMN protein. Following are some of the major strategies:

1) Histone deacetylase (HDAC) inhibitors: The epigenetic landscape near the promoter region of *SMN2* gene can be switched into a transcriptionally active chromatin structure by regulating acetylation of histone proteins as well as methylation of DNA. (Lunke and El-Osta, 2013) This can be achieved by use of various histone deacetylase (HDAC) inhibitors (Brichta et al., 2003; Andreassi et al., 2004; Avila et al., 2007; Garbes et al., 2009; Riessland et al., 2010; Somers et al., 2013). Two of these HDAC inhibitors valproic acid and phenylbutyrate have even been tested in clinical trials of SMA patients, however the conclusions were not evidently successful (Lunke and El-Osta, 2013).

2) Small molecule therapy with antisense oligonucleotides (ASOs): As mentioned earlier *SMN2* gene has an intronic silencer ISS-N1 in intron 7 (Singh et al., 2006). ISS-N1 recruits splicing repressor hnRNP-A1 complex which represses the exon 7 inclusion in the *SMN2*

transcript, thereby producing mainly transcripts lacking exon 7 and generating unstable SMN protein. Nusinersen is an antisense oligonucleotide (ASO) which targets this ISS-N1 site and prevents recruitment of hnRNP-A1 leading to increased amount of stable SMN protein (Hua et al., 2010;Rigo et al., 2014). As one of the major breakthrough in the field of SMA therapeutics (Finkel et al., 2017;Mercuri et al., 2018a) Nusinersen, after showing promising results in clinical trials has recently been approved by the US Food & Drug Administration (FDA) and European Medicines Agency (EMA). Nusinersen treatment although has shown better results than any other previously described method, it is not the final solution for SMA (Talbot and Tizzano, 2017). Moreover, this treatment requires multiple dosage via intrathecal route of drug administration which is painful and could possibly have more complications in long run (Mercuri et al., 2018a).

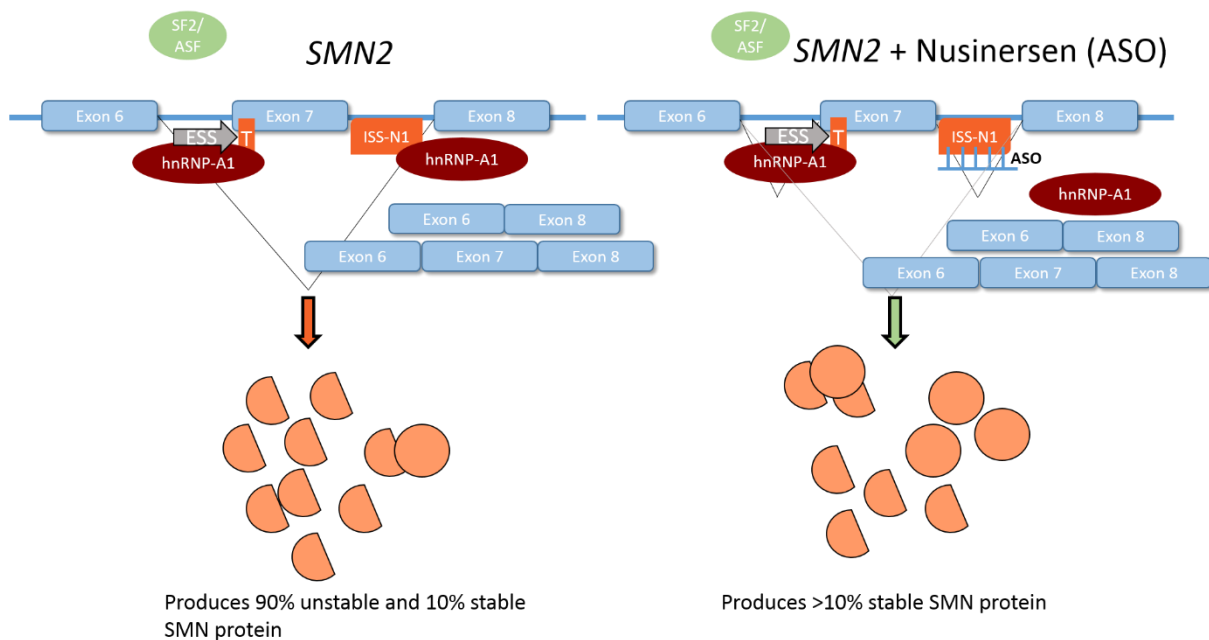


Figure 2 Nusinersen therapy.

Use of an antisense oligonucleotide complimentary to ISS-N1 splicing silencer region, inhibits the binding of splicing repressor protein hnRNP1. This leads to retention of exon 7 in more than 10% of *SMN2* mRNA transcript and higher production of full length, functional SMN protein.

3) Knockdown of *SMN-AS1*: *SMN-AS1* is a neuronally rich long non-coding RNA which acts as a Natural Antisense Transcript (NAT) and binds to the transcription start site (TSS) of *SMN2* gene there by negatively regulating the *SMN2* transcription (d'Ydewalle et al., 2017). *SMN-AS1* recruits polycomb repressor complex-2 (PRC2) to the *SMN2* regulatory regions (Woo et al., 2017). Following this PRC2 recruits certain enzymes which can eventually methylate (di- or tri-) the Lys 27 of histone H3 eventually leading to *SMN2* gene repression (Margueron and Reinberg, 2011). An anti-sense oligonucleotide (ASO) against *SMN-AS1* has been used increase the full length *SMN* transcript as well as the SMN protein level in

SMA therapeutics. However, this approach, by itself, was not sufficient to improve the survival and body weight of SMA mice (d'Ydewalle et al., 2017; Talbot and Tizzano, 2017).

4) Gene replacement therapy: Delivery of exogenous cDNA coding for *SMN1* gene is another approach to increase the SMN protein level in SMA patients. Avexis-101 therapy is based on transduction of a non-pathogenic adeno-associated virus (AAV) of serotype 9 (AAV9) which is known to effectively target motor neurons for delivery of *SMN1* gene (Mendell et al., 2017). A self-complementary form of AAV9 (scAAV) was used to overcome the delay in translation of this transgene. This therapy also is currently in the clinical trials and has shown promising results (Sumner and Crawford, 2018). However high dose of the AAV9 which showed the highest therapeutic potential in SMA patients, has unfortunately resulted in various fatal side effects in non-human primates and piglets (Hinderer et al., 2018). Therefore, the effectivity of this therapy cannot be simply increased by increasing the viral dose but rather needs some other combinatorial therapy to better ameliorate SMA symptoms.

Taken together most therapeutic strategies for SMA involve transcriptional enhancement of *SMN2* gene, which is the primary modifier of SMA. However the most severe as well as most common type of SMA is SMA type I where the individuals may carry even a single allele of *SMN2* (Feldkotter et al., 2002). Considering such a low number of *SMN2* copies, in SMA type I patients, SMA therapeutics would highly benefit from a combinatorial therapy involving SMN independent genetic modifiers (Wirth et al., 2013; Talbot and Tizzano, 2017; Sumner and Crawford, 2018).

1.2 SMA modifiers independent of SMN

One of the most intriguing aspects of genetic diseases originates from the variability of disease phenotypes. This variability in turn is an outcome of numerous genetic and environmental factors, one of them are the disease modifier genes. Particularly, the disturbed homeostasis of diseased individuals with single-gene disorders may disclose the effect of such modifiers otherwise these genes or alleles may not be highly penetrant in healthy individuals (Nadeau, 2001; Genin et al., 2008). Therefore, the study of genetic modifiers has been beneficial for understanding the molecular changes in individuals beyond those afflicted with monogenic conditions (Cutting, 2010; Sankaran et al., 2010).

1.2.1 *Plastin 3*

Particularly in case of SMA, there are some infrequent SMA discordant families, where along with few SMA patients, some asymptomatic individuals have also been reported (Cobben et

al., 1995;Hahnen et al., 1995;Prior et al., 2004;Oprea et al., 2008). These asymptomatic individuals carry homozygous deletion of *SMN1* and only three or four copies of *SMN2*, which usually causes a SMA type II or type III. Characterization of such individuals suggested an additional role of some genetic/ environmental factors in compensation of SMN loss (Wirth et al., 2013). Interestingly, in certain SMA discordant families *Plastin3 (PLS3)* was found to be significantly overexpressed specifically in all asymptomatic individuals but not the symptomatic siblings. Considering the fact, that both symptomatic and asymptomatic individuals carry *SMN1* homozygous deletion and identical *SMN2* copy number, the role of *Plastin3* as a protective modifier of SMA was studied in detail (Oprea et al., 2008). Following this, our group overexpressed *PLS3* which is a Ca^{2+} dependent F-actin bundling protein, ubiquitously in an SMA mouse model. This overexpression was able to restore processes depending on actin dynamics, such as increased F-actin levels, endplate size, NMJ size, synaptic vesicles and active zone numbers (Ackermann et al., 2013). Moreover, we also showed that combination of *PLS3* overexpression along with suboptimal increase in the SMN level (by Nusinersen; SMN antisense oligonucleotide) could even rescue survival of a severe SMA mouse model. This in depth study of the mechanism via which *PLS3* rescues the SMA phenotypes also revealed the indispensable and novel role of endocytosis in the SMA pathology (Hosseinibarkooie et al., 2016).

Endocytosis is a process of internalization of macromolecules by invagination of plasma membrane, eventually forming vesicles with a neck, which then bud off inside the cell via membrane fission. Endocytosis involve de novo production of internal membranes and is also responsible for maintaining the dynamics of plasma membrane composition (Doherty and McMahon, 2009). Various types of endocytosis are classified based on the nature of the molecules being endocytosed (phagocytosis and pinocytosis) as well as the proteins which play major roles like clathrin mediated endocytosis (CME) and caveolin mediated endocytosis (Mayor and Pagano, 2007;Schmid and McMahon, 2007). Nevertheless CME is the major endocytic route, internalizing most cargoes compared to various other types of endocytosis pathways described until now (Kaksonen and Roux, 2018). Endocytosis is impaired in SMA

1.2.2 Neurocalcin delta (*Ncald*)

Our group discovered second SMA modifier gene, Neurocalcin delta (NCALD), which encodes a neuronal calcium sensor protein. In a family with 2 affected (no *SMN1*, 2 copies of *SMN2*) and 5 asymptomatic individuals (no *SMN1*, 4 copies of *SMN2*), NCALD was found to be distinctly downregulated in all five asymptomatic individuals (Riessland et al., 2017). NCALD reduction ameliorated major SMA symptoms in various model systems namely mice,

zebrafish and *Caenorhabditis elegans*. Moreover, NCALD reduction promoted neuronal differentiation, restored the axonal length of motor neurons, improved the NMJ size and structure. Interestingly, NCALD reduction also leads to significantly improved endocytosis in SMA model systems (Riessland et al., 2017). Additionally, it has been shown that NCALD interacts with clathrin in the absence of calcium (Ivings et al., 2002; Riessland et al., 2017). Considering that SMA leads to reduced calcium influx, it has been hypothesized that NCALD can sequester clathrin in low (lower than physiological) calcium concentration thereby hindering the role of clathrin in the endocytosis. Therefore the reduction of NCALD level in SMA physiology, where the calcium influx is reduced, would hinder sequestering of clathrin making it more available. Hence, more availability of clathrin could be the mechanism behind increased endocytosis in SMA upon NCALD reduction.

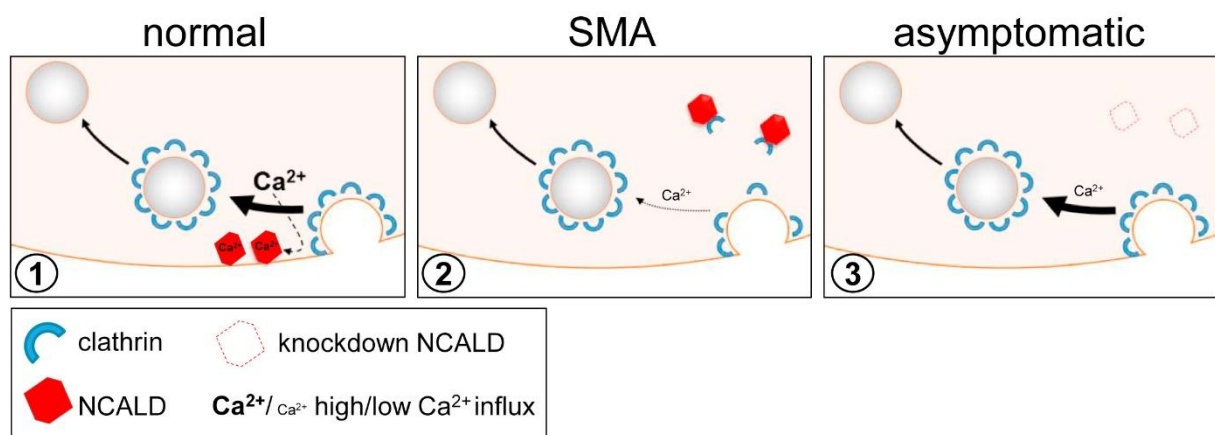


Figure 3 Proposed model depicting the role of NCALD in the endocytosis in normal, SMA and asymptomatic individuals.

NCALD under normal physiological conditions, upon binding to calcium, tethers to cellular membranes. Whereas in SMA conditions the Ca^{2+} homeostasis is disturbed leading to reduced calcium influx and thus NCALD sequesters clathrin. The sequestered clathrin is not available for clathrin mediated endocytosis (CME). However in case of asymptomatic individuals, although Ca^{2+} homeostasis is still impaired but as NCALD levels are reduced, clathrin is not sequestered and is available for CME (Riessland et al., 2017).

1.2.3 Calcineurin-like EF-hand protein 1 (*Chp1*)

In addition to *Pls3* and *Ncald*, we found that a novel PLS3 interacting protein, calcineurin-like EF-hand protein 1 (CHP1) an inhibitor of calcineurin, can also modify SMA (Lin et al., 1999; Janzen et al., 2018). We showed that *Chp1* downregulation can double the survival of SMA mice and restore the impaired axonal growth in SMA motor neurons. Moreover, *Chp1* knockdown in motor neuron like NSC34 cells, tripled macropinocytosis by increasing the calcineurin phosphatase activity. As calcineurin maintains the dynamin phosphorylation during endocytosis we investigated the endocytosis in heterozygous *Chp1* mutant mice on

SMA background. We found that in SMA mice, CHP1 deletion ameliorated the impaired endocytosis, thereby strengthening the role of *SMN* independent modifiers in SMA (Janzen et al., 2018)

1.3 Neurocalcin delta, a neuronal calcium sensor

1.3.1 NCS family

Neuronal calcium sensors (NCS) and other calcium binding proteins are the mediators and regulators of various cellular processes spatially, temporally and in magnitude via their interaction with calcium. NCS family has 14 genes which code for various NCS proteins including Calmodulin, GCAP, Visinin, Visinin like proteins (VILIPs), hippocalcin and neurocalcins (Burgoyne et al., 2004). A group of closely related neuronal calcium sensors forms a subfamily, visinin like proteins (VSNLs), with only 5 members VLIP1, VILIP2, VILIP3, hippocalcin and NCALD. These proteins can transduce the Ca^{2+} signals into specific cellular changes, depending upon their location and interactions with other proteins (Mornet and Bonet-Kerrache, 2001; Burgoyne, 2007). The NCS proteins are characterized by following molecular structure: a Myristoylation signal at N- terminal, two pairs of EF hands (EF1,EF2, EF3,EF4) with Ca^{2+} binding loop and one disabled EF hand near N- terminus (EF1), which varies in each NCS protein imparting them specificity (Ames and Lim, 2012).

As the name, neuronal calcium sensor, suggests these proteins are abundant in the brain or neuronal cells and specifically enriched in certain specific subtypes namely retinal and olfactory neurons (Hidaka and Okazaki, 1993; Kobayashi et al., 1993; Palczewski et al., 1994).

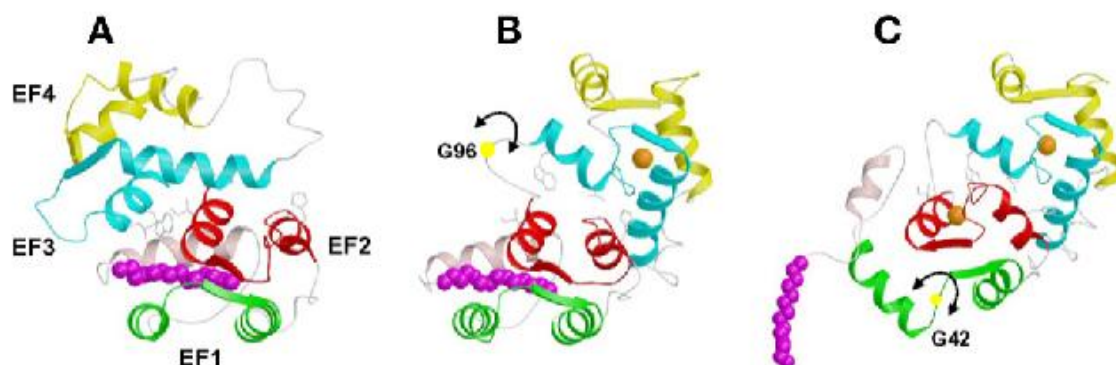


Figure 4 Structure of a neuronal calcium sensor.

NCS proteins have 4 EF hands (2 pairs) which bind to calcium (golden) sequentially (A & B). The binding of calcium causes structural changes in the N terminal domain (EF1 and EF2) and ejects the

myristoyl group (pink) (C). The hydrophobic myristoyl group then enables NCS proteins to integrate into cellular membranes (Ames and Lim, 2012).

1.3.2 Neurocalcin delta

NCALD protein was first purified from the bovine brain, using a calmodulin antagonist W-77 (Nakano et al., 1992; Okazaki et al., 1992). On genomic level, human *NCALD*, which is localized on chromosome 8q22.3 encompasses 438 kb, has 7 exons and produces 30 splice variants, while mouse *Ncald*, which is localized on chromosome 15, encompasses 426 kb, has 7 exons and generates 12 alternative spliced transcripts (Wang et al., 2001) (ENSEMBLE Genome browser).

NCALD protein has a canonical neuronal calcium sensor structure with four EF hand motifs, amongst which three are functional (Terasawa et al., 1992). All three EF hands (EF2, EF3, and EF4) are interdependent on each other and have high affinity to bind to Ca^{2+} ions in unmyristoylated form (Ladant, 1995). The myristoyl chain, which is otherwise sequestered in deep crevice, extrudes from the hydrophobic pocket of EF1 in the presence of minimum 0.6 μM Ca^{2+} , eventually leading to incorporation of NCS proteins into phospholipid membrane (Ladant, 1995). Myristoylated (Myr) NCALD can bind to outer mitochondrial membrane and endoplasmic reticulum (Iino et al., 1995). All the different NCS proteins vary in their binding/sensitivity to calcium thus can direct varied cellular responses to different calcium concentrations (Braunewell and Klein-Szanto, 2009; Ames and Lim, 2012). Interestingly, conformational changes in Myr-NCALD exhibited highest sensitivity to lower calcium concentrations (0 to 0.5 μM) amongst all the tested NCS family members (Viviano et al., 2016b;a).

1.3.3 NCALD abundancy and functions

NCALD is abundant in retinal neurons (Bastianelli et al., 1993; Hidaka and Okazaki, 1993; Porteros et al., 1996; Brinon et al., 1998). Accordingly, NCALD upon binding to calcium, has been shown to regulate the rod outer segment membrane guanylate cyclase, ROS-GC1 in retinal neurons (Venkataraman et al., 2008). ROS-GC1 plays a crucial role in the process of visual and odorant transduction maintaining the cyclic GMP pool in retinal and olfactory neurons (Kumar et al., 1999; Krishnan et al., 2004).

Hippocalcin is a VSNL family member, which shares the highest homology with NCALD and is highly abundant in hippocampus but not in other brain regions (Braunewell and Klein-Szanto, 2009). On other hand, NCALD is known to be abundant in CA3 and dentate gyrus of hippocampus as well as in other brain regions including certain cortical layers (Girard et al., 2015). Hippocalcin (in hippocampal pyramidal neurons) and NCALD (in hippocampal and cortical pyramidal neurons) are known to regulate a particular type of calcium activated potassium current referred to as slow after hyperpolarization (I_{sAHP}) (Tzingounis et al., 2007; Villalobos and Andrade, 2010; Kim et al., 2012). I_{sAHP} is a physiological phenomenon modulated by calcium in neurons as a response to extended periods of excitation (which lead to increase in intracellular calcium) to prevent hyper excitability and seizures (Madison and Nicoll, 1982; Sah, 1996).

Furthermore, VILIP3 (a VSNL family member) has been shown to interact with Cytochrome b_5 (cyb5) and NADH-cytochrome b_5 reductase (B5R). Cyb5 and B5R are ER membrane proteins involved in the microsomal electron transport pathway in mouse brain (Borgese et al., 1993; Honsho et al., 1998; Oikawa et al., 2016). Interestingly, Cyb5 has strong affinity not only towards VILIP3 but also NCALD as well as to other VSNLs (Oikawa et al., 2004; Oikawa et al., 2016). VSNLs bind to Cyb5 only in high calcium concentration, which suggested that only activated VSNLs (myr-VSNLs) which migrate to ER membrane can bind to Cyb5. Furthermore, interaction of NCALD (and other VSNLs) with Cyb5 and B5R has been suggested as calcium dependent modulations of NADH dependent microsomal electron transport pathway (Oikawa et al., 2016).

Nevertheless the localization of NCALD protein is not restricted to the above mentioned cellular and subcellular regions. NCALD has a very broad range of abundance in the brain, however it is highly abundant in specific regions including multiple layers of olfactory bulb, multiple layers of hippocampus, cortical deep layers, striatum, multiple thalamic nuclei and hypothalamus (Girard et al., 2015). Additionally, certain NCALD positive cells are also sparsely present in nucleus accumbens, caudoputamen, medial septal nucleus and cerebellum (Girard et al., 2015). Although few functions of NCALD have been reported in the CNS as mentioned above, the much broader abundance of NCALD in the brain, points toward many more, unexplored, neuronal functions of NCALD.

1.3.4 NCALD implications in various neurological diseases

Studies of diverse neurological patients as well as disease models have implied NCALD's function in various neurological diseases.

1.3.4.1 Neurodegenerative diseases

Neurodegeneration is a general term to describe deficit in structure and function of neurons in certain regions of or whole CNS. Most neurodegenerative diseases are marked by atrophy of brain or spinal cord for example in Alzheimer's disease (AD) and SMA respectively (Kolb and Kissel, 2011; Dos Santos Picanco et al., 2018). Brain neurodegeneration is characterized by (1) decline in neuronal density in specific brain regions, which is directly correlated with extent of neurodegeneration (Zilkova et al., 2006), (2) loss of neurite (dendritic and axonal) complexity not just marks neuronal dysfunction but can even precede neuronal degeneration (Lopez-Domenech et al., 2016) ,(3) yet another hallmark of neurodegeneration is the dysfunctional reactive astrogliosis, where in the inflammatory machinery of brain turn against itself which leads to neuronal apoptosis (Pekny and Pekna, 2016).

AD is a neurodegenerative disease and the most common type of dementia globally, which still remains to be incurable (Wang et al., 2017). Immunostaining analysis of brain tissue biopsies from Alzheimer's patients' revealed significantly lower NCALD levels as compared to healthy controls (Shimohama et al., 1996). Corroborating this, a large-scale transcriptional analysis focusing on the CA1 and CA3 field of the hippocampus showed a significant decrease in NCALD levels, in both CA1 and CA3 brain regions of AD patients compared to controls (Miller et al., 2013b). These findings not only provide insight into the disputed role of calcium sensors and calcium in Alzheimer's disease (Alzheimer's Association Calcium Hypothesis, 2017) but also generated interest in relevance of NCALD physiological function in AD.

1.3.4.2 Neurodevelopmental diseases

Schizophrenia, a cognitive mental disorder, is characterised by disabling psychotic symptoms and does not have any efficient treatment or therapy (Galderisi et al., 2018). Schizophrenia prevalence occurs generally at post-puberty stage, moreover many schizophrenia susceptibility loci are located in neurodevelopmental relevant genes which implies schizophrenia as a neurodevelopmental disorder (Owen et al., 2011). Interestingly, NCALD has been shown to be significantly low in mass spectrometry analysis of plasma membrane and vesicle enriched fraction from pre-frontal cortex (PFC) of neurodevelopmental rat model of schizophrenia (Vercauteren et al., 2007). Additionally, genome-wide association analysis of schizophrenia risk loci has involvement of neuronal calcium signalling (Ripke et al., 2013).

Other neurological diseases associated with NCALD are autism and bipolar disorder. Autism is also a developmental disorder characterized by challenges with social skills, speech and nonverbal communication as well as repetitive behaviors. Pertaining to wide range of conditions characterized as Autism, it is generally referred to as Autism Spectrum Disorder (ASD) (Whyatt and Torres, 2018). On other hand bipolar disorder is also a developmental disorder with onset at adolescence or early adulthood. It is mainly characterized by alternating depression and maniac phases in patients (Power, 2015). Interestingly, single nucleotide polymorphisms (SNPs) in *NCALD* have been associated to autism and bipolar disorder (Ben-David et al., 2011; Xu et al., 2014). In case of such complicated (in genetics and symptoms) diseases, reports on SNPs associated with novel genes not only help to understand the mechanism and pathways involved in the disease but also contribute to the therapeutic development (Jiao et al., 2012; Harvey et al., 2014; Kerner, 2014; Shinozaki and Potash, 2014).

Therefore a further in depth analysis of NCALD function in both neurodegeneration and neurodevelopment can hugely enhance our understanding of NCALD physiological function as well as contribute to deeper understanding of these conditions.

1.3.5 NCALD in other diseases

NCALD abundancy is not restricted to CNS, low levels of NCALD are ubiquitous. However NCALD is comparatively more abundant in certain organs like lung, kidney, ovaries and testis (Wirth lab unpublished results, NCALD protein atlas). NCALD has been associated with various diseases like diabetic nephropathy (Kamiyama et al., 2007), ovarian cancer (Isaksson et al., 2014), lung cancer (Shi et al., 2016) etc. However, as the role of NCALD in other diseases is beyond the scope of this thesis, therefore we need not give a detailed introduction to this topic.

1.4 Modifying role of NCALD reduction in SMA

The project discussed in this thesis is a continuation of previously published findings of Wirth lab (Riessland et al., 2017). We hereby describe in detail the fundamental research that shaped this thesis.

Our group has already shown that treatment of murine NSC34 cells with *Ncald* siRNA, induced neurite outgrowth in these cells even in the absence of retinoic acid. This finding suggested the role of NCALD in the neuronal differentiation and maturation. It was also observed that downregulation of *Ncald* (by injecting morpholinos) restores axonal growth in SMA model of zebrafish, corroborating that NCALD suppression triggers neuronal

differentiation. *Smn* knockdown in zebrafish resulted in reduction of the miniature endplate potential (mEPP) as well as of the endplate potential (EPP), implying disruption of neuronal transmission present in SMA fish model. Intriguingly, the protective effect of *ncald* was seen when knockdown of both *smn* and *ncald* by morpholino injection restored the EPP and mEPP defects to wild-type levels. Strikingly, patch-clamp readings of NSC34 and PC12 cells showed a reduction in the calcium influx when *Smn* was knocked down, which could not be restored upon additional knockdown of *Ncald* which suggested that NCALD most likely acts downstream of Ca^{2+} signals. These results along with other findings implied the role of NCALD in the axon growth and maturation (Yamatani et al., 2010).

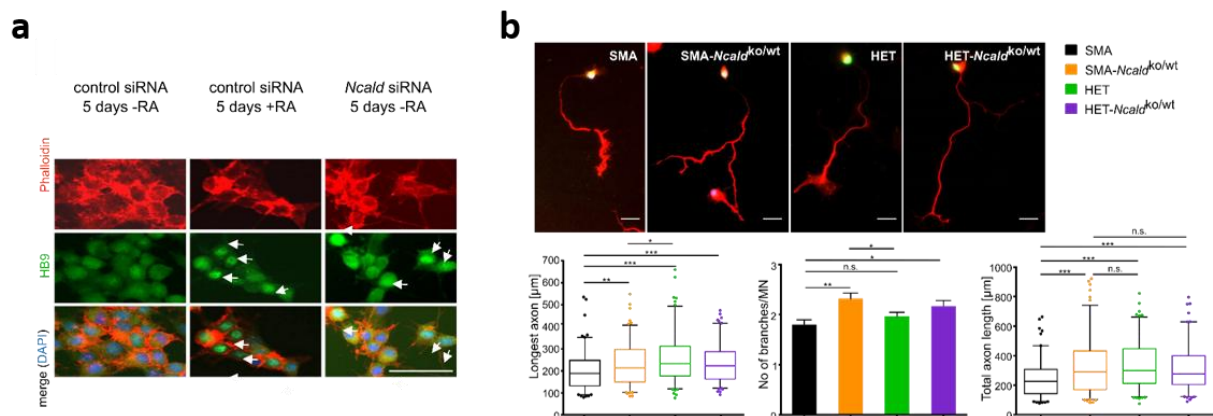


Figure 5 NCALD reduction induces neuronal differentiation and increases axonal length.

(a) NCALD reduction in motor neuron like NSC 34 cells by transfecting them with *Ncald* siRNA induced neuronal differentiation without adding retinoic acid (a differentiation promoting molecule) (b) NCALD reduction in SMA mouse model by cross breeding them with *Ncald* heterozygous knockout animals resulted in augmentation of axonal length as well as branching (Riessland et al., 2017).

NCALD with its protective modifying effects on SMA pathology, could be a potential therapy for SMA. However, the severe SMA mouse model (pups), die before they even reach weaning due to multiple organ failure (Hosseini-barkooie et al., 2016). Therefore, we analysed the effects of NCALD downregulation on SMA background in a mild SMA mouse model. A mild SMA mouse model was generated by treatment of SMA pups (P1) with suboptimum SMN ASO (chemically same as Nusinersen). Reduction of NCALD in SMA background was established by cross breeding heterozygous *Ncald* knockout mouse model with the mild SMA mouse model. The heterozygous *Ncald* knock out model purchased from The Jackson Laboratories, was generated by inserting the Velocigene cassette ZEN-Ub1 the replaced the *Ncald* gene and deleted approximately 29 kbp in chromosome 15 (“JAX Mice Database - 018575 B6N(Cg)-*Ncald* tm1,”).

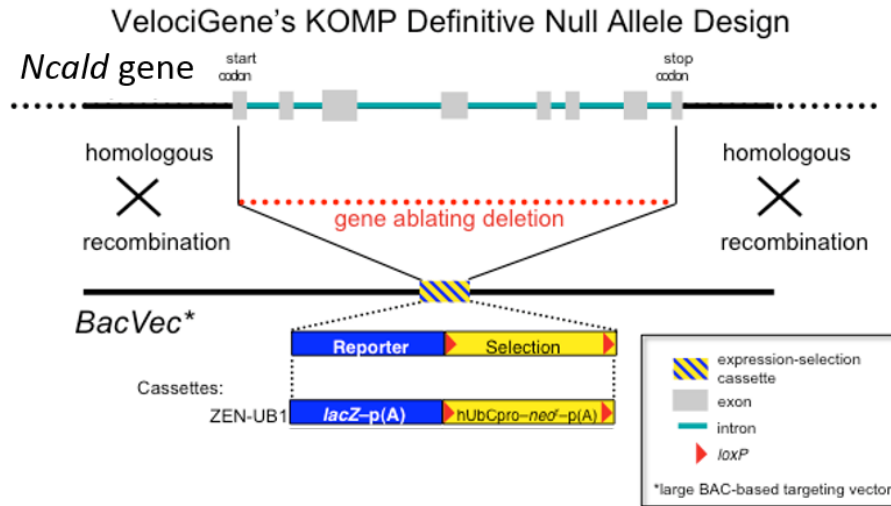


Figure 6 NCALD Knockout mice design.

Insertion of ZEN-UB1 VelociGene cassette containing beta-galactosidase gene, polyadenylation signal, loxP site, promoter from the human ubiquitin C gene and neomycin phosphotransferase replaced the NCALD gene (all coding exons and intervening sequences) by homologous recombination in embryonic stem cells (modified from International Knockout Mouse Consortium website). Further cross breeding removed the neo cassette as well as the Cre transgene from the animals.

Reduction of NCALD by ASO treatment in SMA as well as in HET (control carrying one allele of *Smn1* gene) mice lead to increase in NMJ area and reduced amount of immature NMJs. This reaffirmed the protective modifying effects of NCALD in SMA and we proposed the use of NCALD reduction in SMA therapeutics.

1.4.1 Adult neurogenesis

As this thesis reports a novel link between NCALD and adult neurogenesis, following section is an introduction to adult neurogenesis.

Adult neurogenesis known since more than half decade has been a very interesting and controversial field of study. First report on adult neurogenesis were based on rat model using a radioactive thymidine (Altman and Das, 1965). Generation of new neurons in certain regions of the human brain was first found from post-mortem brain tissues of cancer patients injected with bromodeoxyuridine (BrdU) for cancer diagnosis (Eriksson et al., 1998). BrdU is a thymidine analogue which incorporates into newly synthesised DNA strands and can be detected by probing the tissues with fluorescence labelled anti-BrdU antibody (Dolbeare, 1995). Since then many studies have shown the presence of this process termed as adult neurogenesis in various animal models including various mammals. Although the presence of adult neurogenesis has been confirmed by almost all the rodent model based studies, whether or not adult neurogenesis exists in human brain has remain a controversy (Ming and

Song, 2011). Interestingly the field of human adult neurogenesis was recently shaken by two prominent studies contradicting each other on whether or not new neurons are being born throughout the adulthood (Boldrini et al., 2018; Sorrells et al., 2018). However, understanding the molecular mechanisms involved in generating new neurons in adult brain has widely been accepted as an important step towards neuroregenerative therapy (Kempermann et al., 2018).

2 Aim of the study

NCALD reduction in SMA *in-vitro* and *in-vivo* models resulted in amelioration of major SMA symptoms like increase in the axonal length, axonal branching, NMJ area and maturation, endocytosis and motor functions. Therefore, we proposed NCALD reduction as a SMA therapeutic option, which can be combined with the already available SMN dependent therapies to further enhance the therapeutic impact. However an important question which followed our proposal of NCALD reduction in SMA therapy, was about the potential side effects of NCALD reduction in the physiological system. To answer this question, we need to address an even more primary question about plausible undiscovered physiological roles of NCALD. We attempt answering these two questions in this thesis project by characterizing the *Ncald* heterozygous (*Ncald*^{KO/WT}) as well as homozygous knockout (*Ncald*^{KO/KO}) mouse model, respectively. The *Ncald*^{KO/KO} mouse model used in this study has been generated by The Jackson Laboratories.

In the phenotypic data available for *Ncald* mouse models at International Mouse Phenotyping Consortium (IMPC) website, *Ncald*^{KO/KO} mice show some significant abnormalities namely abnormal neuronal behaviour, hyperactivity, abnormal body mass, impaired pupillary reflex etc (International Mouse Phenotype Consortium, 2016). Considering the data available from IMPC we begin the analysis of brain of NCALD knockout mouse models with following being the main aims:

1. To validate previously published and analyse any new, brain regions with high NCALD abundance in the wildtype mouse brain. These results would narrow down the brain regions as well as cell types we would analyse further. Additionally to analyse the NCALD levels during the brain development that has not been reported yet, to narrow down the age points where NCALD exhibit significant function.
2. To perform an unbiased characterization of the *Ncald*^{KO/KO} animal brain using standard analysis techniques like Nissl staining for morphological analysis, immunostaining analysis for any particular region or cell types based on morphological analysis.
3. To analyse the interactome of NCALD protein to further deepen our understating of its function at the molecular level.
4. Lastly, based on all the results obtained from above mentioned experiment we would finally analyse the specific cell types and molecular pathways which are affected in the *Ncald*^{KO/KO} animals also in the *Ncald*^{KO/WT} animals. To verify the safety and potential side effects of NCALD reduction on physiology of model system, if used in SMA combinatorial therapy.

3 Results

NCALD has been established as an SMN independent protective SMA modifier. NCALD suppression has beneficial effects like increased axonal length, larger NMJ area, decreased number of immature NMJs, enhanced endocytosis and improved motor function in SMA models (Riessland et al., 2017). These findings implied that NCALD reduction can be used as a therapy for SMA in combination with other SMN dependent therapies like nusinersen or Avexis-101 (Hosseini Barkoobae et al., 2017; Riessland et al., 2017). However, these findings also suggested an effective (non-redundant) role of NCALD in the neuronal function and raised a question on any possible side effects that may occur due to reduction of NCALD.

Certain specific neuronal functions of NCALD have been reported earlier like maintenance of cyclic GMP pool in retinal and olfactory neurons (Duda et al., 2004; Krishnan et al., 2004), generation of slow afterhyperpolarization current in cortical as well hippocampal neurons (Villalobos and Andrade, 2010) and calcium dependent modulations of NADH dependent microsomal electron transport pathway (Oikawa et al., 2016). However, all of the above mentioned functions of NCALD were studied based on the role of other NCS family members like GCAP, hippocalcin and VILIP3 respectively. Therefore, an unbiased study of possible non-redundant neuronal functions of NCALD in the brain was an indispensable requirement to further understand the physiological role of NCALD.

In this thesis we have studied NCALD with an unbiased approach via three different genetic backgrounds i.e. wildtype, *Ncald*^{KO/KO}, *Ncald*^{KO/WT}. Using the wildtype animals we studied the abundance and pattern of NCALD as well as its physiological interactions. In *Ncald*^{KO/KO} animals we analyzed the physiological processes that were disturbed in the absence of NCALD, to specifically delineate the role of NCALD in these processes. Lastly, in *Ncald*^{KO/WT} animals we specifically analysed the processes that we found disturbed in *Ncald*^{KO/KO} animals, to verify the safety and effects of NCALD reduction for future SMA therapy.

3.1 NCALD protein, abundance and pattern in wildtype mice

3.1.1 NCALD protein levels rise dramatically during early postnatal stages

To understand the physiological function of NCALD in brain, it was essential to find at which time point during the development of the brain, NCALD is most abundant. As the pattern of NCALD abundance during the brain development has not been reported yet, we analysed the wildtype mouse brains through the development. We investigated the NCALD levels in

embryonic (E16) and early postnatal stages (P1, P10, and P14). Interestingly, NCALD was almost absent at the embryonic stage whereas the NCALD levels increase dramatically from P1 to P14 (Figure 7a). This observation prompted us to analyse postnatal abundance of NCALD. We found that the NCALD expression gradually increase from P1 to P10 and continues to be equally abundant until later stages (P30) in the wildtype brain (Figure 7a). This finding suggested that the function of NCALD is most relevant in postnatal development of the mouse brain.

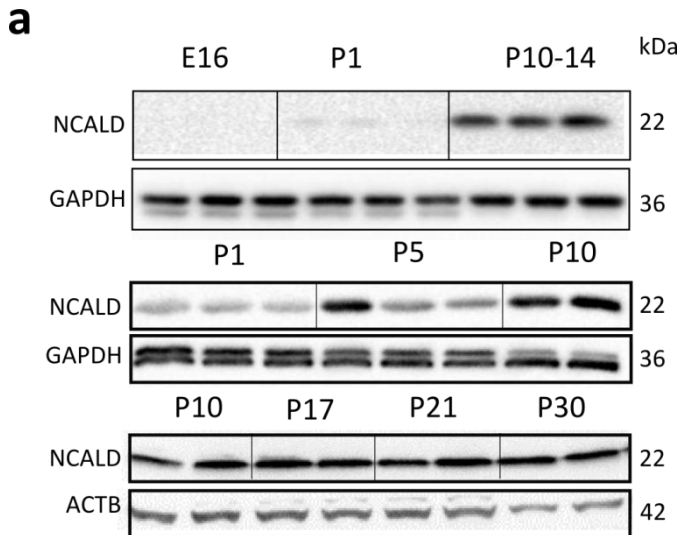


Figure 7 Western blot.

(a) Western blot with brain lysate samples from E16 to P30 showing the dramatic increase from P1 to P10 and high abundance of NCALD until P30.

3.1.2 NCALD is abundant in hippocampus and synaptic punctas

Distribution pattern of NCALD protein within the brain regions like multiple layers of olfactory bulb, multiple layers of hippocampus, cortical deep layers, striatum, multiple thalamic nuclei and hypothalamus have been reported previously (Girard et al., 2015). Nevertheless, we also probed the wildtype brain section with NCALD antibody to reaffirm the previous findings and if possible to find any novel brain region enriched in NCALD.

We therefore analysed the NCALD distribution pattern by NCALD antibody immunostaining of brain sections from P30 wildtype animals. We observed that NCALD is abundant in certain specific regions of the brain namely dentate gyrus (DG) and CA3 in the hippocampus, cortex deep layer (IV-VI), lateral septal nucleus (LS), anteroventral (AVN) and mediodorsal (MDN) thalamic nuclei, stria terminalis (st), agranular insular cortex ventral (AIV) and dorsal (AID) and sparsely presenting in certain other regions like cerebellar cortex, midbrain and pons (Figure 8a). In addition to these regions that corroborated previous finding we also found NCALD highly abundant in presubiculum (PrS), a region that has not been reported in

previous studies on NCALD abundancy (Figure 8a). Furthermore, NCALD has also been found in the pool of neurotransmission related proteins (Vercauteren et al., 2007), synpatosomal fraction (Zareba-Kozioł et al., 2014) as well as co-localizes with synaptic proteins like SV2 at the NMJ (Riessland et al., 2017). However, NCALD localization in the neuronal synapses has not yet been shown. Therefore, to determine more precisely NCALD localization within the neurons, we stained the cultured wildtype hippocampal neurons with NCALD and found a punctate pattern, indicating the presence of NCALD in synapses. This prompted us to co-stain the NCALD with presynaptic markers like Vesicular Glutamate Transporter 1 (VGLUT1) and Vesicular GABA Transporter (VGAT) of excitatory and inhibitory synapses respectively. We found that the NCALD co-localizes with both VGLUT1 and VGAT not in all but only in certain synapses (Figure 8b).

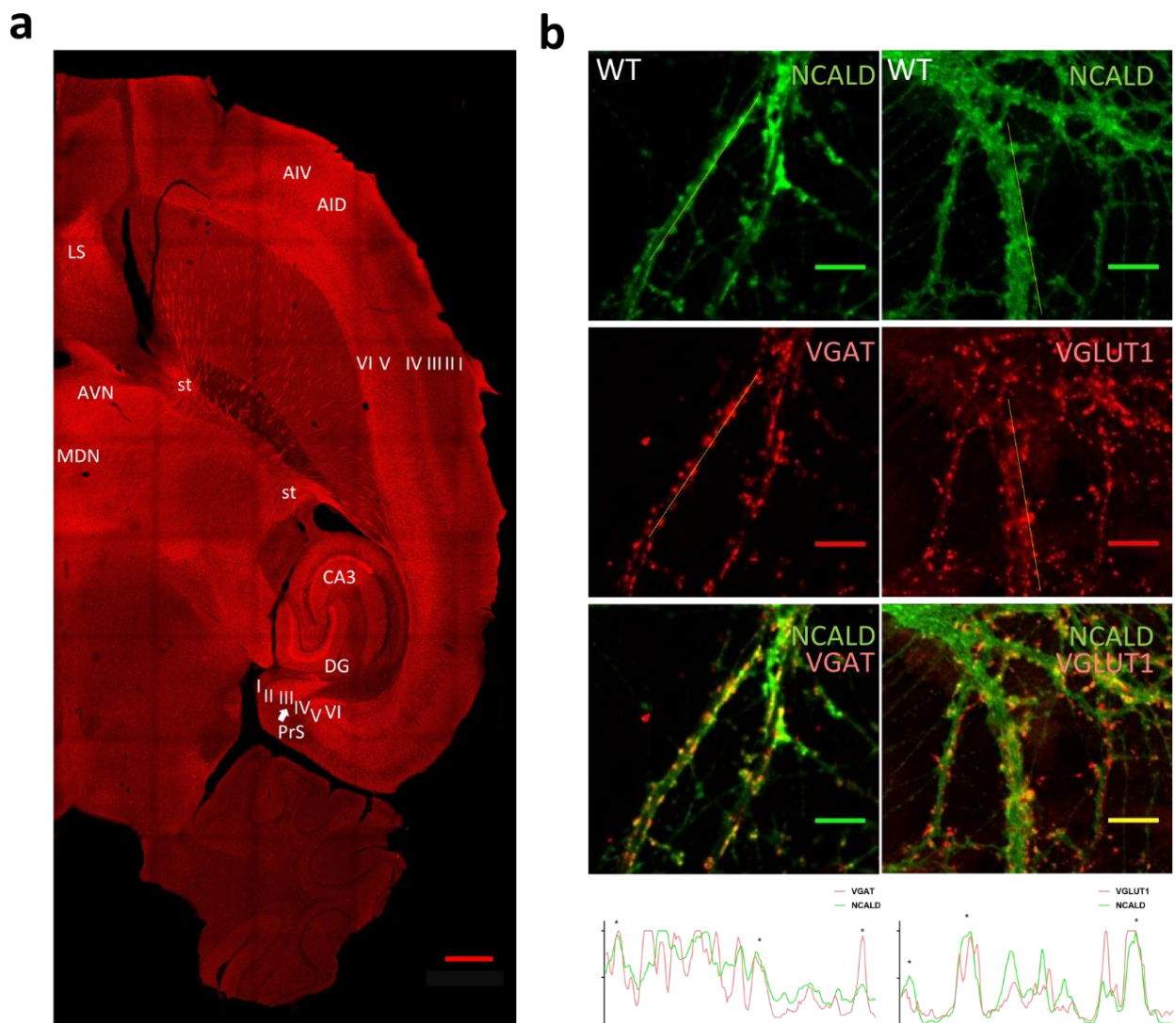


Figure 8 Distributaion and localization of NCALD

(a) Wildtype brain section immunostaining with NCALD antibody depicting the distribution of NCALD in various different brain regions like DG and CA3 in the hippocampus, cortex deep layer (IV-VI),

lateral septal nucleus (LS), anteroventral (AVN) and mediodorsal (MDN) thalamic nuclei, stria terminalis (st), agranular insular cortex ventral (AIV) and dorsal (AID). (b) Representative cultured wildtype hippocampal neurons stained with NCALD antibody and co stained with presynaptic markers VGLUT1 and VGAT. Neurons were imaged with high resolution (40X) for proper visualization of synaptic punctas. A colocalization analysis was performed by ImageJ plot profile function for each channel individually and asterisks represents overlapping peaks of each channel.

3.2 Characterization of *Ncald* knockout mouse

A detailed characterization of *Ncald*^{KO/KO} mice, specifically of the brain would yield deeper insight into novel NCALD neuronal functions. Therefore, we analysed the *Ncald*^{KO/KO} animals and specifically their brains in detail.

3.2.1 *Ncald* knockout causes significant reduction of body weight

Previous unpublished studies in our lab and phenotypic analysis from the International Mouse Phenotyping Consortium show significant reduction in body weight of *Ncald*^{KO/KO} mouse (International Mouse Phenotype Consortium, 2016). To reaffirm these findings we quantified the body weight of 5 month-old male *Ncald*^{KO/KO} animals, and in line with the previous finding we found that adult *Ncald*^{KO/KO} animals weigh significantly less compared to age and sex matched wildtype controls (Figure 9a). Furthermore, the brain from the 4 months old (adult) *Ncald*^{KO/KO} animals and their wildtype littermates were isolated. Interestingly, brain of *Ncald*^{KO/KO} animals also showed significant reduction in their size compared to wildtype littermates (Figure 9b,c). However, when normalized to the reduced body weight, *Ncald*^{KO/KO} brain weigh equivalent to wildtype (Figure 9c).

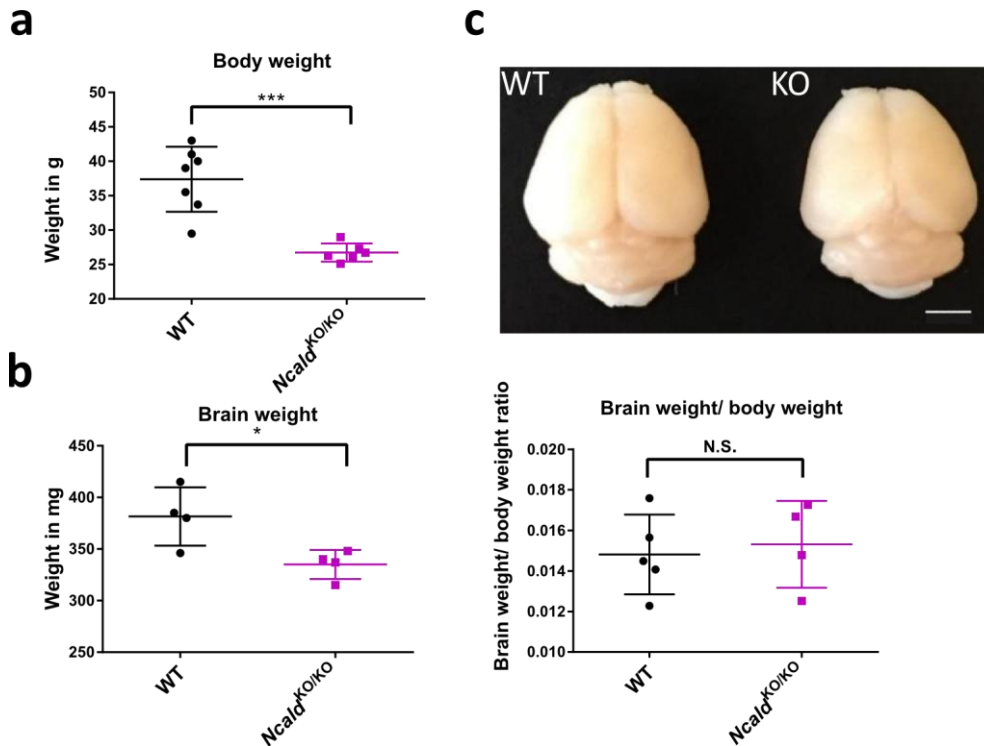


Figure 9 *Ncald* knockout animals show significant reduction in body and brain weight (a) Graph depicting that five months old adult *Ncald*^{KO/KO} males (N=6) weighed significantly less than their age and sex matched wildtype controls (N=7); *** P< 0.001. (b) Graph showing the significant difference in the brain weight of *Ncald*^{KO/KO} animals compared to wildtype littermates; N=4; *P< 0.05. (c) A representative image of *Ncald*^{KO/KO} brain next to a wildtype brain from adult animals. Scale bar 100 pixels and brain weight quantification normalized to body weight. Quantification depicts mean values ± SD; unpaired two-tailed student's t-test; N.S. = non-significant.

3.2.2 Adult *Ncald* knockout brain exhibit gross morphological alterations and reduced dentate gyrus

We analysed the *Ncald*^{KO/KO} mice brain morphology to determine if there are specific brain regions which suffered morphological alterations upon the loss of NCALD as these findings could further focus our study on certain specific brain regions.

We sectioned the brain of 4 month-old *Ncald*^{KO/KO} animals in 40 µm thick consecutive sections. These sections were subjected to Nissl staining for the visualization of the brain morphology. The brain sections from *Ncald*^{KO/KO} animals were compared to that of their wildtype littermates and were probed to morphological analysis. We found enlarged lateral ventricles, smaller hippocampus (especially DG) as well as presubiculum, thinner corpus callosum and cortex in the adult *Ncald*^{KO/KO} brain compared to controls (Figure 10a). Taking into account the conspicuously malformed and smaller DG in hippocampus of adult

Ncald^{KO/KO} animals, we quantified the length of the subgranular zone (SGZ) of the dentate gyrus (DG) in hippocampus. As anticipated, we found that the *Ncald*^{KO/KO} animals have much shorter SGZ length compared to controls (Figure 10b). SGZ is one of the two regions in the brain where the neurogenesis continues throughout the adulthood (Miller et al., 2013a) and also the region which is significantly affected in the Alzheimer's mouse model (Donovan et al., 2006). This finding also marked either a potential loss in the proper development of the dentate gyrus or initial sign of neurodegeneration.

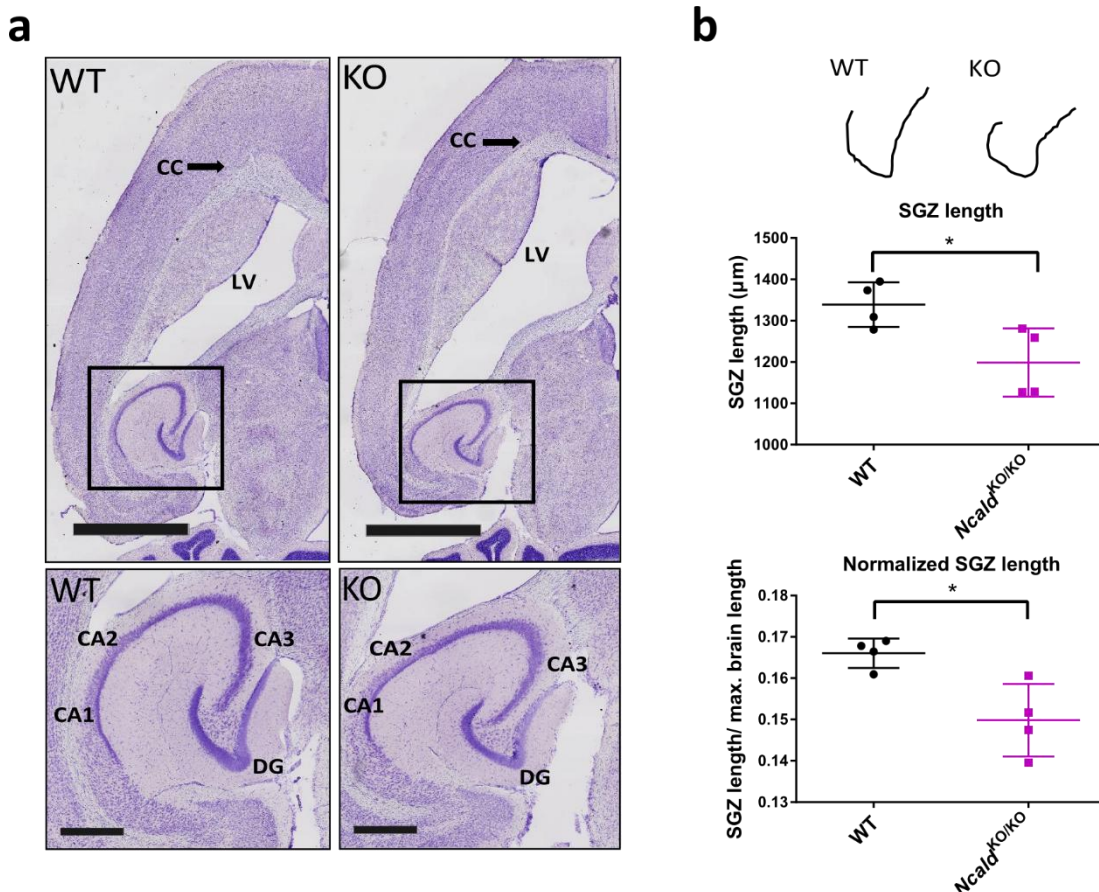


Figure 10 *Ncald*^{KO/KO} brain exhibit gross morphological defects.

(a) Representative nissl staining of brain sections from adult *Ncald*^{KO/KO} animals show morphological defects like enlarged ventricles, corpus callosum atrophy, smaller hippocampus; N=5; scale bar 2mm and 500 μm (magnified inset). (b) Representative outline of the SGZ (in DG) for quantitative analysis, followed by graph depicting significant reduction in the SGZ length in *Ncald*^{KO/KO} brain measured via quantitative analysis; * P<0.05; N=4. The quantitative analysis was also performed by normalizing the length of SGZ to the maximum cross sectional brain length in WT and *Ncald*^{KO/KO} samples; * P<0.05; N=4. Quantification depicts mean values ± SD; unpaired two-tailed student's t-test.

3.2.3 *Ncald* knockout brain do not show progressive neurodegeneration

The observed defects in the morphology of *Ncald*^{KO/KO} brain could be an initial sign of progressive neurodegeneration (Caito et al., 2011). In case of progressive neurodegeneration, the morphological disturbances in the structure of adult *Ncald*^{KO/KO} brain

would worsen with age. Considering this we analysed brain of 18 month-old *Ncald*^{KO/KO} animals and compared it to 4 month-old *Ncald*^{KO/KO} brain. Nevertheless, we did not find exacerbation of the phenotype in the older *Ncald*^{KO/KO} brain (Figure 11a). This result negated the assumption that *Ncald*^{KO/KO} brain underwent neurodegeneration at age of 4 months. To further confirm these results, we analysed some major hallmarks of neurodegeneration like astrogliosis, reduced neuronal density and neuronal complexity (Zilkova et al., 2006; Lopez-Domenech et al., 2016; Pekny and Pekna, 2016) in 4 month-old *Ncald*^{KO/KO} brain. To analyse the astrogliosis, which is marked by upregulation of Glial Fibrillary Acidic Protein (GFAP) and hypertrophy of astrocytic processes (Pekny and Pekna, 2014), we stained the *Ncald*^{KO/KO} brain sections with GFAP an astrocytic marker (Benninger et al., 2016). However, we did not find any signs of astrogliosis in *Ncald*^{KO/KO} brain (Figure 11b). Next, we investigated plausible loss in neuronal density as a sign of neurodegeneration in *Ncald*^{KO/KO} hippocampus (in DG and CA3 region), as it is one of the most severely affected regions in the *Ncald*^{KO/KO} brain. We stained the *Ncald*^{KO/KO} brain sections with NeuN, a marker for mature neurons (Gusel'nikova and Korzhevskiy, 2015), to visualize all the mature neurons and quantify the NeuN⁺ cell density. In line with our previous results, we did not find any significant loss of NeuN⁺ cell density in *Ncald*^{KO/KO} hippocampus compared to controls (Figure 11c). Lastly, we examined loss of dendritic complexity, yet another hallmark of neurodegeneration, in the *Ncald*^{KO/KO} hippocampal neurons. The cultured hippocampal *Ncald*^{KO/KO} neurons were transfected with a plasmid encoding EGFP which marked entire neuronal morphology. We imaged cultured neurons on day *in-vitro* (DIV) 14 and analysed the dendritic morphology using ImageJ sholl analysis tool. Incontestably, the *Ncald*^{KO/KO} neurons when compared to the wildtype neurons did not show any sign of degeneration of dendritic complexity (Figure 11d). These results all together established the fact that *Ncald*^{KO/KO} animals do not incur progressive neurodegeneration.

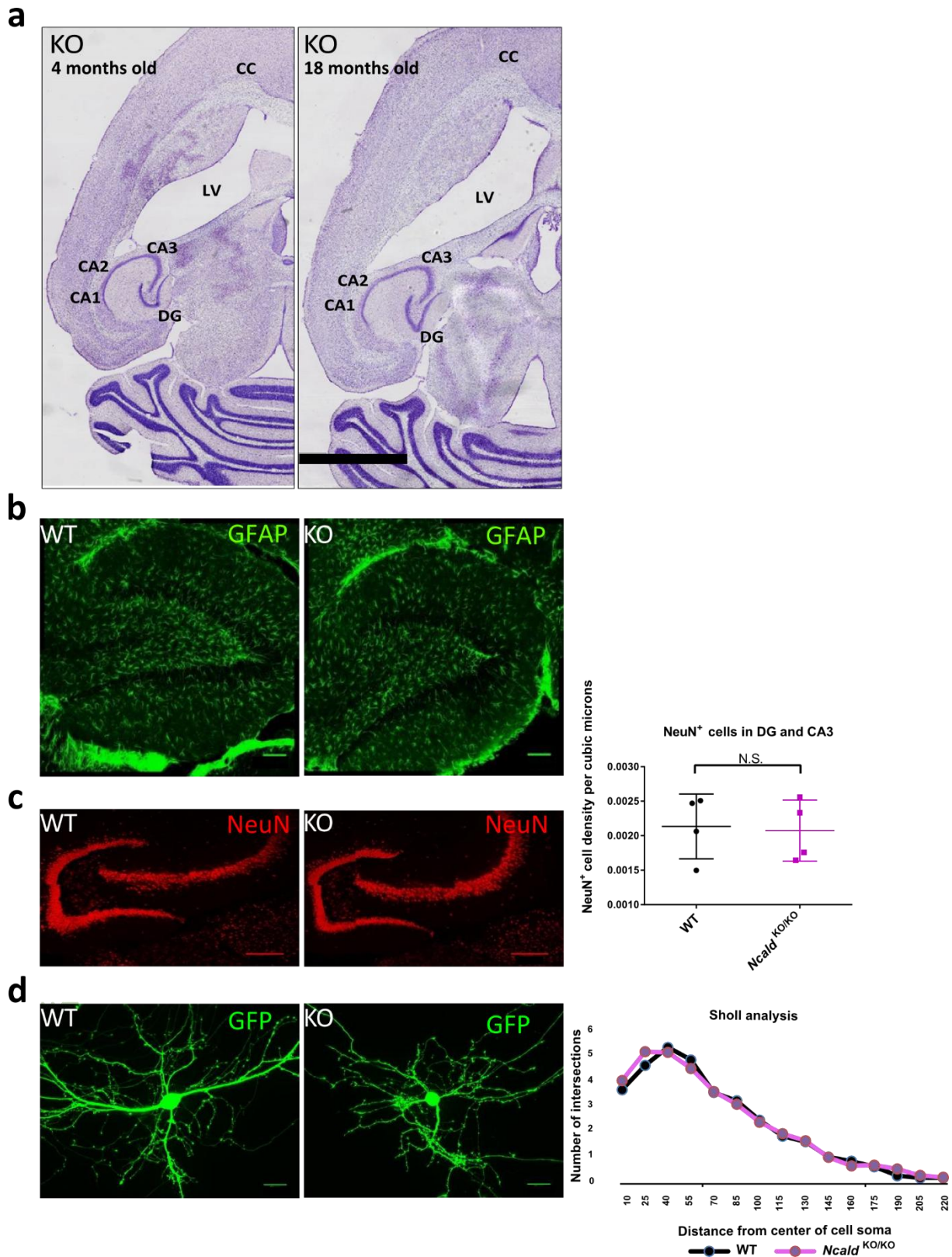


Figure 11 *Ncald*^{KO/KO} brain shows no sign of neurodegeneration.

(a) Representative nissl staining images of 4 months old and 18 months old *Ncald*^{KO/KO} brain, showing no exacerbation of phenotype; N=2; scale bar 2mm. (b) Representative GFAP staining of *Ncald*^{KO/KO} and wildtype brain sections (hippocampus) showing no sign of astrogliosis; N=3. (c) Representative NeuN staining of *Ncald*^{KO/KO} and wildtype brain sections (hippocampus) and graph of quantitative analysis of showing no significant reduction in NeuN⁺ cell density N=4. (d) GFP transfected cultured

hippocampal neurons from *Ncald*^{KO/KO} and wildtype brain and shall analysis graph showing significant loss of dendritic complexity in *Ncald*^{KO/KO} neurons; N=36 & 39 neurons from N=3 pups for each genotype. Quantification depicts mean values ± SD; unpaired two-tailed student's t-test; N.S. = non-significant.

3.2.4 *Ncald* knockout brain show mild morphological defects even before adulthood

We observed none of the major phenotypes of progressive neurodegeneration in *Ncald*^{KO/KO} brain, however 4 month-old *Ncald*^{KO/KO} brain exhibit significant morphological defects especially in dentate gyrus. Considering this, we addressed neurodevelopmental/ maturation defects as the cause of causing the morphological changes in *Ncald*^{KO/KO} brain.

To address whether these defects were originating during the early development of the brain we further analysed some *Ncald*^{KO/KO} animals at 2 weeks (P14) and one month (P30). We found that the younger (P14, 30) *Ncald*^{KO/KO} brain did not show as severe alteration as the adult brain (Figure 12a,b). However, we observed increase in ventricular area in *Ncald*^{KO/KO} animals, since P14, which seemed to be more evident at P30. These findings implied that *Ncald*^{KO/KO} animals most likely accumulate certain neurodevelopmental defects since early post-natal period (P14) through the adolescence (P30) until the adulthood (4 months).

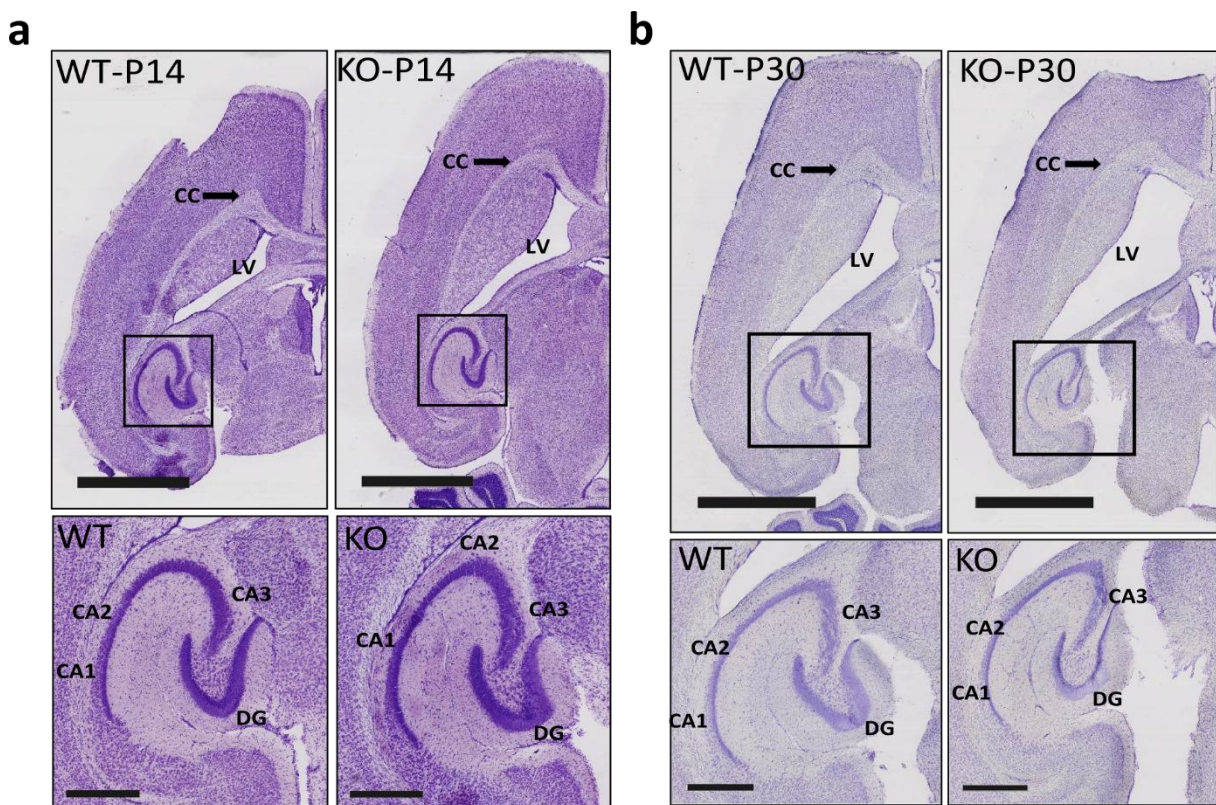


Figure 12 Young (P14 and P30) *Ncald*^{KO/KO} brain exhibit mild morphological defects.

(a) Representative nissl staining of brain sections from P14 *Ncald*^{KO/KO} and wildtype animals, showing mild increase in the lateral ventricles as well as mild atrophy of corpus callosum; N=4; scale bar 2 mm and 500 μm (magnified inset). (b) Representative nissl staining of brain sections from P30 *Ncald*^{KO/KO}

and wildtype animals, showing increase in the lateral ventricles as well as mild atrophy of corpus callosum; N=3; scale bar 2 mm and 500 μ m (magnified inset).

3.2.5 *Ncald* knockout impairs adult neurogenesis

Our initial findings; first, NCALD abundancy increases dramatically during the perinatal period and second, the *Ncald*^{KO/KO} brains most likely undergo some developmental defect, indicated a critical role of NCALD during postnatal brain development/ maturation.

The developmental defects that were observed in the adult *Ncald*^{KO/KO} brain, especially in the hippocampus, could arise due to defects in the cell proliferation (Ferri et al., 2004; Antonelli et al., 2018). To test this hypothesis, we first analysed overall cell proliferation in the *Ncald*^{KO/KO} hippocampus using Ki-67, a general proliferation marker for all actively dividing cells (Scholzen and Gerdes, 2000). We found no significant change in the Ki-67⁺ cell density at *Ncald*^{KO/KO} hippocampus compared to the controls (Figure 13a). Furthermore, we analysed nestin positive adult neural stem cells which are the source of postnatal neurogenesis, but did not find any significant difference between the wildtype and *Ncald*^{KO/KO} brain.

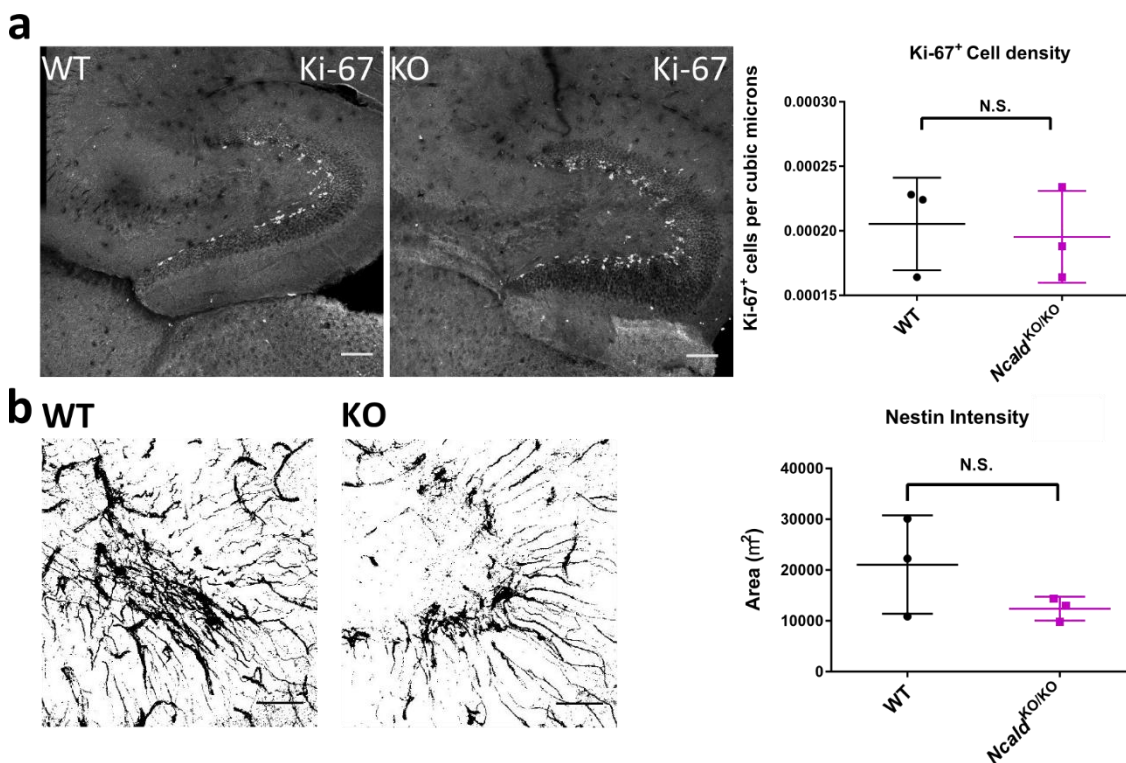


Figure 13 *Ncald*^{KO/KO} hippocampus do not show any defects in general cell proliferation. (a) Representative Ki-67 immunostaining of *Ncald*^{KO/KO} and wildtype hippocampus at P14 and graph representing no significant changes in the Ki-67⁺ proliferating cells in *Ncald*^{KO/KO} hippocampus; N=3; scale bar 100 μ m. (b) Representative intensity mask of nestin immunostaining of *Ncald*^{KO/KO} and wildtype hippocampus at P30 and graph representing no significant changes in the nestin staining in *Ncald*^{KO/KO} hippocampus; N=3; scale bar 45 μ m. Quantification depicts mean values \pm SD; unpaired two-tailed student's t-test; N.S. = non-significant.

Moreover, the volume and morphology of the hippocampus can also be regulated by generation of new neurons in the adulthood a process called adult neurogenesis (Fuss et al., 2014; Baptista and Andrade, 2018). Adult neurogenesis is generation of new neurons from the neural precursor cells (NPCs) which continues from embryonic development until adulthood (Ming and Song, 2011). However in adult animals this process is restricted to certain specific areas of the brain (Bordiuk et al., 2014). There are various stages during the process of differentiation and maturation of adult NPCs into mature granule cells, one such stage of immature granule cells is specifically marked by doublecortin (Couillard-Despres et al., 2005). Doublecortin is a microtubule associated protein known to be expressed specifically in newly generated post mitotic migrating neurons (Gleeson et al., 1999).

Considering this we investigated whether the morphological defects in the *Ncald*^{KO/KO} hippocampus especially in the DG were a result of impaired adult neurogenesis. We analysed specifically the adult born neurons, marked by, immature granule cell marker, doublecortin (DCX) in *Ncald*^{KO/KO} hippocampus and their wildtype littermates. We found that the DCX⁺ cells did not change significantly during P14, however showed a tendency to be more abundant in *Ncald*^{KO/KO} hippocampus (Figure 14a). In contrast to P14, P30 *Ncald*^{KO/KO} hippocampus (DG) displayed a non-significant tendency to have less DCX⁺ neurons compared to controls (Figure 14b). Interestingly, at the age of 4 months the *Ncald*^{KO/KO} hippocampus showed a significant decrease in the DCX⁺ cells compared to their wildtype littermates (Figure 14c). Decrease in DCX⁺ cells in the hippocampus is a hallmark of impaired adult neurogenesis; therefore we concluded that loss of NCALD impairs the adult neurogenesis. Additionally, in adult *Ncald*^{KO/KO} hippocampus we observed a dramatic reduction in dendritic extensions of DCX⁺ neurons (Figure 14c). The functional integration and maturation of newly generated immature DCX⁺ neurons into mature granule cell layer (GCL) of DG is initiated by the extension of spineless dendrites through molecular layer (Toni and Schinder, 2015). Thus, loss of dendritic extensions in DCX⁺ neurons in *Ncald*^{KO/KO} hippocampus questioned the functionality of these neurons. Furthermore, few DCX⁺ neurons which were present in *Ncald*^{KO/KO} DG showed an abnormal tangential migration (Figure 14c). This disorientation in DCX⁺ cells could be a result of general migration defects in *Ncald*^{KO/KO} animals (Evsyukova et al., 2013).

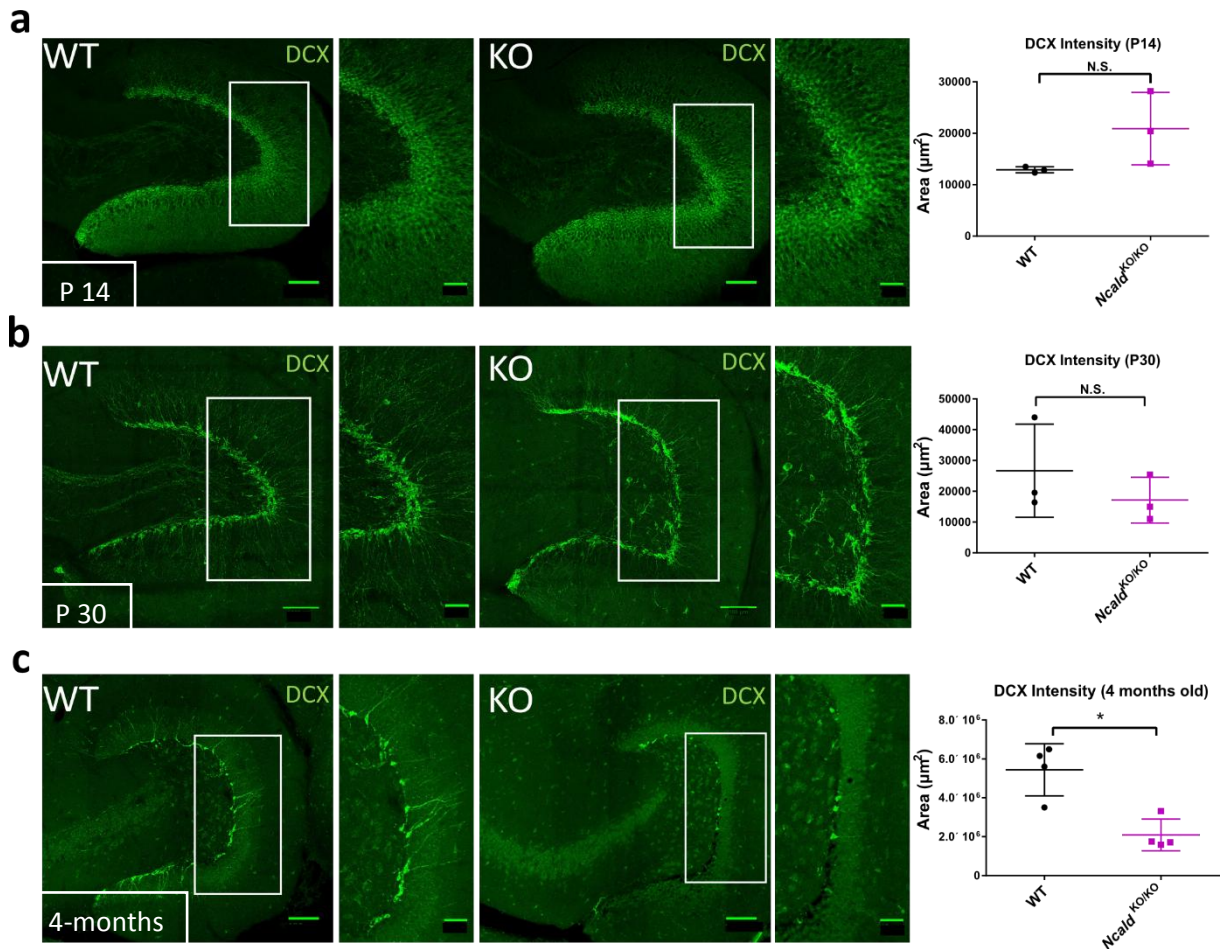


Figure 14 *Ncald*^{KO/KO} brain endure impaired adult neurogenesis.

(a) Representative DCX immunostaining of P14 hippocampus in the *Ncald*^{KO/KO} and the wildtype littermate. A graph representing no significant change in the quantitative analysis of DCX intensity in *Ncald*^{KO/KO} hippocampus compared to controls; N=3; scale bar 100 μm and 40 μm (magnified inset). (b) Representative DCX immunostaining of P30 hippocampus in the *Ncald*^{KO/KO} and the wildtype littermate. A graph representing no significant change in the quantitative analysis of DCX intensity in *Ncald*^{KO/KO} hippocampus compared to controls; N=3; scale bar 100 μm and 40 μm (magnified inset). (c) Representative DCX immunostaining of adult hippocampus in the *Ncald*^{KO/KO} and the wildtype littermate. A graph representing significant reduction in the quantitative analysis of DCX intensity in *Ncald*^{KO/KO} hippocampus compared to controls; N=4; * $P < 0.05$; scale bar 100 μm and 40 μm (magnified inset). Quantification depicts mean values \pm SD; unpaired two-tailed student's t-test; N.S. = non-significant.

3.2.6 *Ncald* knockout does not cause any migrational defects in the cortex

Migration defects observed in DCX⁺ cells in *Ncald*^{KO/KO} hippocampus may not be restricted to hippocampus but could even be occurring in other neuronal migration events such as the migration of neurons during the formation of cortical layers. Migration defects in cortical layers disrupt the standard sequence of deep and superficial layers leading to inversion of these layers (Molyneaux et al., 2007;Lawrenson et al., 2017). Therefore we analysed the

cortical layers and their spatial localization in the *Ncald*^{KO/KO} brain. Superficial and deep cortical layers were stained using the specific markers, Cut-Like Homeobox-1 (CUX1) and T-Box, Brain -1 (TBR1) respectively (Molyneaux et al., 2007). We found that CUX1⁺ and TBR1⁺ cells were located in their proper physiological locations (Figure 15a, b) i.e. we did not find any disturbances in the cortical layer organization in the *Ncald*^{KO/KO} brain.

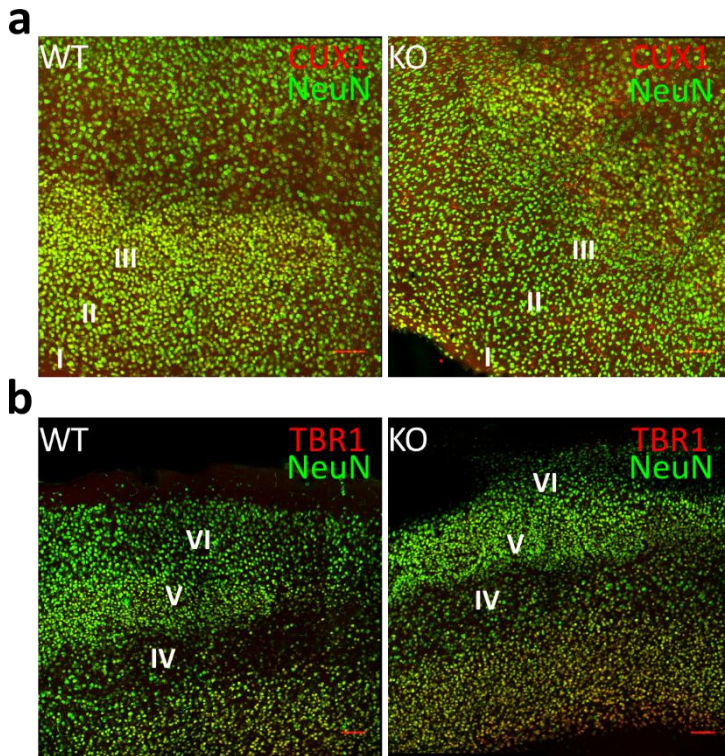


Figure 15 Cortical layers in *Ncald*^{KO/KO} brain do not show migration defects

(a) Representative CUX1 and NeuN immunostaining of cortex in adult *Ncald*^{KO/KO} and wildtype brain. CUX1 labelled superficial layer neurons were correctly localized; scale bar 100 μ m. (b) Representative TBR1 and NeuN immunostaining of cortex in adult *Ncald*^{KO/KO} and wildtype brain. TBR1 labelled deep layer neurons were correctly localized; scale bar 100 μ m.

3.2.7 Myelination is disturbed in *Ncald* knockout brain

Other than generation of new granule cells in the DG, myelination is an important part of postnatal brain development (O'Rourke et al., 2014). Our results indicating possible role of NCALD in postnatal brain development as well as observed thinning of corpus callosum (bundles of myelinated axons) in the *Ncald*^{KO/KO} brain nissl staining images, prompted us to further investigate myelination in *Ncald*^{KO/KO} mouse brain. We stained the brain sections from one month old *Ncald*^{KO/KO} and wildtype animals with Myelin Basic Protein (MBP) antibody. The immunostaining images and western blot analysis of brain lysate showed significantly reduced myelination in the *Ncald*^{KO/KO} brain compared to controls (Figure 16a, b). This finding

suggested loss of NCALD can also impact the process of myelination during the postnatal development of brain.

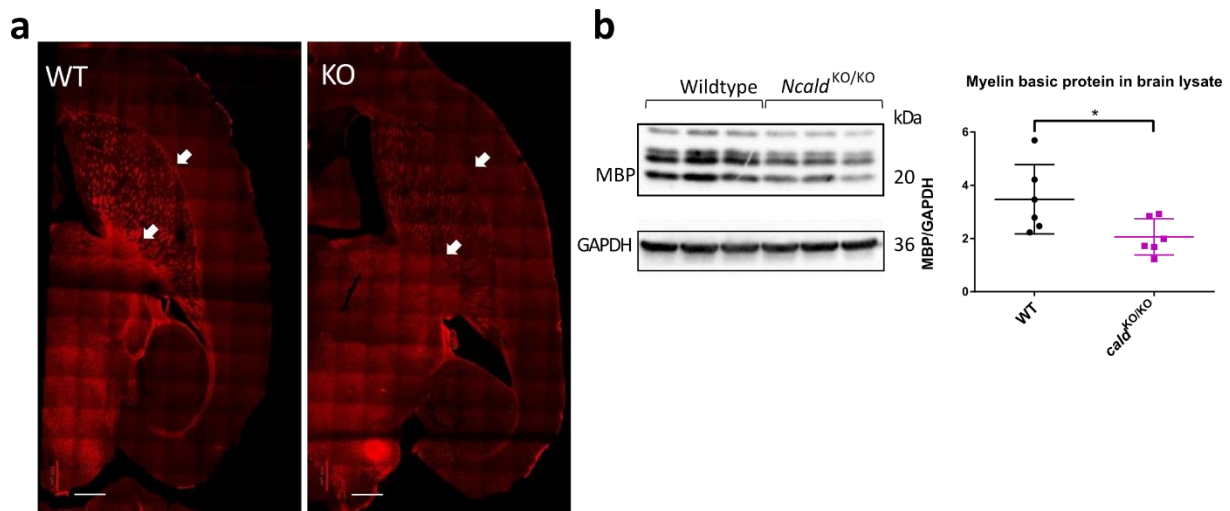


Figure 16 *Ncald*^{KO/KO} brain display reduced myelination
 (a) Representative MBP immunostaining of *Ncald*^{KO/KO} P30 brain showing reduced amount of myelin compared to wildtype littermate; scale bar 500 μ m. (b) Representative western blot from P30 brain lysate also showing reduced levels of myelin in the *Ncald*^{KO/KO} brain compared to controls. A graph representing the quantitative analysis of western blot band intensities; N=6, * P< 0.05. Quantification depicts mean values \pm SD; unpaired two-tailed student's t-test.

3.3 NCALD physiological interactions and function in mouse brain

3.3.1 NCALD is absent in oligodendrocytes

Taking in account the reduced myelination observed in *Ncald*^{KO/KO} brain, we further investigated how NCALD could affect the myelination in physiological context. The myelin sheath is formed via differentiation of specific type of glia cells called oligodendrocytes (Salzer, 2015). To understand further the effect of NCALD on myelination we investigated if NCALD is present in the oligodendrocytes. We co-stained the wildtype brain sections with the oligodendrocyte marker, Anti- adenomatous Polyposis Coli (APC) (Lang et al., 2013) and the NCALD antibody. Interestingly, the co-localization analysis of immunostaining images concluded no co-localization of NCALD with APC (Figure 17a). This finding showed that NCALD is absent in the oligodendrocyte soma and nullified the possibility of NCALD acting directly in the oligodendrocyte. However, there are other factors like neuronal activity which can also regulate the process of myelination (Gibson et al., 2014). Since NCALD is present in neurons and has also been shown to regulate specific neuronal activities (Villalobos and Andrade, 2010), it is a potential possibility that the role of NCALD in neuronal activity may influence myelination.

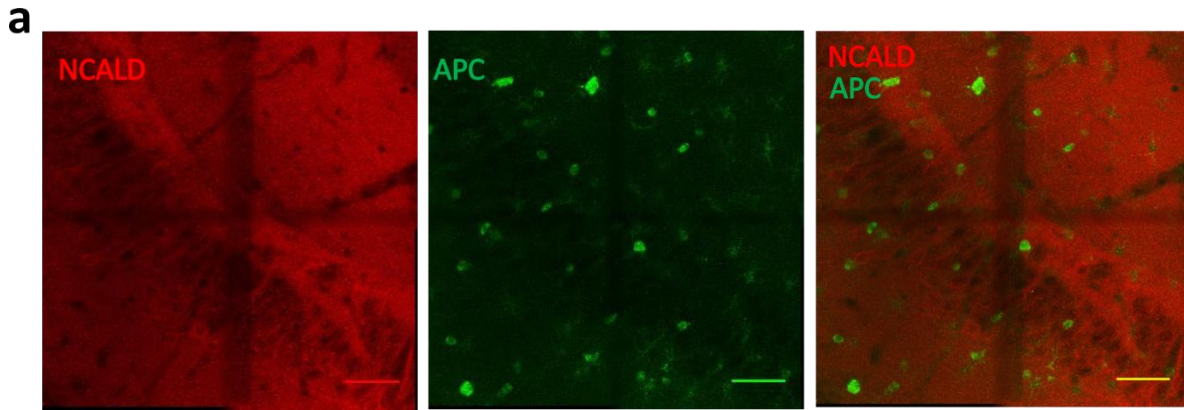


Figure 17 NCALD is absent in oligodendrocytes.

(a) NCALD and APC staining in the wildtype brain section, showing no co-localization of these two proteins; scale bar 50 μ m; $P=0.25$, Mander's coefficient.

3.3.2 NCALD interacts with MAP3K10

To gain deeper insights into the molecular basis of the NCALD function and effect in the mouse brain, we investigated the potential binding partners of NCALD. We addressed this by subjecting the brain lysate from one month-old wildtype and *Ncald*^{KO/KO} mice to immunoprecipitation (IP) using endogenous NCALD antibody. There were three IP groups; (1) wildtype brain lysate IPs (3 samples) (2) *Ncald*^{KO/KO} brain lysate IPs (3 samples) (3) independent negative IP using only the beads (3 wildtype samples). The affinity purified protein complexes (output) from each group were subjected to mass spectrometry (MS) analysis using Orbitrap mass analyzer. Orbitrap generates an electrostatic field using three electrodes, and ionizing peptides segregate by oscillating at a particular frequency based upon their charge and mass ratio. MS analyses determines the composition as well as stoichiometry of the protein complexes (Borch et al., 2005). Therefore, MS is a highly sensitive, mass accurate powerful tool for identification of protein complexes and thus potential novel interaction partners can be investigated by MS analysis.

The data obtained from mass spectrometry of all three groups was compared and further analysed to identify NCALD interactome i.e. candidates present only in wildtype group (group1) but not in the other two groups (**Error! Reference source not found. Appendix Table 6**). The reason behind such strong selection was because NCALD antibody showed some background signals in certain NCALD knockout samples, most likely by binding to close NCALD homologues like VILIP1 or hippocalcin. Therefore, such a strict selection criteria of comparing proteins from all three list, to select proteins that were only present in the wildtype group yielded a very precise final list of only three candidates (Figure 18a). Among the three proteins in the final list, MAP3K10 had the highest number of peptides identified; therefore we first selected this candidate for further analysis. We confirmed

MAP3K10 as an NCALD interacting partner via co-immunoprecipitation analysis from the one month old wildtype brain tissue using the MAP3K10 antibody (Figure 18b). (This part of work was performed by Dr. Seyyedmohsen Hosseinibarkooie, postdoc in AG Wirth).

a

Protein symbols	Protein names	Protein IDs	Peptides	Number of times identified in group 1	Number of times identified in group 2	Number of times identified in group 3
MAP3K10	Mitogen-activated protein kinase kinase kinase 10	D3YXM8	28	3	0	0
DLD	Dihydrolipoyl dehydrogenase, mitochondrial	O08749	4	3	0	0
NCALD	Neurocalcin-delta	Q91X97	5	3	0	0
FMN2	Formin-2	Q9JL04	10	3	0	0

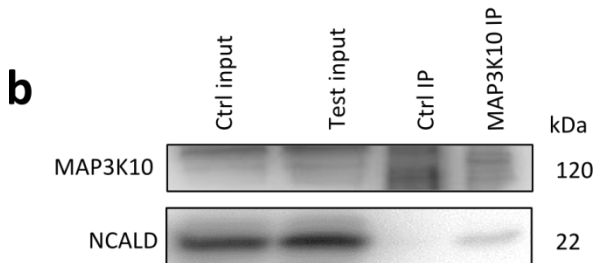


Figure 18 NCALD interacts with MAP3K10.

(a) List of candidate proteins, which may specifically interact with NCALD obtained from mass spectrometry analysis. (b) Co-immunoprecipitation blot confirming the interaction of MAP3K10 and NCALD (fourth lane).

3.3.3 pJNK is upregulated in *Ncald* knockout brain

MAP3K10 is an upstream kinase on the JNK and p38, two major MAP kinase pathways (Hirai et al., 1997). JNK pathway can regulate various processes like neuronal differentiation, axonal growth, axonal branching and apoptosis (Figure 19a) (Coffey, 2014). Interestingly, in addition to these processes, JNK pathway has also been shown to negatively regulate the generation of DCX⁺ cells in adult neurogenesis (Mohammad et al., 2017). Considering our previous finding that adult *Ncald*^{KO/KO} brain exhibited a significant loss in the DCX⁺ cells, we further analysed the JNK and the pJNK (activated JNK) levels in the *Ncald*^{KO/KO} brain. We found significantly higher levels of pJNK (pThr 183 and pTyr 185) in *Ncald*^{KO/KO} brain compared to controls (Figure 19b). Corroborating with the previous studies, we hypothesised that higher pJNK is most likely leading to the loss of DCX⁺ cells in *Ncald*^{KO/KO} brain.

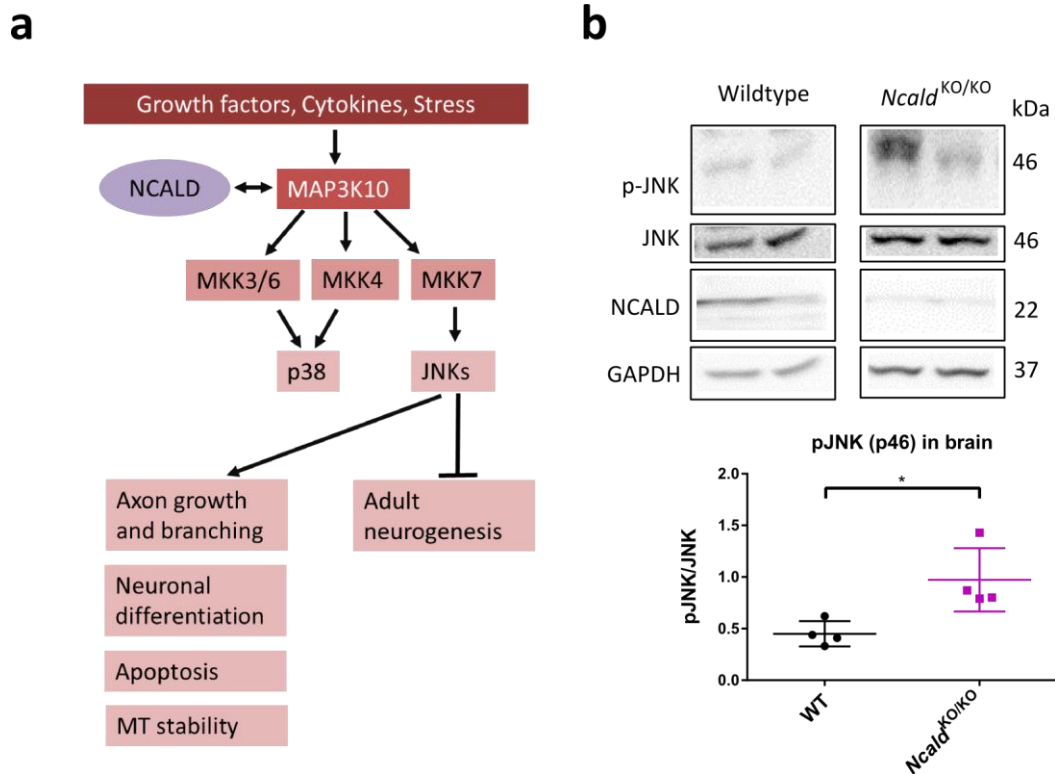


Figure 19 *Ncald*^{KO/KO} brain show increase pJNK levels.

(a) Scheme of JNK pathway and the list of cellular processes regulated by JNK. (b) Representative western blot showing increase in the pJNK level. Graph representing the quantitative analysis of western blot; * $P < 0.05$; $N = 4$. Quantification depicts mean values \pm SD; unpaired two-tailed student's t-test.

3.3.4 Transient inhibition of JNK could not rescue the impairment in adult neurogenesis

To further strengthen the correlation of increased pJNK and loss of DCX⁺ neurons in *Ncald*^{KO/KO} animals, we treated these animals with JNK inhibitor. It has already been shown that use of JNK inhibitor can significantly increase the adult born DCX⁺ cells in mouse hippocampus (Mohammad et al., 2017). Many JNK inhibitors are available and have been used frequently for research purposes, however most of them are not specific to JNK and also inhibit other MAPKs (Bain et al., 2003). Therefore, we chose SR3306, one of the orally available, most effective and highly selective inhibitor of pJNK (Crocker et al., 2011). We treated the *Ncald*^{KO/KO} animals with the JNK inhibitor SR3306 as well as with the vehicle solution. Referring to a previously published protocol (Gao et al., 2017) we first planned to treat the animals intraperitoneally by dissolving the SR3306 in 1X PBS. However, SR3306 was not soluble in 1X PBS at room temperature. Therefore we applied heat by placing the mixture in hot water bath but still could not dissolve the SR3306 in 1X PBS. We also used different DMSO concentrations (2%, 5%, 10%) according to the product protocol to dissolve SR3306, however even with 10% DMSO the SR3306 was not completely soluble. We could not further increase DMSO concentration as it may have toxic effects on the animals (Galvao

et al., 2014). Finally, we could successfully dissolve SR3306 in 45% w/v β -hydroxypropyl cyclodextrin with 0.07% HCl, which has already been published as a solvent for SR3306 (Crocker et al., 2011). This vehicle solution was highly acidic and hence we changed our mode of drug administration from intraperitoneal to oral gavage method. As this drug has neuroprotective effects upon its oral administration in mice, we followed the same protocol (Chambers et al., 2011). We specifically used the 2 months old, young adult brain which displays high rate of adult neurogenesis (Pan et al., 2013) with 3 animals in drug treated group and 3 animals in vehicle treated group for our preliminary analysis. Moreover, to reduce any gender bias we used only females in this experiment. The treatment lasted for six consecutive days, with 7 oral doses of 30 mg/kg SR3306 via gavage, twice on day one and once on days 2-6 and similar treatment was carried out with the vehicle solution (Figure 20). We sacrificed the animals 3 more weeks post treatment, as the percentage DCX⁺ cells (BrdU labelled) has shown to be highest in the second and third week post the BrdU treatment of mouse brain (Snyder et al., 2009),

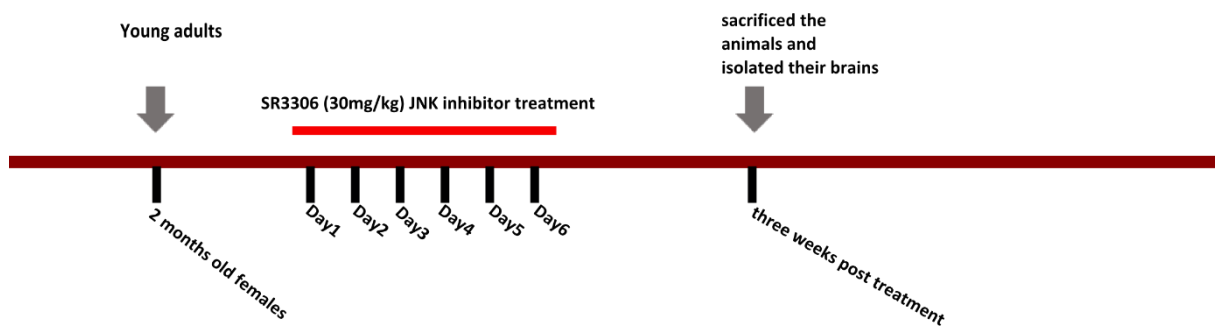


Figure 20 Time line of JNK inhibitor and parallel vehicle treatment.

However, using this treatment protocol we did not find any improvement in the body weight, brain weight, brain morphology or number of DCX⁺ cells in the *Ncald*^{KO/KO} brain (Figure 21a, b, c). These preliminary results were not conclusive; more detailed analysis of wildtype brains under this treatment protocol would specify whether this transient treatment protocol can actually impact the DCX⁺ population. If not, then a longer chronic inhibition of JNK, most likely via mini pump insertion into the animal brain could show a better result as seen in previous studies (Mohammad et al., 2017).

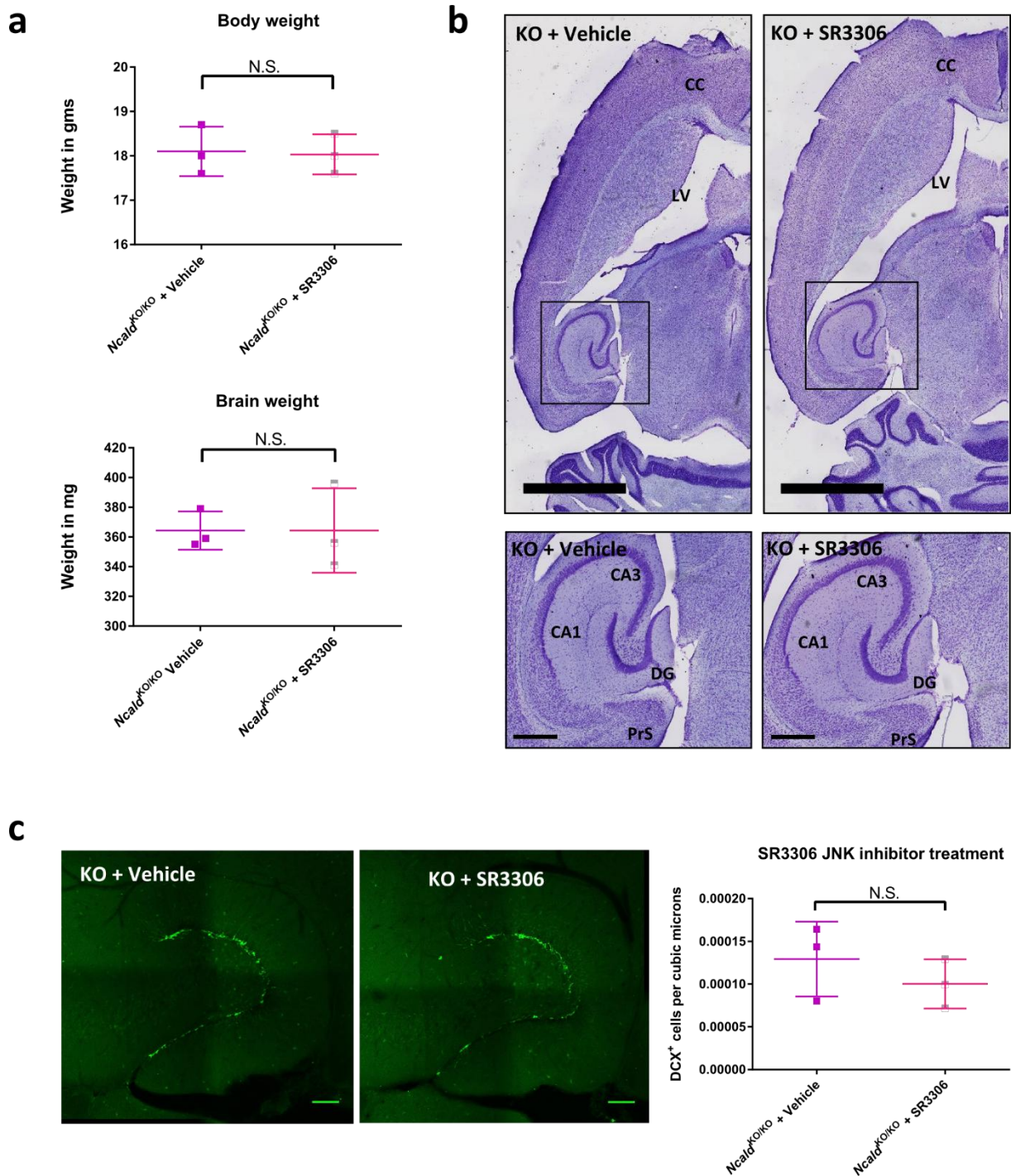


Figure 21 Transient inhibition of JNK does not ameliorate adult neurogenesis in *Ncald*^{KO/KO}. (a) Graph representing the body and brain weight of vehicle treated and SR3306 treated *Ncald*^{KO/KO} animals. SR3306 (JNK inhibitor) treated *Ncald*^{KO/KO} animals did not show any improvement in body or brain weight; N=3. (b) Representative nissl staining of brain sections from vehicle treated and SR3306 treated *Ncald*^{KO/KO} animals. SR3306 (JNK inhibitor) treated *Ncald*^{KO/KO} animals displayed similar defects in hippocampus and lateral ventricles as that of vehicle-treated animals; N =3. (c) Representative DCX immunostaining of brain sections from vehicle-treated and SR3306 treated *Ncald*^{KO/KO} animals. Graph representing SR3306 (JNK inhibitor) treated *Ncald*^{KO/KO} animals displayed similar DCX⁺ cell density as that of vehicle-treated animals; N=3; scale bar 100 μ m. Quantification depicts mean values \pm SD; unpaired two-tailed student's t-test; N.S. = non-significant.

3.3.5 pJNK is not altered in *Ncald* knockout spinal cord

Some studies have reported significant upregulation in pJNK levels in SMA spinal cord (Genabai et al., 2015; Ahmad et al., 2016). Therefore, we also immunoprecipitated the spinal cord lysates from wildtype and *Ncald*^{KO/KO} animals with NCALD antibodies similar to the brain lysate. Further analysis of IP samples with the mass spectrometry also remained the same as that of brain samples (This part of work was performed by Dr. Seyyedmohsen Hosseinibarkooie, postdoc in AG Wirth). Interestingly, spinal cord mass spectrometry analysis corroborated the NCALD interaction with the MAP3K10, therefore we analysed the pJNK level in the *Ncald*^{KO/KO} spinal cord, but did not find any significant changes compared to control samples (Figure 22a).

a

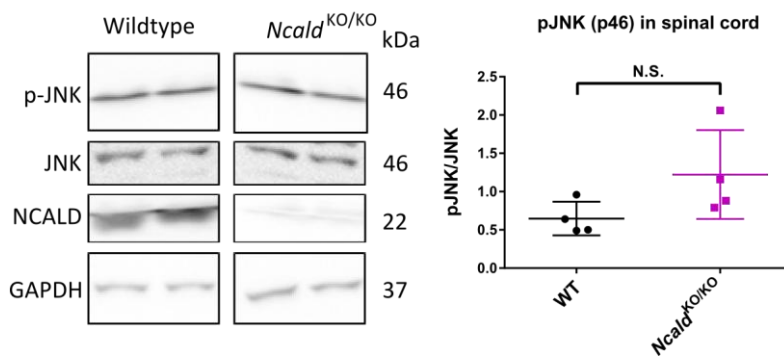


Figure 22 *Ncald*^{KO/KO} spinal cord do not show increased pJNK levels. (a) Representative western blot showing the pJNK levels in *Ncald*^{KO/KO} and wildtype samples. Graph representing the quantitative analysis of the western blot; N=4. Quantification depicts mean values \pm SD; unpaired two-tailed student's t-test; N.S. = non-significant.

3.3.6 RNA sequencing and transcriptomics of *Ncald*^{KO/KO} samples

We further investigated possible changes in physiological gene expression profile upon *Ncald* deletion by analysing the transcriptome of *Ncald*^{KO/KO} animals. Hippocampus, cortex and spinal cord tissues were isolated from the *Ncald*^{KO/KO} and wildtype animals. We used 5 females and 5 males from each genotype. We isolated RNA using the Qiagen kit for high quality RNA purification. Our RNA samples were sequenced in collaboration by the deCODE genetics (Iceland) and the raw data was eventually acquired.

Next part of this experiment was done by Eike Strathmann, a PhD student at AG Wirth. The raw RNA sequencing data was analysed using Kallisto, an open source software. We first analysed the difference between male and female samples within the same tissue type. However, this analysis did not report any unexpected genes with significant differential

expression, but only the genes from sex chromosomes. Therefore, for further analysis we pooled the data obtained from males and females for *Ncald*^{KO/KO} and wildtype samples for each tissue type. We then analysed the raw data for genes that show significant differential expression change (either positively or negatively) upon *Ncald* deletion in each tissue by comparing the pooled *Ncald*^{KO/KO} samples to pooled wildtype samples. We found significant differential expression of 8 genes in hippocampus, 69 genes in spinal cord samples and 371 genes in cortex samples. Unfortunately, during the collection of cortex tissue the limit of 30 mg tissue weight for RNA isolation kit was not known and hence whole cortex tissue was collected, which was much heavier than 30 mg. Consequently, during the RNA isolation only 1/3 of the frozen cortex tissue was used and hence there was no specificity of the sub regions of cortex which were used for analysis. The extremely long list in case of cortex samples could be a result be of this variability within the samples. However, principle component analysis of our transcriptome data revealed three distinct data sets for each tissue thereby reporting the credibility of our samples.

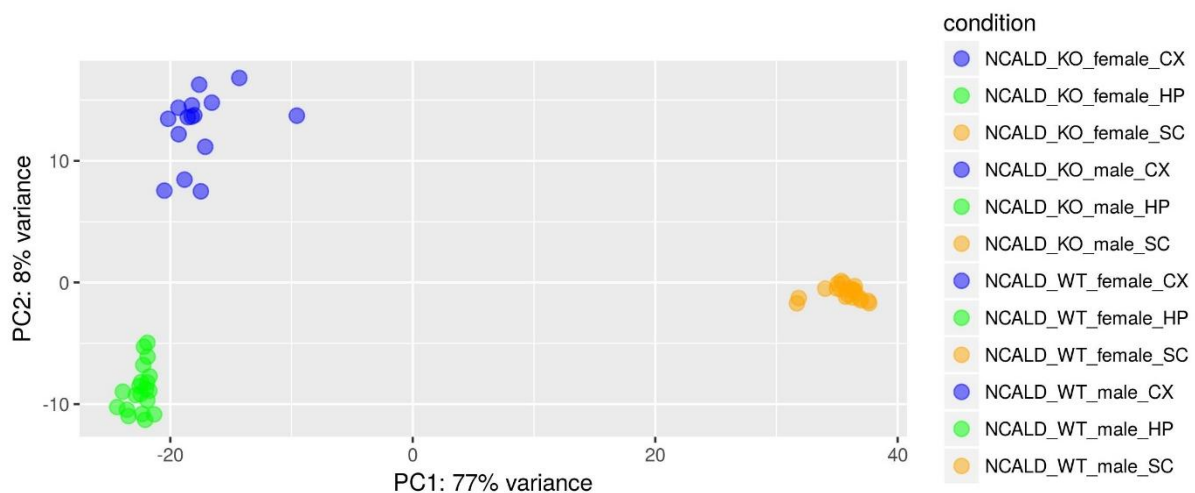


Figure 23 Principle component analysis of transcriptome data from different tissue samples Hippocampus, cortex and spinal cord each tissue showed distinct groups of similarities within each tissue type.

To further pin down interesting candidates for our future investigations, we analysed our data sets for genes which significantly correlate or anti-correlate with expression of the *Ncald*. We found 4 significantly differentially expressed genes in hippocampus, 132 genes in cortex and 19 genes in spinal cord samples in addition to *Ncald* (Appendix Table 7, 8, 9). We also analysed our list of genes based on their annotation in the Kyoto Encyclopedia of Genes and Genomes (KEGG) database for pathway analysis. Details of certain interesting genes and pathways are listed in discussion section in later part of this thesis.

3.4 Characterization of *Ncald*^{KO/WT} animals

NCALD reduction is beneficial on the SMA background and can ameliorate various SMA symptoms, therefore, NCALD reduction has been proposed as a combinatorial therapy option in SMA (Riessland et al., 2017). As mentioned earlier, one of the aims of this thesis was to investigate any possible physiological defects that may arise due to half reduction of NCALD. Taking into account all the physiological defects that we observed in *Ncald*^{KO/KO} animals, we analysed the *Ncald*^{KO/WT} animals specifically for these defects.

3.4.1 *Ncald*^{KO/WT} animals did not exhibit any severe physiological defects

Considering all the phenotypes observed in the *Ncald*^{KO/KO} animals and their brain, we then analysed *Ncald*^{KO/WT} animals. We first quantified the body weight of *Ncald*^{KO/WT} animals, although they showed a strong tendency to weigh less than wildtype animals, *Ncald*^{KO/WT} did not vary significantly in their body weight (Figure 24a). Neither did the brain from *Ncald*^{KO/WT} animals show any significant difference in their weight. Next, we analysed the morphology of adult *Ncald*^{KO/WT} brain in comparison to their wildtype littermates (Figure 24b). However, we did not find significant changes in the lateral ventricles, corpus callosum, cortex or hippocampus, the regions which showed defects in the *Ncald*^{KO/KO} brain (Figure 24c).

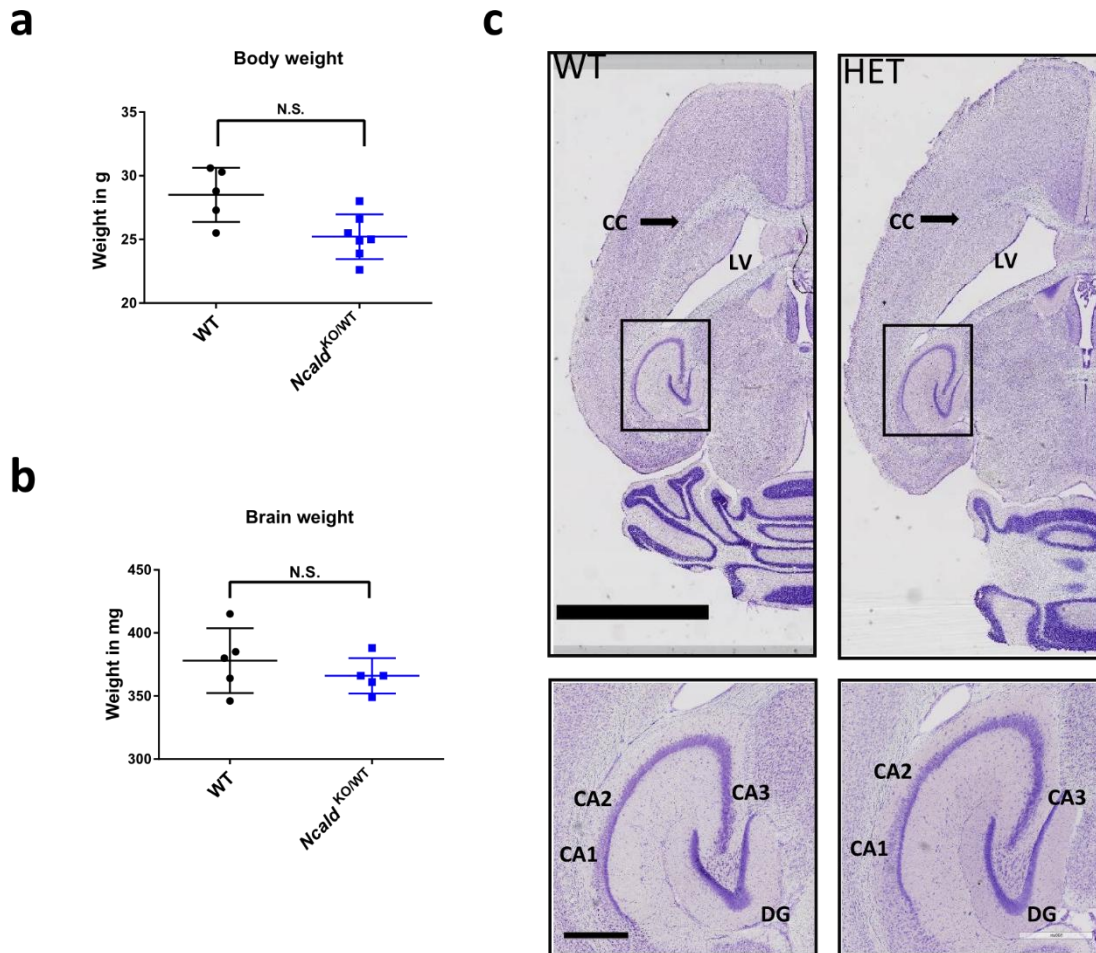


Figure 24 *Ncald*^{KO/WT} animals do not show any severe morphological defects.

(a) Graph representing a strong tendency in *Ncald*^{KO/WT} animal body weight to weigh less, however it was not significant; N=5,6. (b) Graph representing no significant changes in the brain weight; N=5. (c) Representative nissl staining images of *Ncald*^{KO/WT} and wildtype brain section, showing no significant morphological changes; N=4; scale bar 3 mm and 500 μ m (magnified inset). Quantification depicts mean values \pm SD; unpaired two-tailed student's t-test; N.S. = non-significant.

Furthermore, we analysed the DCX⁺ cell density in the *Ncald*^{KO/WT} brain and found no significant alteration compared to controls (Figure 25a). However, the DCX⁺ cells in *Ncald*^{KO/WT} brain showed the tangential migration and loss in the dendritic branching similar to *Ncald*^{KO/KO} (Figure 25a). Following this we analysed the pJNK level and found that there were no significant changes in the *Ncald*^{KO/WT} brain compared to their littermates (Figure 25b).

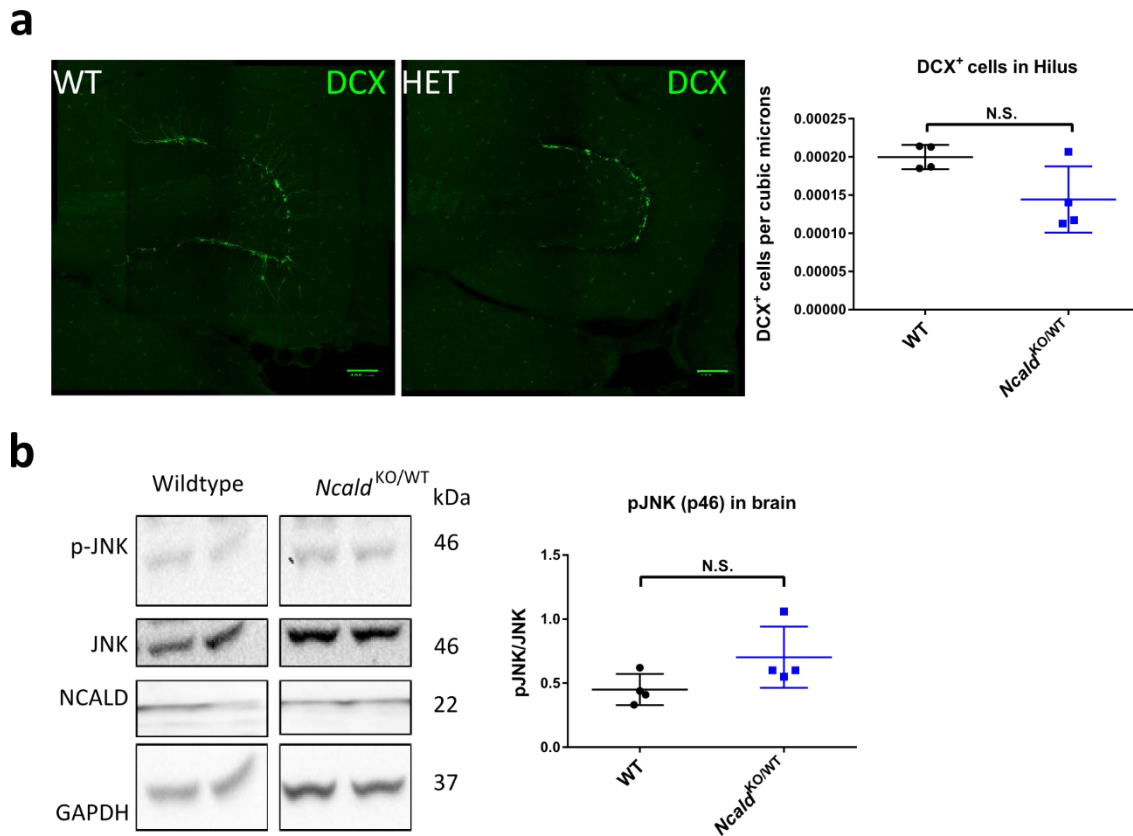


Figure 25 DCX⁺ adult born neuron density is not significantly altered in *Ncald*^{KO/WT} animals. (a) Representative DCX immunostaining of *Ncald*^{KO/WT} and wildtype hippocampus. Graph representing no significant difference in the DCX⁺ cell density in *Ncald*^{KO/WT} and wildtype brain; N=4; scale bar 100 μ m. (b) Representative western blot showing the pJNK levels in *Ncald*^{KO/WT} and wildtype brain. Graph representing no significant difference in the pJNK levels in *Ncald*^{KO/WT} and wildtype brain; N=4. Quantification depicts mean values \pm SD; unpaired two-tailed student's t-test; N.S. = non-significant.

3.4.2 *Ncald*^{KO/WT} and *Ncald*^{KO/KO} motor neurons show elongated axons and increased branching

We have already shown on SMA background that *Ncald*^{KO/WT} genotype positively affects the axonal length and branching (Riessland et al., 2017). Therefore we analysed the cultured wildtype, *Ncald*^{KO/WT} and *Ncald*^{KO/KO} motor neurons at DIV 4. We chose an early time point in culture as the older cultured neurons have very long axons which complicates the axonal analysis. We stained MNs with ChAT, a MN specific marker (MacDonald et al., 2003) and TAU, a microtubule binding protein, to mark the overall morphology of MNs (Bradke and Dotti, 2000). Interestingly, we found longer axonal length and increased branching in both *Ncald*^{KO/WT} and *Ncald*^{KO/KO} motor neurons compared to controls (Figure 26a). This finding supported that not only under SMA condition but also physiologically NCALD reduction acts positively on motor neuron axonal growth and branching.

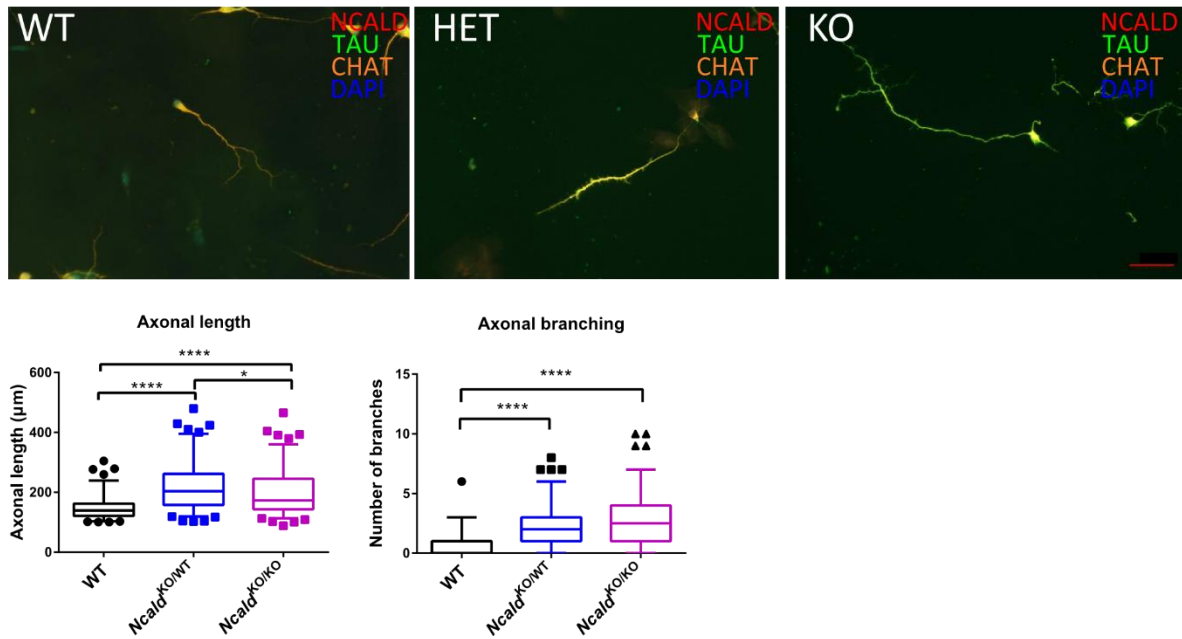
a

Figure 26 *Ncald*^{KO/KO} and *Ncald*^{KO/WT} motor neurons have elongated axons.

(a) Representative images of MN stained with TAU, CHAT, NCALD and DAPI (for nuclear staining) from wildtype, *Ncald*^{KO/KO} and *Ncald*^{KO/WT} cultures. Graph representing quantitative analysis and significant increase in the axonal length and branching; scale bar 20 µm; N= 108, 104, 105 (from 3 embryos each); P< 0.001. Each box plot covered 25-75% values, line represents median and class interval set at <5% and >95%.

3.4.3 *Ncald*^{KO/WT} and *Ncald*^{KO/KO} animals perform well in the motoric test

As crossbreeding of *Ncald*^{KO/WT} animals on the mild SMA background could ameliorate motor function in SMA background such as muscle strength (Riessland et al., 2017), we analysed motor performance of the *Ncald*^{KO/WT} and *Ncald*^{KO/KO} animals by using muscular phenotypic tests such as Rotarod (Brooks and Dunnett, 2009). Rotarod is motor coordination and balance test, where the animals are placed on a rotating rod, specifically designed to test rodent models of neurological deficits (Dunham and Miya, 1957). From our initial data we could see that *Ncald*^{KO/WT} and *Ncald*^{KO/KO} animals spent almost equal amount of time on the rotarod and performed not significantly different than the wildtype animals (Figure 27a,b). This data suggest NCALD reduction or deletion does not have any significant impact on the physiological motor functions.

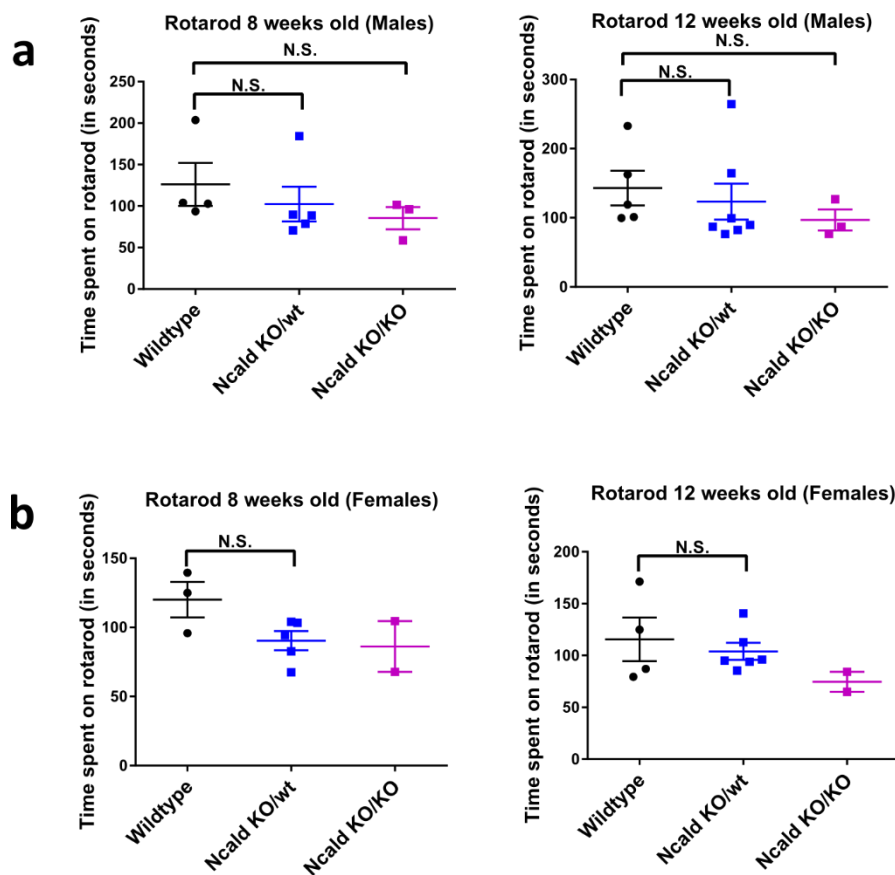


Figure 27 *Ncald*^{KO/KO} and *Ncald*^{KO/WT} animals do not show any changes in motor abilities. (a) Graphs representing time spent by 8 week- old and 12 week- old wildtype, *Ncald*^{KO/KO} and *Ncald*^{KO/WT} males at running on the rotating rod; N = 4, 5, 3 for wildtype, *Ncald*^{KO/KO} and *Ncald*^{KO/WT} respectively. (b) Graphs representing time spent by 8 week- old and 12 week- old wildtype, *Ncald*^{KO/KO} and *Ncald*^{KO/WT} females at running on the rotating rod; N = 4, 5, 2 for wildtype, *Ncald*^{KO/KO} and *Ncald*^{KO/WT} respectively. Quantification depicts mean values \pm SD; unpaired two-tailed student's t-test; N.S. = non-significant.

Taken together, *Ncald*^{KO/WT} animals did not show any severe defects in their brain morphology or adult neurogenesis. Nevertheless, the MN axon length for these animals increased beyond the wildtype control. Conclusively, the reduction of NCALD could most likely be safe therapeutic option for SMA.

4 Discussion

4.1 NCALD in postnatal brain development and maturation

NCALD was almost absent at the embryonic stage whereas the NCALD levels increase dramatically from P1 to P14. This finding suggested that NCALD function is most relevant in postnatal development of the mouse brain.

The postnatal brain development and maturation can be broadly classified into five major processes; 1) Differential expression of molecular attractors and repellents which guide axonal and dendritic projections, 2) Synaptogenesis and facilitated neurotransmission which establishes a dynamic (subjected to processes of refinement and pruning) neuronal network responsive to experiences. 3) Myelination of axons to increase the efficiency and speed to neural communications. 4) Gross structural changes in certain regions like cortex and hippocampus 5) Neurogenesis although diminished with age but still continues throughout the postnatal, adolescence and adult hood (Zelazo et al., 2013). Our finding about NCALD being specifically enhanced since the postnatal stages (P10), marked the importance of further research in NCALD function in various processes that shape the postnatal development and maturation of brain. We would further assemble all the findings on NCALD related to above listed postnatal processes in brain maturation, to clearly draw the future research map on NCALD.

4.1.1 Axonal and dendritic projections

NCALD has been shown to accumulate at the axonal and dendritic growth cones of hippocampal neurons as well as in motor neurons (Yamatani et al., 2010; Riessland et al., 2017). Interestingly, overexpression of NCALD significantly reduced axonal branching in hippocampal neurons (Yamatani et al., 2010), moreover the reduction in NCALD in motor neurons lead to a significant increase in axonal length and branching (Figure 26). Altogether, these results point towards the physiological role of NCALD in axon growth regulation.

4.1.2 Synaptogenesis and neurotransmission

Previous findings show the presence of NCALD in fraction of neurotransmission related proteins (Vercauteren et al., 2007) as well as in synaptosomal fractions (Zareba-Kozioł et al., 2014). Moreover, our previously published results emphasized the role of NCALD in endocytosis which also plays a fundamental role in synaptic functions (Puthenveedu et al., 2007; Riessland et al., 2017). The current study corroborated these findings by reporting the presence of NCALD in the inhibitory as well as excitatory synaptic punctas (Figure 8). We

found that NCALD is present in certain VGLUT1 positive excitatory synapses as well as in certain VGAT positive inhibitory synapses. Intriguingly, NCALD was not present in all the excitatory or inhibitory synapses, which implies the functional specificity of NCALD within the subtypes of synapses.

Furthermore, NCALD has been implied in the Alzheimer's, which, since last decade is being accepted primarily as a synaptic disease. Although our results in regard to hallmarks of neuronal degeneration in *Ncald*^{KO/KO} animals were negative, they did not annul the redundant contribution of NCALD in neuroprotective function (Figure 11). Taken together, these findings affirm the significance of further in-depth analysis of NCALD synaptic functions.

4.1.3 Myelination

We found that although absence of NCALD significantly reduced the myelination (Figure 16), NCALD was not present in the oligodendrocyte soma (glia cell type which generates myelin) (Figure 17) indicating the possibility that certain neuronal function of NCALD may impact myelination. Interestingly, Neurotrophin nerve growth factor (NGF) released from axons acts as a potent regulator of signals that determine the extent of myelination of neurons by regulating their receptivity (Chan et al., 2004). Moreover, role of calcium signaling and neurotransmission in regulation of local myelination on electrically active axons of certain neuronal subtypes has been reported in previous studies (Wake et al., 2011; Wake et al., 2015; Koudelka et al., 2016). However, this is the first study showing a link between NCALD, a neuronal calcium sensor and myelination. These findings also support the reports on neuronal events (release of growth factors or activity) controlled by neuronal proteins, independent of oligodendrocyte activity, can regulate myelination (Miller, 2018).

Furthermore, disturbed white matter integrity, a measure of myelination is strongly linked with schizophrenia as the diffusion tensor imaging of schizophrenia patients brain show disruption in white matter structures (Friedman et al., 2008). Additionally, many myelination-related genes have also been associated with schizophrenia (Chavarría-Siles et al., 2016). Further research of the defects in myelination observed in *Ncald*^{KO/KO} brain and may enhance our understanding of how neuronal calcium sensors which are implicated in schizophrenia pathology (Ripke et al., 2013), functions at molecular level. Moreover, the association of NCALD reduction with schizophrenia (Vercauteren et al., 2007) strengthens the credibility of these further investigations.

4.2 Relevance of NCALD in presubiculum

Although abundance of NCALD in various brain regions have been reported earlier, this is the first study which showed the high abundance of NCALD in presubiculum, part of the parahippocampal region. Presubiculum is composed of head direction cells (53.7%), grid cells (12.8%) and border cells (9%) (Boccarda et al., 2010) that project to various other brain regions relevant for spatial orientation namely medial entorhinal cortex and lateral mammillary nucleus (Huang et al., 2017). Head-direction cells are activated when animals face a particular direction, irrespective of their location and activity; grid cells are neurons which fire periodically and are place-modulated; whereas border cells fire whenever the animal approach any boundary (Boccarda et al., 2010). Therefore, presubiculum is a key brain region which encodes spatial information (Simonnet et al., 2013). Interestingly, we observed a distinct reduction in presubiculum of adult *Ncald*^{KO/KO} animals, which requires further quantification for confirmation (Figure 10). Considering the key role that presubiculum plays in encoding spatial information, it will be very relevant to further investigate the spatial learning and memory in *Ncald*^{KO/KO} animals. One of the well-established spatial learning test is water maze test (D'Hooge and De Deyn, 2001), however considering that IMPC reported anxiety like behaviour in the *Ncald*^{KO/KO} animals, an exposure to water may further contribute to increased anxiety in these animals. Therefore, a spatial learning test which does not involve water exposure would be preferential. One such test is the Barnes maze test, which makes use of distal visual cues placed on a circular platform to assess the spatial memory of the animal (Barnes, 1979).

Moreover, presubiculum has been a region of interest in the Alzheimer's disease. Early studies in Alzheimer's disease found that presubiculum incurred significantly high amount of amyloid deposits, hallmark of Alzheimer's pathology, quite early in the disease progression (Kalus et al., 1989). Hence presubiculum was considered as one of the most severely affected regions in Alzheimer's disease (Carlesimo et al., 2015). However a recent study in the field has altered this consideration, by showing that the amyloid deposits seen in the presubiculum of Alzheimer's patients remain in 'lake like' morphology rather than in form of pathological 'amyloid beta plaques'. Furthermore they showed that presubiculum is comparatively protected than other severely affected surrounding brain regions (Murray et al., 2018). These findings suggested a detailed analysis of presubiculum region as well as the factors which are specific to presubiculum may provide essential inputs in development of protective therapies for Alzheimer's disease. As mentioned earlier significant downregulation of NCALD has been reported in Alzheimer's disease (Miller et al., 2013b). Taking this in account with the remarkably specific and high abundance of NCALD in

presubiculum reported in this study (Figure 8), a further investigation of NCALD into the physiology and pathology of presubiculum could deepen our understanding of protective therapies for Alzheimer's disease.

4.3 Adult neurogenesis, JNK activation and NCALD

Since the initial finding of adult neurogenesis, one of the primary question which remained is, identification of the factors that regulate the proliferation, migration and survival of these rare adult born neurons (Gould and Cameron, 1996). Interestingly, stress and anxiety are major factors which negatively regulates adult neurogenesis (Gould et al., 1998; Tanapat et al., 1998). Stress has also been associated with lower hippocampal volume and reduced adult neurogenesis (Czeh et al., 2001). Furthermore, it has been shown that adult born granule cells can inhibit the mature granule cells in the ventral dentate gyrus thereby increasing the resilience to stress as well as can protect against anxiogenic defects in mouse model for stress (Anacker et al., 2018). Moreover, adult neurogenesis is a crucial determinant of the effect of the anti-depressant therapies and therefore strategies to increase the adult neurogenesis have been proposed as therapeutic options against stress and anxiety (Santarelli et al., 2003).

We found significantly reduced amount of DCX positive neurons in the adult *Ncald*^{KO/KO} hippocampus (Figure 14), which is a hallmark for defects in adult neurogenesis (Balthazart and Ball, 2014). Defects in adult neurogenesis have been linked not only to stress and anxiety but also to short term spatial memory (Denis-Donini et al., 2008). Intriguingly, the behavioural analysis of *Ncald*^{KO/KO} animals at the IMPC showed significant increase in their anxiety like behaviours (International Mouse Phenotype Consortium, 2016). Therefore, a detailed behavioral analysis of *Ncald*^{KO/KO} animals, could further provide evidence for functions of NCALD in stress, anxiety and short term memory and could potentially unravel the mechanism downstream to adult neurogenesis which drives these behavioural deficits.

Adult neurogenesis is known to be mechanistically regulated by electrical activity and intracellular calcium elevations which lead to finer gene expression changes (Spitzer, 2006). Interestingly, detailed information is available on how calcium regulates the neurogenesis during the pre/perinatal development of brain (Toth et al., 2016). However there is a prominent lack of data available on general factors that support specific function of calcium in adult neurogenesis. Our finding which links the loss of NCALD, a neuronal calcium sensor with a loss of DCX positive specific adult born neuronal cell type invigorates further research in understanding the function of calcium in the context of adult neurogenesis.

Adult neurogenesis can also be regulated by the JNK pathway (Mohammad et al., 2017). JNK1 knockout mice showed enhanced levels of DCX positive cells and treatment with JNK inhibitor also significantly increased DCX positive cells and induced anxiolytic response. These findings by Mohammad et al were the first ones to show involvement of JNK in the mechanism of adult neurogenesis. Interestingly, we found NCALD interacts with MAP3K10 (an upstream kinase in JNK pathway) (Figure 18) and *Ncald*^{KO/KO} brain show significantly elevated levels of phosphorylated JNKs (Figure 19). This finding along with the previous results showing loss of DCX positive neurons in *Ncald*^{KO/KO} hippocampus (Figure 14), is the second link between JNK and adult neurogenesis. Our results are in line with the previous findings as we show that elevated pJNK level in *Ncald*^{KO/KO} brain are paralleled by loss in DCX positive neurons and the previous study has shown that inhibition of JNK can increase the DCX positive cells in the dentate gyrus (Mohammad et al., 2017). We further attempted to investigate the effect of transient JNK inhibition on DCX positive cells in *Ncald*^{KO/KO} hippocampus. However, according to our preliminary results we did not see any increase in the DCX positive cells or improvement of any other morphological defects in the *Ncald*^{KO/KO} animal brains (Figure 21) transiently treated for six days with SR3306, a JNK inhibitor (Chambers et al., 2011). This treatment protocol needs further substantial optimization, to determine the effect of JNK inhibition in *Ncald*^{KO/KO} hippocampus, as discussed in the future outlook section.

Adult as well as juvenile born granule cells at dentate gyrus (DG) undergo four consecutive stages of proliferation, differentiation, maturation and survival (Goncalves et al., 2016). These stages are marked by differential genetic expression and has been clustered together via single RNA sequencing (Hochgerner et al., 2018). Expression pattern of *Ncald* within these clusters clearly show that *Ncald* expression is very low at proliferative stages of radial glia like cells and neuroblasts whereas significantly higher in the differentiated immature granule cells, pyramidal cells and GABAergic interneurons, CA3 pyramidal cells (Linarsson lab, 2018) (**Error! Reference source not found.**). Our results from analysis of *Ncald*^{KO/KO} DG particularly showed a reduction of DCX positive cells (Figure 14) which belong into the cluster of immature granule cells (Couillard-Despres et al., 2005). Therefore study of NCALD abundance and function through the various maturation stages of adult born neurons can delineate the mechanisms involved in the process. Another important aspect of adult neurogenesis is the integration of new born neurons into the granule cell layer (Toni and Schinder, 2015). Extension of dendritic arbours from the newly generated DCX positive neurons grow into the granule cell layer and establishes the functional integration of these neurons into granule cell layer (Rosenzweig and Wojtowicz, 2011). Moreover, inhibition of

JNK can significantly increase the dendritic innervations of DCX positive neurons (Mohammad et al., 2017).

***Ncald* expression in differentiation and maturation of DG cells**

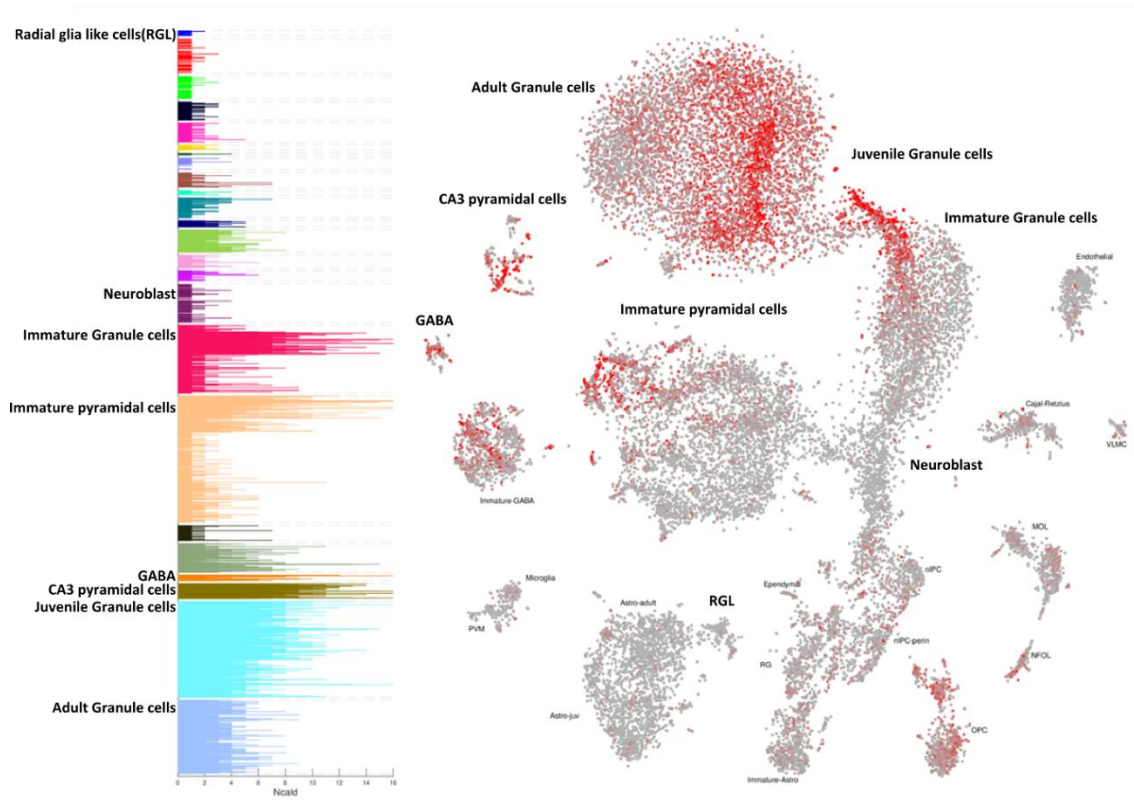


Figure 28 *Ncald* expression pattern in different clusters of dentate gyrus cells. *Ncald* expression is very low during the differentiating neuronal population like radial glia like cells and neuroblasts whereas its expression is highest in the differentiated immature granule cells, pyramidal cells and GABAergic interneurons. *Ncald* has moderate expression in the juvenile and adult granule cells. Adapted from (Linarsson lab, 2018)

We observed loss of these dendritic innervations in DCX positive cells present in the *Ncald*^{KO/KO} DG (Figure 14), which therefore critically questions the functionality of these neurons.

Lastly, transient increase in the JNK levels is observed during the embryonic differentiation and migration of cortical neurons (Hirai et al., 2002). This increase has been associated with the retardation of the radial migration and promotion of tangential migration. As we also observed aberrant tangential migration of DCX positive neurons in the *Ncald*^{KO/KO} DG (Figure 14) and an increase in pJNK (Figure 19), these two findings can also be well connected. Thus, further research on the plausible role of JNK in tangential migration of *Ncald*^{KO/KO} neurons can contribute to our understanding of why and how the neurons switch migration patterns.

4.4 NCALD reduction in SMA

Although recent advances in the field of SMA therapeutics have shown many positive effects, there still remains a demand for complete cure of SMA (Talbot and Tizzano, 2017). Currently, all the approved therapies for SMA focus on enhancing the SMN protein levels, however there are limitations on the amount of SMN protein that can be enhanced via these methods (Sumner and Crawford, 2018). Therefore a combinatorial therapy of SMN dependent and SMN independent strategies is the need of the hour in SMA therapy.

NCALD reduction ameliorates various SMA symptoms like NMJ maturation, motor neurons (MN) inputs, MN axonal length in severe SMA mouse model (Riessland et al., 2017). As the severe SMA mouse suffers through multi-organ failure, a milder SMA model was produced with an early postnatal (P1) injection of SMN-ASO (Nusinersen). NCALD reduction in the mild SMA model significantly improved synaptic endocytosis and motoric function, along with above mentioned symptoms (Riessland et al., 2017). Moreover, analysis of MN axons in SMA zebrafish (generated by *smn* morpholino injections) and motor reflexes in SMA *C.elegans* (lacking *smn-1*) also showed the protective effect of NCALD reduction. These findings established that NCALD reduction can significantly augment the increase in SMN levels in ameliorating SMA symptoms and led to proposal of NCALD reduction as an SMA therapeutic option.

However, significantly low NCALD levels have been related to Alzheimer's a neurodegenerative disease (Shimohama et al., 1996; Miller et al., 2013b) as well as Schizophrenia, a neurodevelopmental disease (Vercauteren et al., 2007). Therefore, the reduction of NCALD along with being beneficial in context of SMA, may additionally have potential physiological side effects in the brain. Hence, in this study we first studied general hallmarks of both neurodegeneration and neurodevelopment upon *Ncald* deletion in *Ncald*^{KO/KO} brain and then specifically analysed these phenotypes in *Ncald*^{KO/WT} brain, as a model of the proposed *Ncald* reduction for SMA therapeutics.

We found no significant changes in the body and brain weight of *Ncald*^{KO/WT} animals. Moreover we did not find any significant changes in pJNK level or the DCX positive cell density at DG of *Ncald*^{KO/WT} animals. Nevertheless, we observed loss in dendritic innervations of the DCX positive cells, which points towards a possible dysfunctionality of these neurons in *Ncald*^{KO/WT} DG and raises concern towards the safety of *Ncald* reduction in SMA therapeutics.

However there are few points which needs to be considered in context of how well the *Ncald*^{KO/WT} brain model the *Ncald* reduction proposed for SMA therapeutics. First, the reduction in the *Ncald* levels for SMA therapy are required only during the initial period of

CNS development, which accounts for the generation and maturation of NMJs. Second, we are currently studying the effect of decrease in *Ncald* levels using ASOs against *Ncald* gene in combination with SMN ASO at P1 to see the combinatorial effect and precise amount of NCALD reduction which can protect the SMA phenotype. Transient *Ncald* reduction by ASO injections at P1 which rescues SMA phenotype, does not sustain the reduction of *Ncald* until adulthood (at 3 months or 6 months) (unpublished data from AG Wirth). Interestingly the severe effects of NCALD deletion/reduction on DCX positive cells were not observed in the initial development of the brain (P14 and P30) but only in adult brain (4 month-old). Therefore the transient *Ncald* reduction in early development most likely would not have the same effect as sustained reduction of *Ncald* in case of *Ncald*^{KO/WT} animals. Nevertheless, this study reported the potential physiological processes to be analysed in order to test the safety of *Ncald* reduction in further studies.

4.5 NCALD in neurodevelopmental disorders

NCALD is linked to multiple neurodevelopmental disorders like schizophrenia (Vercauteren et al., 2007), autism (Ben-David et al., 2011) and bipolar disorder (Xu et al., 2014). Both autism (human patients) and schizophrenia (mouse model) brain show certain morphological defects like enlargement of lateral ventricles (Pletnikov et al., 2008; Movsas et al., 2013). We observed a similar enlargement of lateral ventricle in the *Ncald*^{KO/KO} mice brain, which increased from P14 until 4 months, however did not exacerbate at 18 months. These results pointed towards a defect in the maturation of brain until adulthood or a possible neurodegeneration which did not progress with aging.

Furthermore along with observable changes in the shape and volume of hippocampus, we also found significant decrease in the sub-granular zone length in the *Ncald*^{KO/KO} DG. The physiological shape and overall morphology of hippocampus has been implicated in the maintenance of cognitive functions (Smith et al., 2012; Voineskos et al., 2015). Schizophrenia is marked with smaller hippocampal volume (Sim et al., 2006), additionally various neurodevelopmental disorders including schizophrenia are characterized by severely impaired cognitive functions (Leekam, 2016; Tripathi et al., 2018). Accordingly *Ncald*^{KO/KO} animals can be further analysed for all the major behavioural and morphological phenotypes of neurodevelopmental disorders.

Most of the neurodevelopmental disorders (NDs) like bipolar disorder, autism and schizophrenia are genetically complex and therefore understanding the molecular basis of these diseases using a model organism has been a challenge (Wilson and Terry, 2010).

However, de novo single gene mutations, SNPs or chromosomal deletions found in the genome association studies of NDs patients often reveal causative genes. Additionally, targeted mutations in causative genes has been used to generate mouse models as a translational research tool for various NDs (Crawley, 2012). Interestingly, not only the NCALD abundance was significantly low in schizophrenia rat model but also certain SNPs in *Ncald* are linked to autism and bipolar disorder. Moreover, phenotypic data available at the International Mouse Phenotyping Consortium platform indicate that *Ncald*^{KO/KO} mice are hyperactive and anxious and exhibit severe reduction of body mass (International Mouse Phenotype Consortium, 2016). Henceforth, a detailed study of NCALD function in pathophysiology of schizophrenia and autism, as well as a comprehensive analysis of cognitive behaviour in *Ncald*^{KO/KO} animals have a potential to reveal a novel disease mouse model for neurodevelopmental disorders with subtle behavioural symptoms, thereby improving our understanding of such disorders.

4.6 Interesting candidates and pathways in *Ncald*^{KO/KO} transcriptome analysis

RNA transcriptome analysis comparing *Ncald*^{KO/KO} and wildtype control was performed for hippocampus, cortex and spinal cord tissue. Significant differentially expressed genes were selected and their correlation coefficient with *Ncald* was calculated. Full list of proteins is included in the appendix (**Appendix Table 7****Appendix Table 8****Appendix Table 9**) contains 4 genes in hippocampus, 132 genes in cortex and 19 genes in spinal cord. We discuss physiological functions of certain proteins with minimum value of log₂ fold change as 0.3 (or -0.3) which is equivalent to one- fold increase, as smaller values indicate less significance.

In hippocampus we obtained 3 genes in total with above listed criteria. *Lrp2* was the only gene negatively correlated to *Ncald*, *Lrp2* encodes Low-Density Lipoprotein Receptor-Related Protein 2, an endocytic receptor. Interestingly, loss of *Lrp2* has been shown to impair adult neurogenesis in subependymal zone (SEZ) (Gajera et al., 2010). *Lrp2* regulates bone morphogenetic protein (BMP) signaling and plays a crucial role in balancing proliferative and non-proliferative neural stem cell fate determination during embryonic development as well as adult neurogenesis (Choe et al., 2015). Previous studies have reported loss of *Lrp2* does not affect the adult neurogenesis in sub granular zone (Gajera et al., 2010). Considering that we observe an increase in the *Lrp2* expression and defects in DCX positive adult born neurons in hippocampus upon *Ncald* deletion (Figure 14), even if *Lrp2* plays a role in hippocampus, it is most likely via different mode of action than in the cortex. The other two genes *Sema3c* and *Bok* were positively correlated to *Ncald*. *Sema3c* encodes for Semaphorin 3C, an axon growth and guidance molecule whereas *Bok* encodes for Bcl-2 related Ovarian Killer protein. Semaphorin 3C can act as repellent as well as an attractant for

neurons depending upon the different receptor subunits it recruits (Wolman et al., 2004). As we observed a significantly reduced amount of *Sema3c* transcripts in hippocampus of *Ncald*^{KO/KO} hippocampus, it would be interesting to further analyse the effect of NCALD reduction on hippocampal axon length.

In cortex there were 132 genes with filtered criteria, out of which 130 were negatively correlated to *Ncald*. The top 10 negatively correlated genes were *MS4a15*, *Lhx8*, *Gbx1*, *Ntrk1*, *Gpx6*, *Slc10a4*, *Serpina9*, *Isl1*, *Gdnf* and *Chat*. On the other hand, there were only 2 positively correlated genes namely *Tbc1d9b* and *Cbln4*. Among negatively correlated genes, *Ntrk1* encodes neurotrophic tyrosine kinase, receptor, type 1 and a variant in *Ntrk1* is related to defects in white matter (myelin) structures in young adults (Braskie et al., 2012). Moreover, *Ntrk1* is receptor for neurotrophin growth factor (NGF) which is known to negatively regulate myelination (Chan et al., 2004). Therefore, increase in the *Ntrk1* transcript in *Ncald*^{KO/KO} cortex can be associated with the myelination defects observed in the *Ncald*^{KO/KO} brain (Figure 16).

In spinal cord there were 13 genes with filtered criteria, out of which 4 were negatively correlated to *Ncald* namely *Shh*, *Kctd9*, *Rgs4*, *Tmem56* and 9 were positively correlated to *Ncald* namely *Fbln2*, *Ccnb2*, *Ckap2*, *Mybpc 1*, *Cenpa*, *Ogn*, *Cdc25c*, *Rem1* and *Gsx1*. Among the positively correlated genes, *Fbln2* encodes for Fibulin 2 an extracellular matrix protein which has recently been reported to be involved in axon growth repulsion (de Vega et al., 2009; Schaeffer et al., 2018). It functions via enhancing *Sema3A* an axon repellent cue repulsive activity to promote growth cone collapse and regulates spinal nerve organization in developing embryo (Schaeffer et al., 2018). Taken together the significant increase in MN axon length (Figure 26) and significantly low transcripts of *Fbln2* (with axonal growth repulsive function) in *Ncald*^{KO/KO} motor neurons reported in this study, it would be fascinating to further investigate the role of Fibulin 2 in growth of *Ncald*^{KO/KO} motor neurons.

4.7 Future outlook

1) We found that *Ncald*^{KO/KO} DG have significantly low number of DCX positive cells and on other hand we observed a significant increase in pJNK levels in *Ncald*^{KO/KO} brain. As the inhibition of JNK is reported to increase the DCX positive cells in mouse model (Mohammad et al., 2017), we attempted to inhibit the JNK in *Ncald*^{KO/KO} mouse. We used a very basic inhibition strategy of 7 dosage of SR3306, a JNK specific inhibitor via gavage feeding in the young adult (2 month-old) *Ncald*^{KO/KO} animals, but could not see any increase in the DCX positive cell density. Nevertheless, there can be many reasons behind the negative results, some of them are discussed below with alternate strategies for future research.

- I. The amount of SR3306 used was not sufficient to facilitate the increase in the DCX positive neurons, therefore a gradual and permissible increase in the concentration of JNK inhibitor, SR3306 can be designed to further investigate the effects.
- II. SR3306 is not a potent inhibitor for newly synthesised neurons; as the previous studies showing the effect of SR3306 dealt with post mitotic neurons only, it is possible that using any another JNK inhibitor molecule can be an efficient way to inhibit the JNKs in DCX positive neurons.
- III. Treatment period of six days may not be sufficient to observe the difference in the DCX positive cells as differentiation of each precursor cell into mature granule cell takes about 4-6 weeks. DCX expression increases during the maturation phase of these cells from about 2 weeks to 3 week (Snyder et al., 2009). Hence, longer inhibition of JNK for about 4 weeks long might have better effect on the whole process of differentiation including the maturation of DCX cells.
- IV. Another important factor impacting the effectivity of drug is the mode of administration. We administered SR3306 using a gavage method, which has been effective to protect dopaminergic neurons (Crocker et al., 2011). However, it is possible that DCX positive cells in *Ncald*^{KO/KO} brain need distinct effectivity of JNK inhibition for their survival which can be achieved by a more effective mode of administration namely intracerebral mini pump installation. The effectivity of this method has already been published (Mohammad et al., 2017).

2) Currently, we are analysing the effect of NCALD reduction using *Ncald* ASO in the mild SMA model. As perinatally restricted reduction of NCALD in these animals closely mimics the NCALD reduction proposed for SMA therapy, we would also analyse these animals for the major defects observed in *Ncald*^{KO/KO} brain like gross brain morphology, loss of DCX positive cells and elevated pJNK levels.

3) Certain behavioural tests for social and cognitive deficits, short and long term memory, fear and anxiety would add much value to the *Ncald*^{KO/KO} animals as model system for certain subtle but complex cognitive behaviours of neurodevelopmental diseases like schizophrenia.

4) Analysis of axonal length of cultured hippocampal neurons, will give us further insight, whether the effect of NCALD on axon length is restricted to motor neurons or is a general neuronal function of NCALD.

5) Further analysis of endocytosis in the *Ncald*^{KO/KO} hippocampal as well as motor neurons would yield better understanding of NCALD function in the process of endocytosis, as NCALD has been shown to regulate endocytosis in SMA mice (Riessland et al., 2017).

6) Analysis of top candidate proteins from the NCALD mass spectrometry data like Formin-2 (FMN2), Dihydrolipoyl dehydrogenase mitochondrial (DLD) other than MAP3K10 can unravel yet to be identified physiological functions of NCALD. Moreover, analysis of data obtained from the transcriptome sequencing of wildtype and *Ncald*^{KO/KO} animals would also enhance our understanding of NCALD functions.

7) The antibodies available currently against pJNK, including the one used by us, mark all isoforms of all three JNK encoding genes namely JNK1, 2 and 3. Although JNK1 knockout mice show increase in DCX positive cell density, considering that the JNK inhibitor used by Mohammad et al also targets all the JNK isoforms, it will be interesting to further study adult neurogenesis in context of the JNK2 and JNK3 specifically. Especially as JNK3 is specific to hippocampus (Coffey, 2014), JNK3 knockout is definitely an interesting candidate for adult neurogenesis analysis.

5 Materials and methods

5.1 Materials

5.1.1 Laboratory equipment

Analytical balance	AX2202M	Ohaus
Analytical balance (fine scale)	ARJ 120-4M	Kern
Analytical Column	Poroshell EC120	Agilent
Bacterial incubators	Innova 44	New Brunswick Scientific
	Innova 4230	New Brunswick Scientific
Cell incubator	Heracell™ 150	Heraeus
Cell culture hood	Herasafe™ KS 12	Heraeus
Centrifuges	AllegraX22-R	Beckmann Coulter
	Avanti J-20XPI	Beckmann Coulter
	5415R	Eppendorf
	5415D	Eppendorf
	5804	Eppendorf
	Concentrator 5301	Eppendorf
	Galaxy Mini	VWR
Mass spectrometer	Q Exactive plus	Thermo
Microtome	CM3050 S	Leica
Electrophoresis chambers		
Agarose gels	MGV-620T	C.B.S & Scientific
	SGE-020-02	C.B.S & Scientific
	E-H6	Febicon
SDS-PAA gels	Mini-Protean 3 cell	Bio-Rad
Fibre optic light source	KL 1500 LCD	Leica
Gel documentation	ChemiDoc XRS	Bio-Rad
Heating block	HTMR132	HLC Bio Tech
Heating magnetic stirrer	MR 3001	Heidolph
Horizontal shaker	3015	GFL

Homogenizer	Precellys 24	Peqlab
Microscopes		
Slidescanner	Leica SCN400	Leica
Fluorescent	Axiolmager.M2	Zeiss
	Apotome	Zeiss
Confocal	Leica TCS SP8	Leica
Microscope cameras	AxioCam MRm	Zeiss
	AxioCam ICc 1	Zeiss
	AxioCam ERc 5s	Zeiss
Microwave	R-898 (AL)-A	Sharp
Neubauer chamber	1100000	LO Laboroptik Ltd
pH meter	inoLab pH level	WTW
Photometer	BioPhotometer	Eppendorf
Photometer	NanoDrop 1000	Peqlab
Pipettes		
Research	2.5/10/20/200/1000 µl	Eppendorf
Automatic	Research Pro (10/100 µl)	Eppendorf
Pipettor	Easypet	Eppendorf
Power supplies	PowerPac™ Basic/HC/1000	Bio-Rad
Roller mixer	SRT9	Stuart
	RM5	Hartenstein
Thermocyclers	DNAengine Dyad/Tetrad	MJ Research
	C1000 Touch	Bio-Rad
	S1000	Bio-Rad
Tissue processor	ASP300	Leica
UPLC	EASY nLC 1000	Thermo
Vacuum pump	PM126040-026.3	Biometra
Vortex	444-1372	VWR
Water bath	1083	GFL
Water bath	FBC 620	Fischer Brand
Dissection Microscope	Leica M80	Leica

5.1.2 Mouse work equipment

Ear tag applicator	1005-s1	National Band & Tag Co.
Ear tags	1005-1	National Band & Tag Co.
EP-1 Econo pump	7318142	Bio-Rad
Forceps	BD047R	Aeskulap
	FM002R	Aeskulap
	Dumont #55	Fine Science Tools
Friedman-pearson rongeurs	16020-14	Fine Science Tools
Heating pad	76084	Trixie
Injection needles 27 gauge, Ø-A: 0,31 mm, pst 4	HAMI7803-07	Hamilton
Microliter syringe (5 µl)	75 N SYR	Hamilton
Operating scissors	BC 321R	Aeskulap
	BC 341R	Aeskulap
RotaRod	RotaRod advance systems	TSE systems
Student Vannas Spring Scissors	FD 012R	Fine Science Tool

5.1.3 Chemical

If available, chemicals used in this work had the purity grade “pro analysis”.

β-Mercaptoethanol (99%, p.a)	AppliChem
2-Propanol (≥ 99.5%)	AppliChem
Acetone	AppliChem
Agarose	Sigma
Ammonium persulfate	AppliChem
Ampicillin	AppliChem
Bacto Agar	AppliChem
Bovine serum albumin (BSA)	Sigma
Bromophenol blue	AppliChem
Coomassie Brilliant Blue R-250	AppliChem

Dimethyl sulfoxide	Sigma
Doxycycline hyclate	Sigma
Ethanol ($\geq 99.5\%$, p.a.)	AppliChem
Ethidium bromide (1% in H ₂ O)	AppliChem
Ethylenediaminetetracetic acid (EDTA)	AppliChem
Glycerol (86%, p.a.)	AppliChem
Glycine	AppliChem
Hydrochloric acid (37%)	AppliChem
Hydroxymethylaminoethane (Tris)	AppliChem
Hydroxypropyl- β -cyclodextrin	Sigma
Kanamycin	AppliChem
Methanol ($\geq 99.9\%$, p.a.)	AppliChem
Milk powder (low fat)	AppliChem
Mowiol	Sigma
Paraformaldehyde	Fluka
Sodium chloride (p.a.)	AppliChem
Sodium dodecyl sulfate (SDS)	AppliChem
Sucrose	AppliChem
TBE buffer (10x)	AppliChem
Tetramethylethylenediamine (TEMED)	AppliChem
Tissue Tek	Sakura (Hartenstein)
Triton X-100	AppliChem
Trizma base	Sigma
Tryptone (microbiology base)	AppliChem
Tween-20	AppliChem
Water (HPLC grade)	Sigma
Yeast extract (microbiology grade)	AppliChem

5.2 Reagents

5.2.1 Reagents for molecular biology

10x PCR master mix	New England Biolabs
AquaPlus Mix 40% (29:1) Acrylamide	AppliChem
Bradford reagent	AppliChem
Complete Mini Protease Inhibitors	Roche
DNA ladder (100bp/1kb)	Life Technologies
dNTPs	Peqlab
Horse serum	Life Technologies
Page Ruler Prestained Protein Ladder	Thermo Fisher Scientific
PBS (10x)	Roche
Ponceau S	Sigma
Phosphatase Inhibitor	Thermo Fisher Scientific
Restore Western Blot Stripping Buffer	Sigma
RIPA buffer	Sigma
Super Signal West Pico ECL Substrate	Thermo Fisher Scientific

5.2.2 Cell Culture reagents and media

1x PBS Dulbecco, w/o Ca ²⁺ , Mg ²⁺	Life Technologies
B-27 Supplement (50x) (#17540)	Life Technologies
β-mercaptoethanol 1000x (ME) (#31350-010)	Life Technologies
Amphotericin B	Promocell
Brain derived neurotrophic factor (BDNF)	Peprtech
Borate acid	Sigma
Tetra Borate Sodium	Sigma
Ciliary neurotrophic factor (CNTF)	Peprtech
Cytosine beta-D-arabinofuranoside	Sigma
DMEM (+ 4.5 g/L D-Glucose, +L-Glutami +Pyruvate) (#11995-065)	Life Technologies
DNase I (2000 U/ml)	New England Biolabs
DNase I (2000 U/mg)	Sigma
Fetal Calf Serum (FCS)	Biochrom AG
Gelatin (2%)	Sigma

Geneticin (G418-Sulfate)	Life Technologies
Glial cell-line derive neurotrophic factor (GDNF)	Peprotech
Glucose	Sigma
Glutamax	Life Technologies
Hanks's Balanced Salt Solution (HBSS)	Life Technologies
HEPES	Life Technologies
Insulin	Life Technologies
Leukemia inhibitory factor 1000x (LIF)	Millipore
Lipofectamine® 2000	Life Technologies
Minimum Essential Media	Life Technologies
Mitomycin C (MMC)	Sigma
Neurobasal® Medium (1x) (#21103)	Life Technologies
Non-essential amino acids 100x (NEAA)	Life Technologies
OptiMEM® (1x) (#31985)	Life Technologies
Penicillin/Streptomycin	Life Technologies
Poly-D-Lysine	Applichem
Poly-D-Lysine	Millipore
Pansera ES	PAN-Biotech
Sodium Pyruvate	Life Technologies
Transferrin	Merck
Trypsin	Sigma
Trypsin/EDTA	Life Technologies
Trypsin	Worthington

5.2.3 Reagents for molecular biology

Power SYBR Green Master Mix	Thermo Fisher Scientific
PureYield Plasmid Miniprep System	Promega
PureYield Plasmid Midiprep System	Promega
ProFection mammalian transfection system	Promega
RNeasy Mini Kit	QIAGEN
RNase-free DNase I Set	QIAGEN

Platinum Taq DNA Polymerase High Fidelity	Life Technologies
RNase A	Life Technologies

5.2.4 Antibodies

5.2.4.1 Primary antibodies and staining reagents

α - Actin beta, mouse (A5316)	Sigma
α - Adenomatous Polyposis Coli (APC) (OP80)	Merck
α - Choline Acetyltransferase (ChAT), goat (AB144P)	Millipore
α - Doublecortin (DCX) (AB2253)	Merck
α - GAPDH, Rabbit (G9295)	Sigma
α - Glial Fibrillary Acidic Protein (GFAP) (G3893)	Sigma
α - GFP, mouse (ab13970)	Abcam
α - Homeobox protein cut-like 1 (CUX1) (sc-13024)	Santa Cruz
α - c-Jun N-terminal Kinase (JNK) (9252)	Cell Signalling
α - Ki- 67 (ab15580)	Abcam
α - Myelin Basic Protein (MBP) (SMI94)	Covance
α - Mitogen Activated Protein 3 Kinase 10 (MAP3K10)(NBP1-87737)	Novus Biologicals
α - NeuN (EPR12763)	Abcam
α - Neurocalcin delta, rabbit (12925-1-AP)	Proteintech
α - Phosphorylated c-Jun N-terminal Kinase (pJNK) (sc-6254)	Santa Cruz
α - Tau, mouse (sc-390476)	Santa Cruz
α - T- box brain 1 (TBR1) (ab31940)	Abcam
α - Vesicular GABA Transporter (VGAT) (135011)	Synaptic Systems
α - Vesicular Glutamate Transporter 1 (VGLUT1) (131004)	Synaptic Systems

5.2.4.2 Secondary antibodies and staining reagents

HRP-conjugated goat α -mouse IgG	Dianova
HRP-conjugated goat α -rabbit	Cell Signaling
Goat α -mouse Alexa 488 IgG	Thermo Fisher Scientific

Donkey α -rabbit Alexa 488	Thermo Fisher Scientific
Donkey α -goat Alexa 568 IgG	Thermo Fisher Scientific
Goat α -mouse Alexa 568 IgG	Thermo Fisher Scientific

5.2.5 Solutions and media

5.2.5.1 Cell culture media

All cell culture media was stored at 4°C.

Hippocampal neuron culture basic media

Minimum Essential @Medium	1 L
Glucose	5 g
NaHCO ₃	200 mg
Transferrin	100 mg

Hippocampal neuron culture plating media

Hippocampal neuron culture basic media	100 ml
FCS	10 ml
L-Glutamine (200mM)	0.25 ml
Insuline solution	0.2 ml
Pen/Strep	1.1 ml

➔ sterile filtered before use

Hippocampal neuron culture growth media

Hippocampal neuron culture basic media	100 ml
FCS	10 ml
L-Glutamine (200mM)	0.25 ml
B27	2 ml
Pen/Strep	1.1 ml

➔ sterile filtered before use

HBSS solution

Sodium Pyruvate	5 ml
HEPES buffer	5 ml
Pen/Strep	5.1 ml
Commercial HBSS solution	500 ml
→ adjust pH to 7.3-7.4	
→ sterile filtered before use	
<u>Digestion solution</u>	
NaCl (5M)	1.37 ml
KCl (3M)	83 µl
HEPES buffer (1M)	1.25 ml
Na ₂ HPO ₄ (120 mM)	2.9 ml
MilliQ water	to the final volume of 50 ml
→ adjust pH to 7.2	
→ sterile filtered before use	
<u>Dissociation solution</u>	
MgSO ₄ ·7H ₂ O	148 mg
HBSS solution	50 ml
<u>Motor neuron culture media</u>	
Neurobasal®Medium	500 ml
B-27 supplement (50x)	10 ml
L-Glutamine	5 ml
Pen/Strep	7 ml
Amphotericin B	1.25 ml
BDNF	50 ng/ml
CNTF	50 ng/ml
GDNF	50 ng/ml
<u>Motor neuron plating media (for 50 ml)</u>	
DMEM	45 ml
FKS	2.5 ml
Glucose (20%)	1.5 ml

Pen/Strep	0.7 ml
-----------	--------

Amphotericin B	0.15 ml
----------------	---------

→ sterile filtered before use
7.5 g

→ autoclave and store at 4°C

5.2.5.2 Solutions to work with DNA

Tail lysis buffer (pH 7.4, for 500 ml)

EDTA (0.5 M)	5 ml
--------------	------

NaCl (5 M)	20 ml
------------	-------

SDS (20%)	5 ml
-----------	------

Tris/HCl (1 M, pH 8.5)	50 ml
------------------------	-------

Deionized H ₂ O	to the final volume of 500 ml
----------------------------	-------------------------------

→ Proteinase K (200 µg/ml) added freshly before use

TE⁻⁴ buffer (for 100 ml):

Tris (1 M, pH 8.0)	1 ml
--------------------	------

EDTA (0.5 M, pH 8.0)	20 µl
----------------------	-------

Deionized H ₂ O	to the final volume of 100 ml
----------------------------	-------------------------------

→ RNase A (50 µg/ml) added freshly before use

5.2.5.3 Solutions to work with Proteins

Ammonium Persulfate (APS) solution (10%, for 10 ml):

APS	1 g
-----	-----

Deionized H ₂ O	to the final volume of 10 ml
----------------------------	------------------------------

→ aliquoted and stored at -20°C

Blocking solution (6%, for 100 ml)

Milk powder (low fat)	6 g
-----------------------	-----

TBS Tween buffer	to the final volume of 100 ml
------------------	-------------------------------

Electrophoresis buffer (10x, for 1 L)

Trizma® base	30.29 g
--------------	---------

Glycine	144.13 g
SDS	10 g
Deionized H ₂ O	to the final volume of 1 L

Laemmli buffer for SDS page (3x, for 10 ml)

Tris/HCl (1M, pH 6.8)	2.4 ml
Glycerol	3 ml
SDS (20%)	3 ml
Bromophenol blue	6 mg
β-mercaptoethanol	1.6 ml

Separating gel for SDS PAGE (12%, for 10ml)

Deionized H ₂ O	4.85 ml
AquaPlus Mix (39:1) Acrylamide	2.55 ml
Tris (1.5 M, pH 8.8)	2.6 ml
SDS (10%)	0.1 ml
APS (10%)	0.1 ml
TEMED	40 µl

Stacking gel for SDS PAGE (for 4 ml)

Deionized H ₂ O	2.96 ml
AquaPlus Mix (39:1) Acrylamide	0.52 ml
Tris (1 M, pH 6.8)	0.52 ml
SDS (10%)	40 µl
APS (10%)	40 µl
TEMED	4 µl

TBS Tween buffer (for 5 L)

Tris (20 mM)	12.1 g
NaCl (137 mM)	40 g
Tween-20 (0.5%)	25 ml
Deionized H ₂ O	to the final volume of 5 L

→ adjust pH to 7.56

Transfer buffer (for 5 L)

Trizma® Base	12.1 g
Glycine	56.3 g
Methanol	1 L
Deionized H ₂ O	to the final volume of 5 L

Tris-HCl (1 M, pH 6.8, for 100 ml)

Tris-HCl	15 g
Deionized H ₂ O	to the final volume of 100 ml

→ adjust pH to 6.8 with 37% HCl

Tris-HCl (1.5 M, pH 8.8, for 200 ml)

Tris-HCl	45.25 g
Deionized H ₂ O	to the final volume of 200 ml

→ adjust pH to 8.8 with 37% HCl

5.2.5.4 Solutions for histology and immunohistology

Blocking solution (motor neurons for 10 ml)

BSA (4%)	0.4 g
1% Tween/1x PBS	2 ml
1x PBS	to the final volume of 10 ml

Ringer solution (for perfusion)

NaCl (0.85%)	4.25 g
KCl (0.025%)	0.125 g
NaHCO ₃ (0.02%)	0.1 g
Deionized H ₂ O	to the final volume of 500 ml

4% paraformaldehyde (PFA) in PBS (pH 7.3, for 1 L)

PFA	40 g
-----	------

Deionized H ₂ O	to the volume of 900 ml
→ adjust pH to 7.3	
Deionized H ₂ O	to the volume of 1 L
→ aliquot and store at -20°C	

Phosphate buffer (for immunostaining)

0.4M

NaH ₂ PO ₄ H ₂ O	27.6 g
Na ₂ HPO ₄ H ₂ O	35.6 g
Deionized H ₂ O	to the final volume of 500 ml

0.125M

Mix 31.25 ml of 0.4M phosphate buffer with 68.75 ml of deionized water for final volume of 100 ml

DMSO solution (for storing perfused brain and brain sections)

Phosphate buffer (0.4M)	31.25 ml
Glycerin	20 ml
DMSO	2 ml
Deionized H ₂ O	to the final volume of 100 ml

Gelatin solution (for mounting brain sections)

Gelatin	0.2 g
Tris-HCl (pH 7.6)	to the final volume of 100 ml

5.2.6 Primers and oligoneucleotides

Sequences for primers purchased as lyophilized from Integrated DNA Technologies. Stock solutions at a concentration of 100 pmol/μl were prepared from lyophilized products and subsequently diluted to 10 pmol/μl.

Table 1: Primers for genotyping

Application	Name		Sequence	Amplicon length (bp)	Annealing temp (°C)
Genotyping	<i>Ncald</i> mut	fwd	CGGTCGCTACCATTACCAGT	824	60
		rev	GCATGTGTGACAACAGACCC		
	<i>Ncald</i> wt	fwd	AGCATTCTGCCTTGCTGAT	201	58
		rev	TTCCCTTACGGGGATGCT		

5.2.7 Plasmid

pEGFP-N1 plasmid with vector backbone of pEGFP-N and a CMV promoter, a generous gift from Kononeko lab (CECAD, Cologne) was used in the work presented in this thesis. The vector can be ordered at Snap-gene.

5.2.8 Software packages and internet database

- 1D Scan EX (densitometric analysis) Scanalytics Inc.
- EndNoteX7 (reference organization) Thomson Research
- Fiji (ImageJ) (image analysis) Open Source
- GraphPad Prism (graph design, statistical analysis) GraphPad Software
- Inkscape (figure design) Inkscape Community
- Kallisto (RNA sequencing analysis) Open source
- MaxQuant (mass spectrometry analysis) Open source
- Office 2013 (text processing, data analysis) Microsoft
- OMERO (image analysis) Open source
- Quantity One 4.5.1 Bio-Rad

- (image acquisition and analysis)
- ZEN Zeiss
- (image acquisition and analysis)
- Ensembl <http://www.ensembl.org/>
- GeneCards <http://www.genecards.org/>
- Medline <https://www.ncbi.nlm.nih.gov/pubmed>
- NCBI <http://www.ncbi.nlm.nih.gov/>
- OMIM <http://www.ncbi.nlm.nih.gov/omim>
- UniProt <http://www.uniprot.org/>

5.2.9 Mice

Ncald^{KO/KO} – homozygous knockout animals were acquired from The Jacksons Laboratories. Detailed description of the design of mouse has been discussed in Figure 6

5.3 Methods

Unless stated otherwise, all molecular biology methods were adapted from the standard reference work “Molecular Cloning: A Laboratory Manual (volume 1-3)” by Joseph Sambrook and David W. Russell. The culture, transfection and selection of ES cells was performed according to the guidelines from the work “Laboratory protocols for conditional gene targeting” by Raul M. Torres and Ralf Kühn.

5.3.1 Working with nucleic acids

5.3.1.1 RNA isolation

RNA was isolated from tissues (hippocampus, spinal cord and piece of cortex weighing max 30 mg), by incubating them in RLT buffer (Qiagen) supplemented with 10 µl/ml β-mercaptoethanol. Next, the samples were homogenized using automated homogenizer (Peglab) and transferred using RNase free filter tips to sterile tubes. Extraction of RNA was performed using RNeasy Mini Kit (Qiagen) according to the manufacturer’s protocol. Genomic DNA contaminations were prevented in all cases by incubating samples in DNase I digestion for 20 min at RT. Finally, RNase free water was used to extract RNA and samples were stored at -80°C. The QuBit RNA assay Kit was used to measure exact RNA concentrations according to the manufacturer’s protocol. Briefly, 1 µl RNA BR reagent was mixed with 199 µl RNA BR buffer to prepare a master mix. Reference RNA standards were used to calibrate the QuBit machine, 10 µl of each standard were mixed with 190 µl of master mix. Finally, RNA concentration by 1 µl RNA sample were added in 199 µl master mix. After incubating for 2 min at RT, the RNA concentrations were calculated using the RNA broad range assay of the QuBit system.

5.3.1.2 Isolation of DNA

For genotyping the animals, tail tip/ ear punch were collected. The tissues were immersed in Tail lysis buffer (493 μ l) and proteinase K solution was (7 μ l, 200 μ g/ml) added freshly. The mixture was incubated at 55°C on a shaker/incubator until the tissue completely dissolved. Suspension containing fully dissolved tissue was centrifuged at maximum speed (16200 x g) for 5 min to pellet extra debris. The clear supernatant was transferred in a new 1.5 ml tube containing 500 μ l isopropanol. By gentle shaking (12 times gentle flipping of tube) and centrifugation for 10 min (13000 rpm) DNA was precipitated. The pellet was washed with 70% ethanol (200 μ l) to remove residual salt by 5 min centrifugation (13000 rpm) whereas the supernatant was discarded. The ethanol was discarded and the pellet was dried for 10 min in a vacuum concentrator centrifuge and resuspended in TE (100 μ l) with RNase at 37°C for approx. 1 h. subsequently, a genotyping PCR was performed using 1 μ l of the DNA suspension.

5.3.1.3 Polymerase Chain Reaction (PCR)

A polymerase chain reaction was used to amplify the specific genomic fragment for genotyping, PCR developed in 1980s by Kary Mullis (Mullis et al., 1986) is one of the most important and fundamental molecular technique. It is an enzymatic DNA amplification technique that initially uses complementary oligonucleotides (primers) which flank the DNA fragment of interest. Subsequently, a thermostable DNA polymerase termed Taq polymerase from *Thermophilus aquaticus* is used to amplify the DNA fragment of interest. Taq polymerase synthesizes new DNA starting from the 3' end of a single-strand DNA template. A PCR reaction mix is composed of: a template DNA (mainly genomic DNA, but also cDNA), target specific primers, Taq polymerase, $MgCl_2$ necessary co-factor for polymerase, all dNTPs to synthesize the PCR product, enzymatic buffer and water. Currently, many manufacturers offer all PCR components (except template DNA and primers) as convenient and inexpensive ready-to-use Master mixes which are optimized for a wide range of annealing temperatures. For genotyping, such a 2x Master mix (New England Biolabs) was routinely used. An exemplary PCR composition with individual components or with a Master mix is given in Table 2.

Table 2: A standard 20 µl PCR composition

Left side – with individual components, right side – with 2x Master Mix

Components	Volume [µl]	Components	Volume [µl]
10x PCR buffer	2	2x Master mix	10
100 mM of dNTP	3		
MgCl ₂	0.75		
Taq polymerase	0.15		
ddH ₂ O	11.1	ddH ₂ O	7
Primer fwd (10 pmol)	1		
Primer rev (10 pmol)	1		
Template DNA	1		

Each PCR consists of a series of three steps: denaturation, primer annealing and elongation; these three steps together constitute one PCR cycle. Each step requires different temperature conditions: the denaturation is performed at 95°C to separate two strands of the template DNA, the primer annealing depends on the sequence of an individual primer (specifically on its length and CG/AT proportion) and the elongation depends on the amplicon length, as the amplification speed of the Taq polymerase is ~ 1 kb/min. An exemplary PCR program is given in Table 3.

Table 3: A standard thermocycler PCR program

Step	Duration	Temperature [°C]
1. Initial denaturation	5 min	95
2. Denaturation	30 sec	95

3. Primer annealing	30 sec	Primer dependent, usually 58-62°C
4. Elongation	1 min per 1 kb	72
Repeat steps 2-4 for 35x		
5. Final elongation	10 min	72
Cooling	-	4

5.3.1.4 Agarose gel electrophoresis

In a agarose gel DNA fragments are separated depending on their size using an electric field. As the DNA molecules carry negative charge, they migrate towards positively charged anode in the gel.

Generally 1% gels were prepared by dissolving agarose powder in 1x TBE buffer by heating the solution in a microwave. Once the agarose was completely dissolved, the solution was cooled down on a stirrer and ethidium bromide solution was added into agarose gel solution with a final concentration 1 µg/ml. In parallel, a gel chamber was set with well combs and the agarose solution was poured into the chamber to solidify. Before loading the samples, the agarose gel chamber was filled with 1x TBE and then the combs were removed to load the samples in the empty wells. The PCR samples (along with loading dye) were cautiously pipetted into the wells of agarose gel. Finally, the gel was run for about 20-30 min at 100-120 V to separate the bands of different sizes and was imaged using the ChemiDoc XRS Imaging System from Bio-Rad.

5.3.2 Working with proteins

Proteins being highly sensitive biomolecules are easily degraded at temperatures higher than ice-cold, therefore all protein work was carried out at ice-cold temperatures (4°C). Additionally, the lysis buffer was supplemented with a cocktail of protease inhibitors (Roche) and phosphatase inhibitor (Thermo Scientific).

5.3.2.1 Isolation of proteins from tissues

The tissues were collected during mice dissection and snap-frozen for protein isolation without any degradation. Using Precellys24 device (Peqlab) the tissue samples were

homogenized for protein isolation: the sample was placed in a 2 ml eppendorf with ceramic beads and cold RIPA buffer in sufficient amount. The homogenization of the tissues was carried out for 25 sec at 5500 rpm. The samples were further sonicated for 5 minutes using Bioruptor® Plus device (Diagenova). Sonication fragments the DNA and thereby prevents smearing on SDS-PAGE blot. Lastly, the tissue lysate was centrifuged at 4°C for 30 min at 13000 rpm and clear supernatant was collected for further analysis.

5.3.2.2 Bradford assay

Bradford assay was used to measure the protein concentration in the tissue lysates (Bradford, 1976). Upon binding to protein, a shift takes place in Bradford reagent absorption maximum from 470 to 595 nm, which can be measured photometrically. A photometer was first calibrated for the Bradford assay using a standard curve of BSA dilutions. 1 µl of the lysate of unknown protein concentration was mixed with 499 µl of Bradford solution and incubated for 15 min at room temperature; in parallel, a blank containing 1 µl of the lysis buffer (routinely RIPA buffer) with 499 µl of the Bradford solution was prepared. First the absorption of the blank, and then of all samples was measured at a wavelength of 595 nm and the protein concentration was calculated from the measured values by comparison to the BSA standard curve.

5.3.2.3 SDS polyacrylamide gel electrophoresis (SDS-PAGE)

The protein lysates were run on SDS-PAGE followed by Western blot analysis. First, a certain required amount of protein lysate (20-40 µg) was mixed with 3x Laemmli buffer and denatured at 95°C for 5 min. The proteins were given a strong negative charge exceeding their native charge by addition of the SDS both in the Laemmli buffer and the polyacrylamide (PAA) gel gives. This allows the separation of all proteins irrespective of their intrinsic charge solely based on their molecular weight.

A 12% PAA separating and a stacking gel were prepared in a 0.5 mm spacer glass and a thin glass plates. These two gel types differ in their composition by the PAA concentration and pH. The stacking gel contains less PAA and forms larger pores, so that the proteins can migrate easily and concentrate at the border between both gels. The separating gel contains more amount of PAA and therefore forms smaller pores, thus bigger proteins migrate slowly and can be identified in the upper part of the SDS-PAGE gel, while smaller proteins move easily to the bottom part of the gel.

The separating gel was poured first and covered with isopropanol which helps to form smooth edge of the gel. Once the gel was polymerized, the isopropanol was washed out.

Subsequently, the stacking gel was pipetted on top of the solidified separating gel and well combs were carefully inserted.

The protein lysates were loaded into the wells along with 3x Laemmli loading buffer of the stacking gel. Additionally, a protein ladder PAGE Ruler Plus (Thermo Fisher Scientific) was loaded a marker to estimate the size of analyzed proteins. PAA SDS-PAGE gel electrophoresis was performed in the Mini-Protean 3 cell system (Bio-Rad) at 50-100 V and partially filled with 1x electrophoresis buffer.

5.3.2.4 Western blot

Once separated by SDS-PAGE according to size, the samples were transferred from the gel to a nitrocellulose membrane (Hartenstein) by semi dry or wet blotting in the transfer system (Bio-Rad). The gel transfer was arranged from the following components (all of them previously equilibrated in the transfer buffer): a sponge pad (only for wet transfer), a Whatman paper layer, the PAA gel with separated proteins, the nitrocellulose membrane, again a Whatman paper layer and finally a sponge pad (only for wet transfer). All components were fixed in a transfer stack and placed in a transfer chamber fully filled with transfer buffer. The protein transfer was carried out at 4°C for 2 h at 110 V. During the transfer negatively charged proteins migrate to the positively charged anode in the electric field and adhere to the membrane by hydrophobic interaction.

5.3.2.5 Immunochemical detection of proteins

The membrane with freshly transferred proteins was washed with TBS-T to remove residual methanol and stained with the Ponceau solution to visualize the quality of the transfer. The membrane was washed with TBS-T to remove the Ponceau dye and was incubated in the blocking solution (6% milk solution) for at least 1 h. Subsequently, the membrane was incubated overnight with the primary antibody diluted in 3% milk solution at 4°C. After the sufficient incubation time, the membrane was washed with TBS-T 3x 10 min each. Subsequently, membrane was incubated with the secondary antibody solution. The primary and secondary antibodies with the respective dilutions and incubation times are listed in Table 4. Finally, the membrane was again washed 3x 10 min with TBS-T and incubated for 5 min in the SuperSignal® Wets Pico Chemiluminiscent Substrate (Thermo Fisher Scientific) in order to visualize the proteins stained with the specific antibodies. The visualization was performed using ChemiDoc XRS Imaging System (Bio-Rad).

Table 4: Primary and secondary antibodies used for protein detection

Antibody	Dilution	Incubation time
HRP anti-β-actin	1:10000	2 h
anti-GAPDH	1:5000	2 h
anti-NCALD	1:1000	o.n
anti-MBP	1:1000	o.n.
anti-MAP3K10	1:500	o.n.
anti-pJNK	1:500	o.n.
anti-JNK	1:1000	o.n.
Secondary antibody		
anti-mouse-HRP	1:5000	1 h
anti-rabbit-HRP	1:5000	1 h

5.3.2.6 Co-immunoprecipitation

This technique was performed by Dr. Seyyedmohsen Hosseinibarkooie, postdoc in AG Wirth. The brain and spinal cord samples were collected at P30 and P14, respectively (From both wild type and *Ncald*^{KO/KO} mice). The tissue samples were homogenized and lysed in the NP40 based lysis buffer (50mM Tris-HCl, 1% NP40, 100mM NaCl, 2mM MgCl₂ including protease inhibitor (Roche). 10μl of Control rabbit IgG (SantaCruz) and NCALD polyclonal antibody were used for immunoprecipitation using protein A paramagnetic MicroBeads (Miltenyi) following the manufacturer's instruction. Finally, the IP columns were washed at least 6 times with lysis buffer. The bound fraction of proteins was directly used for further mass spectrometry analysis.

5.3.2.7 Mass spectrometry and data analysis

This technique was performed by Dr. Seyyedmohsen Hosseinibarkooie, postdoc in AG Wirth. All samples were analysed on a Q-Exactive Plus (Thermo Scientific) mass spectrometer coupled to an EASY nLC 1000 UPLC (Thermo Scientific). The protocol used in this work was followed from a published study (Dafinger et al., 2018). Peptides were loaded with solvent A (0.1% formic acid in water) onto an in-house packed analytical column (50 cm × 75 µm I.D., filled with 2.7 µm Poroshell EC120 C18, Agilent). Peptides were chromatographically separated at a constant flow rate of 250 nL/min using the following gradient: 5-30% solvent B (0.1% formic acid in 80 % acetonitrile) within 66 min, 30-50% solvent B within 13 min, followed by washing and column equilibration. The mass spectrometer was operated in data-dependent acquisition mode. The MS1 survey scan was acquired from 300-1750 m/z at a resolution of 70,000. The top 10 most abundant peptides were isolated within a 1.8 Th window and subjected to HCD fragmentation at a normalized collision energy of 27%. The AGC target was set to 5e5 charges, allowing a maximum injection time of 120 ms. Product ions were detected in the Orbitrap at a resolution of 35,000. Precursors were dynamically excluded for 20 s.

All mass spectrometric raw data were processed with Maxquant (version 1.5.3.8) using default parameters. Briefly, MS2 spectra were searched against the Uniprot MOUSE.fasta (downloaded at: 18.47.2017) database, including a list of common contaminants. False discovery rates on protein and PSM level were estimated by the target-decoy approach to 1% (Protein FDR) and 1% (PSM FDR) respectively. The minimal peptide length was set to 7 amino acids and carbamidomethylation at cysteine residues was considered as a fixed modification. Oxidation (M) and Acetyl (Protein N-term) were included as variable modifications. The match-between runs option was enabled. LFQ quantification was enabled using default settings.

5.3.3 Working with mice and mouse tissues

5.3.3.1 Mouse strain

We used highly homozygous inbred mouse strains, as the genetic background of each strain has been shown to affect the gene expression and therefore the phenotypic outcome (Linder, 2006). In this work experiments were performed on C57BL/6N mice with a genetically pure background. All mice were housed 12 h day/night cycle in the mouse facility of the Institute of Genetics, Cologne as well as Center for Molecular Medicine, Cologne. The experiments used in this work are described in detail in an animal experimental protocol which was permitted by the local animal protection committee under the reference number 84-02.04.2014.A126. Each mouse was humanly euthanized according to protocols approved by the Landesamt für Natur, Umwelt and Verbraucherschutz of Northrhine Westfalia (LANUV NRW).

5.3.3.2 *Ncald*^{ko/ko} mice

The B6N.Cg-Ncaldtm1.1(KOMP)Vlclg/J mice were acquired from the Jackson Laboratory (Stock number #018575). These mice were generated using the VelociGene strategy developed by the Regeneron Company by the Knockout Mouse Phenotyping Program (KOMP²) to target most difficult genes. The VelociGene cassette ZEN-Ub1 (beta-galactosidase coding sequence from *E. coli lacZ* gene; polyadenylation signal; loxP site; promoter from the human ubiquitin C gene; neomycin phosphotransferase; polyadenylation signal; loxP site) was inserted to replace 28620 bp between positions 37298567-37327186 of chromosome 15 (Genome Build37) deleting all exons and intervening sequences. Subsequently, the neomycin cassette used for colony selection was excised by Cre expression. The *Ncald*^{KO/KO} mice were viable and fertile, but in our observation the fertility of homozygous knock-out mice was severely diminished compared to wildtype. Breeding of *Ncald*^{ko/ko} animals was very inefficient and produced infrequent litters, which did not seldom survived due to lack of parental care. Therefore, *Ncald*^{KO/WT} animals generated by cross breeding wildtype mice with *Ncald*^{KO/KO} mice were used to for breeding with efficient breeding performance. Moreover, breeding of *Ncald*^{KO/WT} produced wildtype, *Ncald*^{KO/WT} and *Ncald*^{KO/KO} littermates which were used for further experiments

5.3.3.3 Generation of primary motor neurons

Primary motor neurons culture were prepared from spinal cords of E13.5 of embryos following the previously published protocol . The beginning of pregnancy was determined by regular plug check. On E13.5, the pregnant female was sacrificed and embryos were carefully separated from the uterus. Subsequently, the embryo was placed on a Sylgard-filled Petri dish filled with 1x PBS. In order to open the embryo dorsally, it was carefully fixed ventrally using forceps and fine minuten pins without damaging the dorsal part of embryo. Subsequently, the skin of the embryo above the spinal cord was carefully removed and spine was released by scratching out along the vertebrae with sharp pins. Surrounding glial cells and meninges membrane were neatly removed without damaging the spinal cord. The clean spinal cord tissue was placed in a 1.5 ml tube with 500 µl of 1x PBS and centrifuged at 4°C and 1000 x g for 10 min.

All work with cell lines was performed in a laminar flow culture hood in sterile conditions. Additionally, antibiotics and anti-fungal agents were added to cell culture media to prevent contamination. Cells were placed in sterile cell incubators at 37°C with 5% CO₂. Following this, the 1x PBS was pipetted off and the spinal cord was resuspended in 500 µl of 1% Trypsin in 1x PBS and incubated for 10 min at 37°C. Afterwards, resuspended spinal cord was

centrifuged again for 7 min at 4°C and 1000 x g. Finally, the supernatant Trypsin solution was removed and 500 µl of motor neuron plating medium with DNase I (100 U/ml) was added and the tissue was completely dissolved by slow and repetitive pipetting. This is a crucial step as even little rigorous pipetting can damage motor neurons. After 2 min incubation at RT, the undissolved debris settled at the bottom of the tube and the cell suspension was transferred to a fresh 1.5 ml tube. 10 µl of cell suspension was pipetted out and the cells were counted using the Neubauer chamber. 75,000 cells/well were plated on poly-D-lysine (PDL) coated coverslips in a 12-well plate containing 2 ml of plating medium (For immunofluorescent staining to determine axonal length). Increasing the cell density did not allow visualization of distinct axons, whereas decreasing the seeding density did not allow the cells to grow properly due to lack of cell to cell interaction. Next day, the plating medium was replaced with Neurobasal® medium with growth factors. For the staining, the motor neurons were cultured for 4 days.

5.3.3.4 Generation of primary hippocampal neurons

The protocol used for this experiment has been published earlier (Kononenko et al., 2017). Post-Natal (P1-P4) pups were sacrificed without damaging their heads. The brain were carefully removed from the heads in a sterile dissection hood and collected in a small petri dish containing 20% fetal calf serum (fcs) dissolved in Hank's Balanced Salt Solution (HBBS). Hippocampi from both sides of the cortex were dissected under a dissection microscope and placed in a dish containing 20% FCS dissolved in HBBS. This dish needs to be kept on top of ice cooked metal plate, do prevent any degradation of tissue. The Hippocampi were carefully cut into small pieces with sharp blades. This step is crucial, as rough handling of the blade can damage neurons. Following this, the small pieces of hippocampi along with the 20% FCS HBBS solution were transferred to a 15ml falcon tube using 5ml glass pipette. Once the small pieces of hippocampi settled down the tube, the supernatant solution was aspirated carefully. Hippocampi pieces were washed two times with 5 ml of 20% FCS HBBS solution and the two times with 5 ml HBBS supplemented with Trypsin (10 mg/2ml) and DNase I (10 µl/2ml) and filtered to be added on the hippocampi after aspirating the last washing solution. The tube with Hippocampi pieces in digestion solution was incubated in the sterile incubator for 15 minutes at 37°C. Subsequently, the hippocampi pieces were washed two times with 5ML of 20% FCS HBBS solution and then two times with 5ML HBBS supplemented with penicillin and streptomycin. After aspirating the last washing solution 2ml of dissociation solution freshly supplemented with DNase I (10 µl/2ml) was added on the hippocampi pieces. Glass Pasteur pipette was carefully melted at the tip, to prepare a very small opening which allows passing of more or less single cell suspension. Such a glass pipette was used to homogenize the hippocampi pieces into single

cell suspension by gently pipetting up and down. Homogenized cell suspension was centrifuged at 300 g at 4°C. Supernatant was carefully aspirated, this step is crucial as the pellet is very loose and can easily get aspirated along with the supernatant. Cells were diluted in the desired amount of plating media and 10 µl of cell suspension was pipetted out and the cells were counted using the Neubauer chamber. 70,000 cells/well were plated on poly-D-lysine (PDL) coated coverslips in a 6-well plate and left to firmly attach onto the coverslip surface for one hour. Subsequently, 2 ml of plating medium was added onto each well. Next day the plating medium was replaced with growth medium. Hippocampal neurons were cultured for 14 days.

5.3.3.5 Transfection of primary hippocampal neurons

The protocol used for this experiment has been published earlier (Kononenko et al., 2017). The hippocampal neurons were transfected at DIV 7-9 using the calcium phosphate transfection kit from Promega and following the manufacturer's protocol. The HBSS solution and the NBA media were equilibrated by placing them in the cell culture incubator for 1 h before the transfection. Osmolarity of HBSS and NBA solution used for transfection needs to be adjusted to the osmolarity of growth media of the cells to be transfected, otherwise the cells may not survive the harsh transfection conditions. Therefore, the osmolarity of HBSS and NBA was measured and adjusted to the cell growth medium osmolarity. Precipitation reaction mixture was prepared by mixing the DNA (Plasmid) that needs to be transfected into the cells, CaCl₂ and water in one tube and corresponding amount of HEPES in 14 ml falcon tube. The DNA, CaCl₂ and water solution was added dropwise into HEPES solution along with gentle stirring on the vortex in 2-3 minutes and was incubated for 20 mins in dark. Coverslips with hippocampal neurons were transferred into a plate containing NBA and about 100 µl of precipitates were added on top of the coverslips. This plate was incubated for 30 minutes in the cell culture incubator. Afterwards, the transfection media was aspirated from the plate and coverslips were washed to remove any precipitate which sediment on the neurons with pre-warm HBSS solution. Finally, the coverslips were brought back to original plate with growth medium.

5.3.3.6 Immunofluorescent staining of primary neurons

The proteins of interest are specifically detected using a primary antibody, which is subsequently visualized by the binding of a fluorophore-conjugated secondary antibody. Cells were seeded out and cultured on coverslips for immunofluorescent staining. The cells grow in culture incubator for a given time, depending upon each experiment. To start with immunostaining, cells were washed with 2x PBS and fixed with 4 % PFA (supplemented with

4 % sucrose in case of motor neurons) for 15 min . After the fixation cells were washed again and permeabilized with 1 % Triton detergent in 1x PBS for 5 minutes. Subsequently, cells were blocked with 4 % BSA and 0.2 % Triton in PBS for 1 h at room temperature. After blocking Primary antibodies (listed above) were diluted in the blocking solution and pipetted on the cells and incubated o.n. at 4°C. Next day, the cells were washed with 1x PBS 3x for 5 min and then incubated with secondary antibodies in a dark chamber (listed above) at room temperature diluted in 1x PBS for 1h. Following this, the cells were again washed to remove residual salts 3X with 1X PBS and 1X ddH₂O. Finally, the coverslips were mounted on glass slides with Mowiol and stored at 4°C for further microscopic analysis.

5.3.3.7 Gavage treatment

Ncald homozygous knockout animals were treated with the JNK inhibitor SR3306 as well as with the vehicle solution. As this drug has been shown to have neuroprotective effects upon its oral administration in mice, the same protocol was followed (Chambers et al). SR3306 was dissolved in 45% W/V solution of beta- Hydroxy propyl Cyclodextrin and 0.07% HCl and the same solution without SR3306 to be used as the vehicle control. Two months old age point has also been used in Muhammad et al for the treatment of JNK inhibitor which showed the increase in adult neurogenesis, therefore we choose the same age for our treatment. We treated the animals orally using the well-established oral gavage method with 7 doses, twice on day one and once on days 2-6 (as described in Chambers et al). As the DCX expression in the newly born neurons in mice brain, peaks at about 2-3 weeks after the beginning of differentiation NSCs, we started the treatment in 2 months old animals and waited for 3 more weeks after the treatment has finished to sacrifice the animal.

5.3.3.8 Transcardial perfusion fixation

Fixation of larger tissues like whole brain does not work well if directly placed in a fixative solution, as the fixative cannot reach the regions of the tissue. Therefore, whole animal perfusion fixation allows usage of the physiological circulatory system of the animal to evenly distribute the fixative inside tissues like brain (Gage et al., 2012). Moreover, perfusion of the animal cleans the blood from the body organs before fixing them thereby supporting cleaning background signals in immunohistological analysis which may arise due to blood vessel.

Animals were anesthetised with specific amount of narcotic solution (0.1 ml/10 g ketamine/xylazine) based on their body weight. Once the animals reach a sleeping state termed surgical plane, where they no longer respond to strong pinching stimuli between their toes, they were fixed on a Styrofoam plate. The skin and muscles above the heart were carefully cut open to expose the heart and a very fine needle (27 G) connected to the perfusion tube was inserted into the left ventricle of heart. Subsequently, a small cut was

made on the right atrium of the heart to allow the outflow of the blood. The perfusion pump was set at low speed (7ml/min) to allow drop by drop flow of the perfusion solutions. Firstly freshly prepared ringer solution was pumped through the body to clear the blood, color of the tongue and liver was used to observe the clearance of the blood. After sufficiently clearing the blood from the body, 4 % PFA solution was pumped through the tube. The efficiency of fixation was measured by the observed stiffness of head and tail, when sufficiently stiff perfusion was stopped and the brain were carefully removed using special Friedman-pearson rongeurs. The isolated brain were transferred in a tube containing 4 % PFA at incubated overnight at 4 ° C and then next day were transferred to 2 % DMSO solution to be stored until further processing.

5.3.3.9 Serial sectioning and Nissl staining of brain sections

PFA fixed brains in DMSO solution were sectioned using a freezing microtome device. The microtome stage was cooled down to -30°C. Tissue-tek (Hartenstein) solution was frozen to prepare a raising base on stage and brain was fixed on this base. Stage was covered completely with finely crushed dry ice to freeze the whole brain. Once frozen and solid, 40 um thick brain sectioned were generated with a sharp blade adhered to the microtome and each section was collected in a series of 6 tubes containing 2 % DMSO solution. These tubes were stored in -80°C until further processing.

In this study Nissl staining was used to stain brain sections for a gross histological analysis of brain morphology. Sections were first incubated in Cresyl violet solution for 8-10 minutes then washed 3 times with water and subsequently were dehydrated in a series of increasing EtOH concentrations (50 % , 70 % , 80 % , 96 % + acetic acid , 100 % , 2 min each) and lastly were incubated in Xylol. Finally, sections were mounted with Entellan and a coverslip.

5.3.3.10 Immunohistochemical staining of brain sections

For immunofluorescent staining of brain sections, firstly the sections were washed 3X 10 min each, to remove any DMSO solution in which they were stored. Similar dorso-ventral brain sections were selected from wildtype and *Ncald*^{KO/KO}. After washing, the brain sections were permeabilized using a 1 % triton solution in phosphate buffer (0.125 M) for 2 h. Following this the sections were incubated with the blocking solution (3 % BSA and 0.3 % triton X) for 1 h. Subsequently, the sections were incubated with primary antibodies diluted in blocking solution at 4 °C overnight. Next day sections were washed 3X 5 min each, with phosphate buffer (0.125 M) and then incubated with secondary antibodies diluted in blocking solution for 2 h. Finally, the sections were washed 3X 5 min each and then mounted on glass slides with

Mowiol. Slides were stored at 4°C until further microscopic analysis. The following antibodies were used: anti-NCALD (1:100, 12925-1-AP, Proteintech), anti-NeuN (1:500, EPR 12763, Abcam), anti- TBR1 (1:500, ab31940), anti- CUX1 (1:200 sc-13024, Santa Cruz), anti- GFAP (1:500, G3893, Sigma), anti- Ki-67 (1:500, ab15580 Abcam), anti- DCX (1:500, AB2253, Merck), anti- APC (1:500, OP80, Merck), anti- MBP (1:1000 SMI94, Covance).

5.3.3.11 Microscopic image acquisition and analysis

All bright field images of Nissl stained brain sections were imaged using high throughput automated SCN400 Slide Scanner (Leica) whereas fluorescent images of brain sections with Z stacks (1 um thickness) were acquired using laser scanning confocal microscope SP8 (Leica). On other hand, all fluorescent images of fixed cells were acquired with a fully motorized fluorescence microscope AxiomagerM2 equipped with an AxioCam MRm camera and an ApoTome device for optical sectioning (Zeiss). The images included in this thesis represent the maximum intensity projections of the Z stacks. The image analysis was performed with the Aperio ImageScope (Leica), ZEN (Zeiss), Fiji software (Open Source) and OMERO software.

5.3.3.11.1 Hippocampal culture colocalization analysis

Hippocampal neurons were imaged with high resolution (40X) using AxiomagerM2 and images were analysed using ImageJ software for colocalization analysis of NCALD with synaptic markers. As the co-localization was visibly restricted to certain punctas, a random stretch of neurites with certain observable punctas with co-localization (yellow) signal was chosen. A line was drawn on this stretch and ImageJ plot profile function was used for each channel individually to calculate the intensity plot through the line. These intensity values was plotted against the XY value on the line for each channel in GraphPad Prism 6 software. Subsequently, the plots for NCALD and each synaptic marker were superimposed. The asterisks represents overlapping peaks of each channel, thus showing the co-localization

5.3.3.11.2 Analysis of sub granular zone nissl staining

OMERO software was used for measuring the SGZ length. Draw polyline function was used to accurately draw a line over the SGZ length and draw line function was used to measure the cerebral length of whole section. This method has already been published (Antonelli et al., 2018).

5.3.3.11.3 Sholl Analysis

Dendritic complexity of cultured hippocampal neurons was done using ImageJ software. Cells were imaged centring the cell soma in each image and then a line was drawn from centre of cell soma until longest neurite length. Sholl analysis function of ImageJ was used to draw virtual concentric circles around the cell soma until the length of manually drawn line, with specified interval distance. Number of intersections at each circle was calculated as a measure of dendritic complexity and plotted against distance from soma in GraphPad Prism 6 software.

5.3.3.11.4 Cell density analysis

Cell density for NeuN and DCx positive cells in the brain sections was calculated using ImageJ software. Three different ROIs were drawn across DG and CA3 (for NeuN) or hilus (for DCX) and the plane with highest number of cells was selected for each image and number of cells was counted using Cell counter function in ImageJ. As the thickness of each stack was 1 μm , the dimensions of ROI (length * breadth) were multiplied to obtain the volume of each ROI and then number of cells in the ROI were divided with this volume to obtain the cell density.

5.3.3.11.5 Intensity analysis

Intensity of DCX and nestin staining for each brain section was measured using ImageJ software. All images were converted to 8 bit type and certain intensity threshold which sufficiently superimposed immunostaining, was set using a wildtype section. Each image was opened with the same threshold and the stained area of image was measured.

5.3.3.11.6 Motor neuron morphological analysis

Motor neuron (MN) axon length was measured by tracing the longest neurite in each cell with 'spiral line' tool of ZEN software (Zeiss) whereas MN branching was calculated by manually counting the number of outgrowth on the longest axon.

5.3.3.12 Rotarod

Rota rod is a motoric performance test where the mice are placed on a rotating rod and are allowed to run on a rod for about 300 seconds. Amount of time (in seconds) which a mice spends running on the rod before it falls off the rod is calculated a sensing metallic floor below the rods and is automatically stored in the connecting computer. The amount of time

that each mice spend on the rotation rod gives a measurement of their balance, coordination, physical condition and motoric abilities. 8 weeks or 12 week old animals were placed on such a machine and the seconds spent on the rod were calculated for each animal.

5.3.3.13 Transcriptome analysis

This analysis was done by Eike Strathmann, a PhD student at AG Wirth RNA sequencing data were analyzed using the program Kallisto (Bray et al., 2016) and the R plugin DESeq2 (Love et al., 2014) as well as custom R scripts. Kallisto uses the raw data (fastq files) to estimate the transcript abundance using a method based on pseudoalignment.

5.3.3.14 Statistical analysis

The GraphPad Prism 6 software was used to perform all statistical analysis. One-way ANOVA test was used to analyze wildtype, heterozygous and homozygous motor neuron axon length and branching; with Tukey's correction for multiple comparisons. Histological analyses the SGZ length, neuronal density, DCX intensity, were tested for significance by assessing determined with two-tailed unpaired student's tests.

P<0.05 values were considered significant and further statistical significance were represented by: *P<0.05, **P<0.01 and ***P<0.001.

6 References

- Ackermann, B., Krober, S., Torres-Benito, L., Borgmann, A., Peters, M., Hosseini Barkoobe, S.M., Tejero, R., Jakubik, M., Schreml, J., Milbradt, J., Wunderlich, T.F., Riessland, M., Tabares, L., and Wirth, B. (2013). Platin 3 ameliorates spinal muscular atrophy via delayed axon pruning and improves neuromuscular junction functionality. *Hum Mol Genet* 22, 1328-1347.
- Ahmad, S., Bhatia, K., Kannan, A., and Gangwani, L. (2016). Molecular Mechanisms of Neurodegeneration in Spinal Muscular Atrophy. *J Exp Neurosci* 10, 39-49.
- Altman, J., and Das, G.D. (1965). Autoradiographic and histological evidence of postnatal hippocampal neurogenesis in rats. *J Comp Neurol* 124, 319-335.
- Alzheimer's Association Calcium Hypothesis, W. (2017). Calcium Hypothesis of Alzheimer's disease and brain aging: A framework for integrating new evidence into a comprehensive theory of pathogenesis. *Alzheimers Dement* 13, 178-182 e117.
- Ames, J.B., and Lim, S. (2012). Molecular structure and target recognition of neuronal calcium sensor proteins. *Biochim Biophys Acta* 1820, 1205-1213.
- Anacker, C., Luna, V.M., Stevens, G.S., Millette, A., Shores, R., Jimenez, J.C., Chen, B., and Hen, R. (2018). Hippocampal neurogenesis confers stress resilience by inhibiting the ventral dentate gyrus. *Nature* 559, 98-102.
- Andreassi, C., Angelozzi, C., Tiziano, F.D., Vitali, T., De Vincenzi, E., Boninsegna, A., Villanova, M., Bertini, E., Pini, A., Neri, G., and Brahe, C. (2004). Phenylbutyrate increases SMN expression in vitro: relevance for treatment of spinal muscular atrophy. *Eur J Hum Genet* 12, 59-65.
- Antonelli, F., Casciati, A., Tanori, M., Tanno, B., Linares-Vidal, M.V., Serra, N., Belles, M., Pannicelli, A., Saran, A., and Pazzaglia, S. (2018). Alterations in Morphology and Adult Neurogenesis in the Dentate Gyrus of Patched1 Heterozygous Mice. *Front Mol Neurosci* 11, 168.
- Avila, A.M., Burnett, B.G., Taye, A.A., Gabanella, F., Knight, M.A., Hartenstein, P., Cizman, Z., Di Prospero, N.A., Pellizzoni, L., Fischbeck, K.H., and Sumner, C.J. (2007). Trichostatin A increases SMN expression and survival in a mouse model of spinal muscular atrophy. *J Clin Invest* 117, 659-671.
- Bain, J., Mclauchlan, H., Elliott, M., and Cohen, P. (2003). The specificities of protein kinase inhibitors: an update. *Biochem J* 371, 199-204.
- Balthazart, J., and Ball, G.F. (2014). Doublecortin is a highly valuable endogenous marker of adult neurogenesis in canaries. Commentary on Vellema M et al. (2014): Evaluating the predictive value of doublecortin as a marker for adult neurogenesis in canaries (*Serinus canaria*). *J Comparative Neurol* 522:1299-1315. *Brain Behav Evol* 84, 1-4.
- Baptista, P., and Andrade, J.P. (2018). Adult Hippocampal Neurogenesis: Regulation and Possible Functional and Clinical Correlates. *Front Neuroanat* 12, 44.
- Barnes, C.A. (1979). Memory deficits associated with senescence: a neurophysiological and behavioral study in the rat. *J Comp Physiol Psychol* 93, 74-104.
- Bastianelli, E., Okazaki, K., Hidaka, H., and Pochet, R. (1993). Neurocalcin immunoreactivity in rat olfactory bulb. *Neurosci Lett* 161, 165-168.
- Ben-David, E., Granot-Herskovitz, E., Monderer-Rothkoff, G., Lerer, E., Levi, S., Yaari, M., Ebstein, R.P., Yirmiya, N., and Shifman, S. (2011). Identification of a functional rare variant in autism using genome-wide screen for monoallelic expression. *Hum Mol Genet* 20, 3632-3641.
- Benninger, F., Glat, M.J., Offen, D., and Steiner, I. (2016). Glial fibrillary acidic protein as a marker of astrocytic activation in the cerebrospinal fluid of patients with amyotrophic lateral sclerosis. *J Clin Neurosci* 26, 75-78.
- Boccarda, C.N., Sargolini, F., Thoresen, V.H., Solstad, T., Witter, M.P., Moser, E.I., and Moser, M.B. (2010). Grid cells in pre- and parasubiculum. *Nat Neurosci* 13, 987-994.
- Boldrini, M., Fulmore, C.A., Tartt, A.N., Simeon, L.R., Pavlova, I., Poposka, V., Rosoklija, G.B., Stankov, A., Arango, V., Dwork, A.J., Hen, R., and Mann, J.J. (2018). Human

- Hippocampal Neurogenesis Persists throughout Aging. *Cell Stem Cell* 22, 589-599 e585.
- Borch, J., Jorgensen, T.J., and Roepstorff, P. (2005). Mass spectrometric analysis of protein interactions. *Curr Opin Chem Biol* 9, 509-516.
- Bordiuk, O.L., Smith, K., Morin, P.J., and Semenov, M.V. (2014). Cell proliferation and neurogenesis in adult mouse brain. *PLoS One* 9, e111453.
- Borgese, N., D'arrigo, A., De Silvestris, M., and Pietrini, G. (1993). NADH-cytochrome b5 reductase and cytochrome b5 isoforms as models for the study of post-translational targeting to the endoplasmic reticulum. *FEBS Lett* 325, 70-75.
- Bradford, M.M. (1976). A rapid and sensitive method for the quantitation of microgram quantities of protein utilizing the principle of protein-dye binding. *Anal Biochem* 72, 248-254.
- Bradke, F., and Dotti, C.G. (2000). Differentiated neurons retain the capacity to generate axons from dendrites. *Curr Biol* 10, 1467-1470.
- Braskie, M.N., Jahanshad, N., Stein, J.L., Barysheva, M., Johnson, K., McMahon, K.L., De Zubicaray, G.I., Martin, N.G., Wright, M.J., Ringman, J.M., Toga, A.W., and Thompson, P.M. (2012). Relationship of a variant in the NTRK1 gene to white matter microstructure in young adults. *J Neurosci* 32, 5964-5972.
- Braunewell, K.H., and Klein-Szanto, A.J. (2009). Visinin-like proteins (VSNLs): interaction partners and emerging functions in signal transduction of a subfamily of neuronal Ca²⁺-sensor proteins. *Cell Tissue Res* 335, 301-316.
- Bray, N.L., Pimentel, H., Melsted, P., and Pachter, L. (2016). Near-optimal probabilistic RNA-seq quantification. *Nat Biotechnol* 34, 525-527.
- Brichta, L., Hofmann, Y., Hahnen, E., Siebzehnrubl, F.A., Raschke, H., Blumcke, I., Eyupoglu, I.Y., and Wirth, B. (2003). Valproic acid increases the SMN2 protein level: a well-known drug as a potential therapy for spinal muscular atrophy. *Hum Mol Genet* 12, 2481-2489.
- Brinon, J.G., Arevalo, R., Crespo, C., Bravo, I.G., Okazaki, K., Hidaka, H., Aijon, J., and Alonso, J.R. (1998). Neurocalcin immunoreactivity in the rat main olfactory bulb. *Brain Res* 795, 204-214.
- Brooks, S.P., and Dunnett, S.B. (2009). Tests to assess motor phenotype in mice: a user's guide. *Nat Rev Neurosci* 10, 519-529.
- Brzustowicz, L.M., Lehner, T., Castilla, L.H., Penchaszadeh, G.K., Wilhelmsen, K.C., Daniels, R., Davies, K.E., Leppert, M., Ziter, F., Wood, D., and Et Al. (1990). Genetic mapping of chronic childhood-onset spinal muscular atrophy to chromosome 5q11.2-13.3. *Nature* 344, 540-541.
- Burgoyne, R.D. (2007). Neuronal calcium sensor proteins: generating diversity in neuronal Ca²⁺ signalling. *Nat Rev Neurosci* 8, 182-193.
- Burgoyne, R.D., O'callaghan, D.W., Hasdemir, B., Haynes, L.P., and Tepikin, A.V. (2004). Neuronal Ca²⁺-sensor proteins: multitasking regulators of neuronal function. *Trends Neurosci* 27, 203-209.
- Caito, S.W., Milatovic, D., Hill, K.E., Aschner, M., Burk, R.F., and Valentine, W.M. (2011). Progression of neurodegeneration and morphologic changes in the brains of juvenile mice with selenoprotein P deleted. *Brain Res* 1398, 1-12.
- Carlesimo, G.A., Piras, F., Orfei, M.D., Iorio, M., Caltagirone, C., and Spalletta, G. (2015). Atrophy of presubiculum and subiculum is the earliest hippocampal anatomical marker of Alzheimer's disease. *Alzheimers Dement (Amst)* 1, 24-32.
- Cartegni, L., and Krainer, A.R. (2002). Disruption of an SF2/ASF-dependent exonic splicing enhancer in SMN2 causes spinal muscular atrophy in the absence of SMN1. *Nat Genet* 30, 377-384.
- Chambers, J.W., Pachori, A., Howard, S., Ganno, M., Hansen, D., Jr., Kamenecka, T., Song, X., Duckett, D., Chen, W., Ling, Y.Y., Cherry, L., Cameron, M.D., Lin, L., Ruiz, C.H., and Lograsso, P. (2011). Small Molecule c-jun-N-terminal Kinase (JNK) Inhibitors Protect Dopaminergic Neurons in a Model of Parkinson's Disease. *ACS Chem Neurosci* 2, 198-206.

- Chan, J.R., Watkins, T.A., Cosgaya, J.M., Zhang, C., Chen, L., Reichardt, L.F., Shooter, E.M., and Barres, B.A. (2004). NGF controls axonal receptivity to myelination by Schwann cells or oligodendrocytes. *Neuron* 43, 183-191.
- Chavarria-Siles, I., White, T., De Leeuw, C., Goudriaan, A., Lips, E., Ehrlich, S., Turner, J.A., Calhoun, V.D., Gollub, R.L., Magnotta, V.A., Ho, B.C., Smit, A.B., Verheijen, M.H., and Posthuma, D. (2016). Myelination-related genes are associated with decreased white matter integrity in schizophrenia. *Eur J Hum Genet* 24, 381-386.
- Choe, Y., Pleasure, S.J., and Mira, H. (2015). Control of Adult Neurogenesis by Short-Range Morphogenic-Signaling Molecules. *Cold Spring Harb Perspect Biol* 8, a018887.
- Cobben, J.M., Van Der Steege, G., Grootsholten, P., De Visser, M., Scheffer, H., and Buys, C.H. (1995). Deletions of the survival motor neuron gene in unaffected siblings of patients with spinal muscular atrophy. *Am J Hum Genet* 57, 805-808.
- Coffey, E.T. (2014). Nuclear and cytosolic JNK signalling in neurons. *Nat Rev Neurosci* 15, 285-299.
- Couillard-Despres, S., Winner, B., Schaubeck, S., Aigner, R., Vroemen, M., Weidner, N., Bogdahn, U., Winkler, J., Kuhn, H.G., and Aigner, L. (2005). Doublecortin expression levels in adult brain reflect neurogenesis. *Eur J Neurosci* 21, 1-14.
- Crawley, J.N. (2012). Translational animal models of autism and neurodevelopmental disorders. *Dialogues Clin Neurosci* 14, 293-305.
- Crocker, C.E., Khan, S., Cameron, M.D., Robertson, H.A., Robertson, G.S., and Lograsso, P. (2011). JNK Inhibition Protects Dopamine Neurons and Provides Behavioral Improvement in a Rat 6-hydroxydopamine Model of Parkinson's Disease. *ACS Chem Neurosci* 2, 207-212.
- Cutting, G.R. (2010). Modifier genes in Mendelian disorders: the example of cystic fibrosis. *Ann N Y Acad Sci* 1214, 57-69.
- Czeh, B., Michaelis, T., Watanabe, T., Frahm, J., De Biurrun, G., Van Kampen, M., Bartolomucci, A., and Fuchs, E. (2001). Stress-induced changes in cerebral metabolites, hippocampal volume, and cell proliferation are prevented by antidepressant treatment with tianeptine. *Proc Natl Acad Sci U S A* 98, 12796-12801.
- D'hooge, R., and De Deyn, P.P. (2001). Applications of the Morris water maze in the study of learning and memory. *Brain Res Brain Res Rev* 36, 60-90.
- D'yedewalle, C., Ramos, D.M., Pyles, N.J., Ng, S.Y., Gorz, M., Pilato, C.M., Ling, K., Kong, L., Ward, A.J., Rubin, L.L., Rigo, F., Bennett, C.F., and Sumner, C.J. (2017). The Antisense Transcript SMN-AS1 Regulates SMN Expression and Is a Novel Therapeutic Target for Spinal Muscular Atrophy. *Neuron* 93, 66-79.
- Dafinger, C., Rinschen, M.M., Borgal, L., Ehrenberg, C., Basten, S.G., Franke, M., Hohne, M., Rauh, M., Gobel, H., Bloch, W., Wunderlich, F.T., Peters, D.J.M., Tasche, D., Mishra, T., Habbig, S., Dotsch, J., Muller, R.U., Bruning, J.C., Persigehl, T., Giles, R.H., Benzing, T., Schermer, B., and Liebau, M.C. (2018). Targeted deletion of the AAA-ATPase Ruvbl1 in mice disrupts ciliary integrity and causes renal disease and hydrocephalus. *Exp Mol Med* 50, 75.
- De Vega, S., Iwamoto, T., and Yamada, Y. (2009). Fibulins: multiple roles in matrix structures and tissue functions. *Cell Mol Life Sci* 66, 1890-1902.
- Denis-Donini, S., Dellarole, A., Crociara, P., Francese, M.T., Bortolotto, V., Quadrato, G., Canonico, P.L., Orsetti, M., Ghi, P., Memo, M., Bonini, S.A., Ferrari-Toninelli, G., and Grilli, M. (2008). Impaired adult neurogenesis associated with short-term memory defects in NF-kappaB p50-deficient mice. *J Neurosci* 28, 3911-3919.
- Doherty, G.J., and McMahon, H.T. (2009). Mechanisms of endocytosis. *Annu Rev Biochem* 78, 857-902.
- Dolbeare, F. (1995). Bromodeoxyuridine: a diagnostic tool in biology and medicine, Part I: Historical perspectives, histochemical methods and cell kinetics. *Histochem J* 27, 339-369.
- Donovan, M.H., Yazdani, U., Norris, R.D., Games, D., German, D.C., and Eisch, A.J. (2006). Decreased adult hippocampal neurogenesis in the PDAPP mouse model of Alzheimer's disease. *J Comp Neurol* 495, 70-83.

- Dos Santos Picanco, L.C., Ozela, P.F., De Fatima De Brito Brito, M., Pinheiro, A.A., Padilha, E.C., Braga, F.S., De Paula Da Silva, C.H.T., Dos Santos, C.B.R., Rosa, J.M.C., and Da Silva Hage-Melim, L.I. (2018). Alzheimer's Disease: A Review from the Pathophysiology to Diagnosis, New Perspectives for Pharmacological Treatment. *Curr Med Chem* 25, 3141-3159.
- Duda, T., Fik-Rymarkiewicz, E., Venkataraman, V., Krishnan, A., and Sharma, R.K. (2004). Calcium-modulated ciliary membrane guanylate cyclase transduction machinery: constitution and operational principles. *Mol Cell Biochem* 267, 107-122.
- Dunham, N.W., and Miya, T.S. (1957). A note on a simple apparatus for detecting neurological deficit in rats and mice. *J Am Pharm Assoc Am Pharm Assoc* 46, 208-209.
- Eriksson, P.S., Perfilieva, E., Bjork-Eriksson, T., Alborn, A.M., Nordborg, C., Peterson, D.A., and Gage, F.H. (1998). Neurogenesis in the adult human hippocampus. *Nat Med* 4, 1313-1317.
- Evsyukova, I., Plestant, C., and Anton, E.S. (2013). Integrative mechanisms of oriented neuronal migration in the developing brain. *Annu Rev Cell Dev Biol* 29, 299-353.
- Fan, L., and Simard, L.R. (2002). Survival motor neuron (SMN) protein: role in neurite outgrowth and neuromuscular maturation during neuronal differentiation and development. *Hum Mol Genet* 11, 1605-1614.
- Feldkotter, M., Schwarzer, V., Wirth, R., Wienker, T.F., and Wirth, B. (2002). Quantitative analyses of SMN1 and SMN2 based on real-time lightCycler PCR: fast and highly reliable carrier testing and prediction of severity of spinal muscular atrophy. *Am J Hum Genet* 70, 358-368.
- Ferri, A.L., Cavallaro, M., Braida, D., Di Cristofano, A., Canta, A., Vezzani, A., Ottolenghi, S., Pandolfi, P.P., Sala, M., Debiasi, S., and Nicolis, S.K. (2004). Sox2 deficiency causes neurodegeneration and impaired neurogenesis in the adult mouse brain. *Development* 131, 3805-3819.
- Finkel, R.S., Mercuri, E., Darras, B.T., Connolly, A.M., Kuntz, N.L., Kirschner, J., Chiriboga, C.A., Saito, K., Servais, L., Tizzano, E., Topaloglu, H., Tulinius, M., Montes, J., Glanzman, A.M., Bishop, K., Zhong, Z.J., Gheuens, S., Bennett, C.F., Schneider, E., Farwell, W., De Vivo, D.C., and Group, E.S. (2017). Nusinersen versus Sham Control in Infantile-Onset Spinal Muscular Atrophy. *N Engl J Med* 377, 1723-1732.
- Finkel, R.S., Mercuri, E., Meyer, O.H., Simonds, A.K., Schroth, M.K., Graham, R.J., Kirschner, J., Iannaccone, S.T., Crawford, T.O., Woods, S., Muntoni, F., Wirth, B., Montes, J., Main, M., Mazzone, E.S., Vitale, M., Snyder, B., Quijano-Roy, S., Bertini, E., Davis, R.H., Qian, Y., Sejersen, T., and Group, S.M.a.C. (2018). Diagnosis and management of spinal muscular atrophy: Part 2: Pulmonary and acute care; medications, supplements and immunizations; other organ systems; and ethics. *Neuromuscul Disord* 28, 197-207.
- Fischer, U., Liu, Q., and Dreyfuss, G. (1997). The SMN-SIP1 complex has an essential role in spliceosomal snRNP biogenesis. *Cell* 90, 1023-1029.
- Friedman, J.I., Tang, C., Carpenter, D., Buchsbaum, M., Schmeidler, J., Flanagan, L., Golembo, S., Kanellopoulou, I., Ng, J., Hof, P.R., Harvey, P.D., Tsopelas, N.D., Stewart, D., and Davis, K.L. (2008). Diffusion tensor imaging findings in first-episode and chronic schizophrenia patients. *Am J Psychiatry* 165, 1024-1032.
- Fuss, J., Biedermann, S.V., Falfan-Melgoza, C., Auer, M.K., Zheng, L., Steinle, J., Horner, F., Sartorius, A., Ende, G., Weber-Fahr, W., and Gass, P. (2014). Exercise boosts hippocampal volume by preventing early age-related gray matter loss. *Hippocampus* 24, 131-134.
- Gage, G.J., Kipke, D.R., and Shain, W. (2012). Whole animal perfusion fixation for rodents. *J Vis Exp*.
- Gajera, C.R., Emich, H., Lioubinski, O., Christ, A., Beckervordersandforth-Bonk, R., Yoshikawa, K., Bachmann, S., Christensen, E.I., Gotz, M., Kempermann, G., Peterson, A.S., Willnow, T.E., and Hammes, A. (2010). LRP2 in ependymal cells regulates BMP signaling in the adult neurogenic niche. *J Cell Sci* 123, 1922-1930.

- Galderisi, S., Mucci, A., Buchanan, R.W., and Arango, C. (2018). Negative symptoms of schizophrenia: new developments and unanswered research questions. *Lancet Psychiatry* 5, 664-677.
- Galvao, J., Davis, B., Tilley, M., Normando, E., Duchon, M.R., and Cordeiro, M.F. (2014). Unexpected low-dose toxicity of the universal solvent DMSO. *FASEB J* 28, 1317-1330.
- Gao, S., Howard, S., and Lograsso, P.V. (2017). Pharmacological Inhibition of c-Jun N-terminal Kinase Reduces Food Intake and Sensitizes Leptin's Anorectic Signaling Actions. *Sci Rep* 7, 41795.
- Garbes, L., Riessland, M., Holker, I., Heller, R., Hauke, J., Trankle, C., Coras, R., Blumcke, I., Hahnen, E., and Wirth, B. (2009). LBH589 induces up to 10-fold SMN protein levels by several independent mechanisms and is effective even in cells from SMA patients non-responsive to valproate. *Hum Mol Genet* 18, 3645-3658.
- Genabai, N.K., Ahmad, S., Zhang, Z., Jiang, X., Gabaldon, C.A., and Gangwani, L. (2015). Genetic inhibition of JNK3 ameliorates spinal muscular atrophy. *Hum Mol Genet* 24, 6986-7004.
- Genin, E., Feingold, J., and Clerget-Darpoux, F. (2008). Identifying modifier genes of monogenic disease: strategies and difficulties. *Hum Genet* 124, 357-368.
- Gibson, E.M., Purger, D., Mount, C.W., Goldstein, A.K., Lin, G.L., Wood, L.S., Inema, I., Miller, S.E., Bieri, G., Zuchero, J.B., Barres, B.A., Woo, P.J., Vogel, H., and Monje, M. (2014). Neuronal activity promotes oligodendrogenesis and adaptive myelination in the mammalian brain. *Science* 344, 1252304.
- Girard, F., Venail, J., Schwaller, B., and Celio, M.R. (2015). The EF-hand Ca(2+)-binding protein super-family: a genome-wide analysis of gene expression patterns in the adult mouse brain. *Neuroscience* 294, 116-155.
- Gleeson, J.G., Lin, P.T., Flanagan, L.A., and Walsh, C.A. (1999). Doublecortin is a microtubule-associated protein and is expressed widely by migrating neurons. *Neuron* 23, 257-271.
- Goncalves, J.T., Schafer, S.T., and Gage, F.H. (2016). Adult Neurogenesis in the Hippocampus: From Stem Cells to Behavior. *Cell* 167, 897-914.
- Gould, E., and Cameron, H.A. (1996). Regulation of neuronal birth, migration and death in the rat dentate gyrus. *Dev Neurosci* 18, 22-35.
- Gould, E., Tanapat, P., McEwen, B.S., Flugge, G., and Fuchs, E. (1998). Proliferation of granule cell precursors in the dentate gyrus of adult monkeys is diminished by stress. *Proc Natl Acad Sci U S A* 95, 3168-3171.
- Gusel'nikova, V.V., and Korzhewskiy, D.E. (2015). NeuN As a Neuronal Nuclear Antigen and Neuron Differentiation Marker. *Acta Naturae* 7, 42-47.
- Hahnen, E., Forkert, R., Marke, C., Rudnik-Schoneborn, S., Schonling, J., Zerres, K., and Wirth, B. (1995). Molecular analysis of candidate genes on chromosome 5q13 in autosomal recessive spinal muscular atrophy: evidence of homozygous deletions of the SMN gene in unaffected individuals. *Hum Mol Genet* 4, 1927-1933.
- Harvey, P.D., Siever, L.J., Huang, G.D., Muralidhar, S., Zhao, H., Miller, P., Aslan, M., Mane, S., Mcnamara, M., Gleason, T., Brophy, M., Przygodzki, R., O'leary, T.J., Gaziano, M., and Concato, J. (2014). The genetics of functional disability in schizophrenia and bipolar illness: Methods and initial results for VA cooperative study #572. *Am J Med Genet B Neuropsychiatr Genet* 165B, 381-389.
- Hidaka, H., and Okazaki, K. (1993). Neurocalcin family: a novel calcium-binding protein abundant in bovine central nervous system. *Neurosci Res* 16, 73-77.
- Hinderer, C., Katz, N., Buza, E.L., Dyer, C., Goode, T., Bell, P., Richman, L.K., and Wilson, J.M. (2018). Severe Toxicity in Nonhuman Primates and Piglets Following High-Dose Intravenous Administration of an Adeno-Associated Virus Vector Expressing Human SMN. *Hum Gene Ther* 29, 285-298.
- Hirai, S., Katoh, M., Terada, M., Kyriakis, J.M., Zon, L.I., Rana, A., Avruch, J., and Ohno, S. (1997). MST/MLK2, a member of the mixed lineage kinase family, directly phosphorylates and activates SEK1, an activator of c-Jun N-terminal kinase/stress-activated protein kinase. *J Biol Chem* 272, 15167-15173.

- Hirai, S., Kawaguchi, A., Hirasawa, R., Baba, M., Ohnishi, T., and Ohno, S. (2002). MAPK-upstream protein kinase (MUK) regulates the radial migration of immature neurons in telencephalon of mouse embryo. *Development* 129, 4483-4495.
- Hochgerner, H., Zeisel, A., Lonnerberg, P., and Linnarsson, S. (2018). Conserved properties of dentate gyrus neurogenesis across postnatal development revealed by single-cell RNA sequencing. *Nat Neurosci* 21, 290-299.
- Hoffmann, J. (1893). Dritter Beitrag zur Lehre von der hereditären progressiven spinalen Muskelatrophie im Kindesalter. *Dtsch Z Nervenheilk* 18, 217-222.
- Honsho, M., Mitoma, J.Y., and Ito, A. (1998). Retention of cytochrome b5 in the endoplasmic reticulum is transmembrane and luminal domain-dependent. *J Biol Chem* 273, 20860-20866.
- HosseiniBarkooie, S., Peters, M., Torres-Benito, L., Rastetter, R.H., Hupperich, K., Hoffmann, A., Mendoza-Ferreira, N., Kaczmarek, A., Janzen, E., Milbradt, J., Lamkemeyer, T., Rigo, F., Bennett, C.F., Guschlbauer, C., Buschges, A., Hammerschmidt, M., Riessland, M., Kye, M.J., Clemen, C.S., and Wirth, B. (2016). The Power of Human Protective Modifiers: PLS3 and CORO1C Unravel Impaired Endocytosis in Spinal Muscular Atrophy and Rescue SMA Phenotype. *Am J Hum Genet* 99, 647-665.
- HosseiniBarkooie, S., Schneider, S., and Wirth, B. (2017). Advances in understanding the role of disease-associated proteins in spinal muscular atrophy. *Expert Rev Proteomics* 14, 581-592.
- Hua, Y., Sahashi, K., Hung, G., Rigo, F., Passini, M.A., Bennett, C.F., and Krainer, A.R. (2010). Antisense correction of SMN2 splicing in the CNS rescues necrosis in a type III SMA mouse model. *Genes Dev* 24, 1634-1644.
- Huang, L.W., Simonnet, J., Nassar, M., Richevaux, L., Lofredi, R., and Fricker, D. (2017). Laminar Localization and Projection-Specific Properties of Presubicular Neurons Targeting the Lateral Mammillary Nucleus, Thalamus, or Medial Entorhinal Cortex. *eNeuro* 4.
- Iino, S., Kobayashi, S., Okazaki, K., and Hidaka, H. (1995). Neurocalcin-immunoreactive receptor cells in the rat olfactory epithelium and vomeronasal organ. *Neurosci Lett* 191, 91-94.
- International Mouse Phenotype Consortium (2016). *Ncald* homozygous knockout.
- Isaksson, H.S., Sorbe, B., and Nilsson, T.K. (2014). Whole genome expression profiling of blood cells in ovarian cancer patients -prognostic impact of the CYP1B1, MTSS1, NCALD, and NOP14. *Oncotarget* 5, 4040-4049.
- Ivings, L., Pennington, S.R., Jenkins, R., Weiss, J.L., and Burgoyne, R.D. (2002). Identification of Ca²⁺-dependent binding partners for the neuronal calcium sensor protein neurocalcin delta: interaction with actin, clathrin and tubulin. *Biochem J* 363, 599-608.
- Janzen, E., Mendoza-Ferreira, N., HosseiniBarkooie, S., Schneider, S., Hupperich, K., Tschanz, T., Grysko, V., Riessland, M., Hammerschmidt, M., Rigo, F., Bennett, C.F., Kye, M.J., Torres-Benito, L., and Wirth, B. (2018). CHP1 reduction ameliorates spinal muscular atrophy pathology by restoring calcineurin activity and endocytosis. *Brain*.
- Jiao, Y., Chen, R., Ke, X., Cheng, L., Chu, K., Lu, Z., and Herskovits, E.H. (2012). Single nucleotide polymorphisms predict symptom severity of autism spectrum disorder. *J Autism Dev Disord* 42, 971-983.
- Kaksonen, M., and Roux, A. (2018). Mechanisms of clathrin-mediated endocytosis. *Nat Rev Mol Cell Biol* 19, 313-326.
- Kalus, P., Braak, H., Braak, E., and Bohl, J. (1989). The presubicular region in Alzheimer's disease: topography of amyloid deposits and neurofibrillary changes. *Brain Res* 494, 198-203.
- Kamiyama, M., Kobayashi, M., Araki, S., Iida, A., Tsunoda, T., Kawai, K., Imanishi, M., Nomura, M., Babazono, T., Iwamoto, Y., Kashiwagi, A., Kaku, K., Kawamori, R., Ng, D.P., Hansen, T., Gaede, P., Pedersen, O., Nakamura, Y., and Maeda, S. (2007). Polymorphisms in the 3' UTR in the neurocalcin delta gene affect mRNA stability, and confer susceptibility to diabetic nephropathy. *Hum Genet* 122, 397-407.

- Kashima, T., and Manley, J.L. (2003). A negative element in SMN2 exon 7 inhibits splicing in spinal muscular atrophy. *Nat Genet* 34, 460-463.
- Kempermann, G., Gage, F.H., Aigner, L., Song, H., Curtis, M.A., Thuret, S., Kuhn, H.G., Jessberger, S., Frankland, P.W., Cameron, H.A., Gould, E., Hen, R., Abrous, D.N., Toni, N., Schinder, A.F., Zhao, X., Lucassen, P.J., and Frisen, J. (2018). Human Adult Neurogenesis: Evidence and Remaining Questions. *Cell Stem Cell* 23, 25-30.
- Kerner, B. (2014). Genetics of bipolar disorder. *Appl Clin Genet* 7, 33-42.
- Kim, K.S., Kobayashi, M., Takamatsu, K., and Tzingounis, A.V. (2012). Hippocalcin and KCNQ channels contribute to the kinetics of the slow afterhyperpolarization. *Biophys J* 103, 2446-2454.
- Kobayashi, M., Takamatsu, K., Saitoh, S., Miura, M., and Noguchi, T. (1993). Molecular cloning of hippocalcin, a novel calcium-binding protein of the recoverin family exclusively expressed in hippocampus. *Biochem Biophys Res Commun* 196, 1017.
- Kolb, S.J., and Kissel, J.T. (2011). Spinal muscular atrophy: a timely review. *Arch Neurol* 68, 979-984.
- Kononenko, N.L., Classen, G.A., Kuijpers, M., Puchkov, D., Maritzen, T., Tempes, A., Malik, A.R., Skalecka, A., Bera, S., Jaworski, J., and Haucke, V. (2017). Retrograde transport of TrkB-containing autophagosomes via the adaptor AP-2 mediates neuronal complexity and prevents neurodegeneration. *Nat Commun* 8, 14819.
- Koudelka, S., Voas, M.G., Almeida, R.G., Baraban, M., Soetaert, J., Meyer, M.P., Talbot, W.S., and Lyons, D.A. (2016). Individual Neuronal Subtypes Exhibit Diversity in CNS Myelination Mediated by Synaptic Vesicle Release. *Curr Biol* 26, 1447-1455.
- Krishnan, A., Venkataraman, V., Fik-Rymarkiewicz, E., Duda, T., and Sharma, R.K. (2004). Structural, biochemical, and functional characterization of the calcium sensor neurocalcin delta in the inner retinal neurons and its linkage with the rod outer segment membrane guanylate cyclase transduction system. *Biochemistry* 43, 2708-2723.
- Kumar, V.D., Vijay-Kumar, S., Krishnan, A., Duda, T., and Sharma, R.K. (1999). A second calcium regulator of rod outer segment membrane guanylate cyclase, ROS-GC1: neurocalcin. *Biochemistry* 38, 12614-12620.
- Ladant, D. (1995). Calcium and membrane binding properties of bovine neurocalcin delta expressed in Escherichia coli. *J Biol Chem* 270, 3179-3185.
- Lang, J., Maeda, Y., Bannerman, P., Xu, J., Horiuchi, M., Pleasure, D., and Guo, F. (2013). Adenomatous polyposis coli regulates oligodendroglial development. *J Neurosci* 33, 3113-3130.
- Lawrenson, I.D., Krebs, D.L., Linossi, E.M., Zhang, J.G., McLennan, T.J., Collin, C., Mcrae, H.M., Kolesnik, T.B., Koh, K., Britto, J.M., Kueh, A.J., Sheikh, B.N., El-Saafin, F., Nicola, N.A., Tan, S.S., Babon, J.J., Nicholson, S.E., Alexander, W.S., Thomas, T., and Voss, A.K. (2017). Cortical Layer Inversion and Deregulation of Reelin Signaling in the Absence of SOCS6 and SOCS7. *Cereb Cortex* 27, 576-588.
- Leekam, S. (2016). Social cognitive impairment and autism: what are we trying to explain? *Philos Trans R Soc Lond B Biol Sci* 371, 20150082.
- Lefebvre, S., Burglen, L., Frezal, J., Munnich, A., and Melki, J. (1998). The role of the SMN gene in proximal spinal muscular atrophy. *Hum Mol Genet* 7, 1531-1536.
- Lefebvre, S., Burglen, L., Reboullet, S., Clermont, O., Burlet, P., Viollet, L., Benichou, B., Cruaud, C., Millasseau, P., Zeviani, M., and Et Al. (1995). Identification and characterization of a spinal muscular atrophy-determining gene. *Cell* 80, 155-165.
- Lefebvre, S., Burlet, P., Liu, Q., Bertrand, S., Clermont, O., Munnich, A., Dreyfuss, G., and Melki, J. (1997). Correlation between severity and SMN protein level in spinal muscular atrophy. *Nat Genet* 16, 265-269.
- Lin, X., Sikkink, R.A., Rusnak, F., and Barber, D.L. (1999). Inhibition of calcineurin phosphatase activity by a calcineurin B homologous protein. *J Biol Chem* 274, 36125-36131.
- Linarsson Lab (2018). Dentate gyrus- *Ncald*.
- Linder, C.C. (2006). Genetic variables that influence phenotype. *ILAR J* 47, 132-140.

- Liu, Q., and Dreyfuss, G. (1996). A novel nuclear structure containing the survival of motor neurons protein. *Embo J* 15, 3555-3565.
- Lopez-Domenech, G., Higgs, N.F., Vaccaro, V., Ros, H., Arancibia-Carcamo, I.L., Macaskill, A.F., and Kittler, J.T. (2016). Loss of Dendritic Complexity Precedes Neurodegeneration in a Mouse Model with Disrupted Mitochondrial Distribution in Mature Dendrites. *Cell Rep* 17, 317-327.
- Lorson, C.L., Hahnen, E., Androphy, E.J., and Wirth, B. (1999). A single nucleotide in the SMN gene regulates splicing and is responsible for spinal muscular atrophy. *Proc Natl Acad Sci U S A* 96, 6307-6311.
- Love, M.I., Huber, W., and Anders, S. (2014). Moderated estimation of fold change and dispersion for RNA-seq data with DESeq2. *Genome Biol* 15, 550.
- Lunke, S., and El-Osta, A. (2013). Applicability of histone deacetylase inhibition for the treatment of spinal muscular atrophy. *Neurotherapeutics* 10, 677-687.
- Macdonald, S.C., Fleetwood, I.G., Hochman, S., Dodd, J.G., Cheng, G.K., Jordan, L.M., and Brownstone, R.M. (2003). Functional motor neurons differentiating from mouse multipotent spinal cord precursor cells in culture and after transplantation into transected sciatic nerve. *J Neurosurg* 98, 1094-1103.
- Madison, D.V., and Nicoll, R.A. (1982). Noradrenaline blocks accommodation of pyramidal cell discharge in the hippocampus. *Nature* 299, 636-638.
- Margueron, R., and Reinberg, D. (2011). The Polycomb complex PRC2 and its mark in life. *Nature* 469, 343-349.
- Mayor, S., and Pagano, R.E. (2007). Pathways of clathrin-independent endocytosis. *Nat Rev Mol Cell Biol* 8, 603-612.
- Mcwhorter, M.L., Monani, U.R., Burghes, A.H., and Beattie, C.E. (2003). Knockdown of the survival motor neuron (Smn) protein in zebrafish causes defects in motor axon outgrowth and pathfinding. *J Cell Biol* 162, 919-931.
- Mendell, J.R., Al-Zaidy, S., Shell, R., Arnold, W.D., Rodino-Klapac, L.R., Prior, T.W., Lowes, L., Alfano, L., Berry, K., Church, K., Kissel, J.T., Nagendran, S., L'italien, J., Sproule, D.M., Wells, C., Cardenas, J.A., Heitzer, M.D., Kaspar, A., Corcoran, S., Braun, L., Likhite, S., Miranda, C., Meyer, K., Foust, K.D., Burghes, A.H.M., and Kaspar, B.K. (2017). Single-Dose Gene-Replacement Therapy for Spinal Muscular Atrophy. *N Engl J Med* 377, 1713-1722.
- Mercuri, E., Darras, B.T., Chiriboga, C.A., Day, J.W., Campbell, C., Connolly, A.M., Iannaccone, S.T., Kirschner, J., Kuntz, N.L., Saito, K., Shieh, P.B., Tulinius, M., Mazzone, E.S., Montes, J., Bishop, K.M., Yang, Q., Foster, R., Gheuens, S., Bennett, C.F., Farwell, W., Schneider, E., De Vivo, D.C., Finkel, R.S., and Group, C.S. (2018a). Nusinersen versus Sham Control in Later-Onset Spinal Muscular Atrophy. *N Engl J Med* 378, 625-635.
- Mercuri, E., Finkel, R.S., Muntoni, F., Wirth, B., Montes, J., Main, M., Mazzone, E.S., Vitale, M., Snyder, B., Quijano-Roy, S., Bertini, E., Davis, R.H., Meyer, O.H., Simonds, A.K., Schroth, M.K., Graham, R.J., Kirschner, J., Iannaccone, S.T., Crawford, T.O., Woods, S., Qian, Y., Sejersen, T., and Group, S.M.a.C. (2018b). Diagnosis and management of spinal muscular atrophy: Part 1: Recommendations for diagnosis, rehabilitation, orthopedic and nutritional care. *Neuromuscul Disord* 28, 103-115.
- Miller, J.A., Nathanson, J., Franjic, D., Shim, S., Dalley, R.A., Shapouri, S., Smith, K.A., Sunkin, S.M., Bernard, A., Bennett, J.L., Lee, C.K., Hawrylycz, M.J., Jones, A.R., Amaral, D.G., Sestan, N., Gage, F.H., and Lein, E.S. (2013a). Conserved molecular signatures of neurogenesis in the hippocampal subgranular zone of rodents and primates. *Development* 140, 4633-4644.
- Miller, J.A., Woltjer, R.L., Goodenbour, J.M., Horvath, S., and Geschwind, D.H. (2013b). Genes and pathways underlying regional and cell type changes in Alzheimer's disease. *Genome Med* 5, 48.
- Miller, R.H. (2018). Calcium control of myelin sheath growth. *Nat Neurosci* 21, 2-3.
- Ming, G.L., and Song, H. (2011). Adult neurogenesis in the mammalian brain: significant answers and significant questions. *Neuron* 70, 687-702.

- Mohammad, H., Marchisella, F., Ortega-Martinez, S., Hollos, P., Eerola, K., Komulainen, E., Kuleskaya, N., Freemantle, E., Fagerholm, V., Savontous, E., Rauvala, H., Peterson, B.D., Van Praag, H., and Coffey, E.T. (2017). JNK1 controls adult hippocampal neurogenesis and imposes cell-autonomous control of anxiety behaviour from the neurogenic niche. *Mol Psychiatry*.
- Molyneaux, B.J., Arlotta, P., Menezes, J.R., and Macklis, J.D. (2007). Neuronal subtype specification in the cerebral cortex. *Nat Rev Neurosci* 8, 427-437.
- Mornet, D., and Bonet-Kerrache, A. (2001). Neurocalcin-actin interaction. *Biochim Biophys Acta* 1549, 197-203.
- Movsas, T.Z., Pinto-Martin, J.A., Whitaker, A.H., Feldman, J.F., Lorenz, J.M., Korzeniewski, S.J., Levy, S.E., and Paneth, N. (2013). Autism spectrum disorder is associated with ventricular enlargement in a low birth weight population. *J Pediatr* 163, 73-78.
- Mullis, K., Faloona, F., Scharf, S., Saiki, R., Horn, G., and Erlich, H. (1986). Specific enzymatic amplification of DNA in vitro: the polymerase chain reaction. *Cold Spring Harb Symp Quant Biol* 51 Pt 1, 263-273.
- Murray, C.E., Gami-Patel, P., Gkanatsiou, E., Brinkmalm, G., Portelius, E., Wirths, O., Heywood, W., Blennow, K., Ghiso, J., Holton, J.L., Mills, K., Zetterberg, H., Revesz, T., and Lashley, T. (2018). The presubiculum is preserved from neurodegenerative changes in Alzheimer's disease. *Acta Neuropathol Commun* 6, 62.
- Nadeau, J.H. (2001). Modifier genes in mice and humans. *Nat Rev Genet* 2, 165-174.
- Nakano, A., Terasawa, M., Watanabe, M., Usuda, N., Morita, T., and Hidaka, H. (1992). Neurocalcin, a novel calcium binding protein with three EF-hand domains, expressed in retinal amacrine cells and ganglion cells. *Biochem Biophys Res Commun* 186, 1207-1211.
- O'rourke, M., Gasperini, R., and Young, K.M. (2014). Adult myelination: wrapping up neuronal plasticity. *Neural Regen Res* 9, 1261-1264.
- Oikawa, K., Kimura, S., Aoki, N., Atsuta, Y., Takiyama, Y., Nagato, T., Yanai, M., Kobayashi, H., Sato, K., Sasajima, T., and Tateno, M. (2004). Neuronal calcium sensor protein visinin-like protein-3 interacts with microsomal cytochrome b5 in a Ca²⁺-dependent manner. *J Biol Chem* 279, 15142-15152.
- Oikawa, K., Odero, G.L., Nafez, S., Ge, N., Zhang, D., Kobayashi, H., Sate, K., Kimura, S., Tateno, M., and Albensi, B.C. (2016). Visinin-Like Protein-3 Modulates the Interaction Between Cytochrome b 5 and NADH-Cytochrome b 5 Reductase in a Ca(2+)-Dependent Manner. *Cell Biochem Biophys* 74, 449-457.
- Okazaki, K., Watanabe, M., Ando, Y., Hagiwara, M., Terasawa, M., and Hidaka, H. (1992). Full sequence of neurocalcin, a novel calcium-binding protein abundant in central nervous system. *Biochem Biophys Res Commun* 185, 147-153.
- Oprea, G.E., Krober, S., Mcwhorter, M.L., Rossoll, W., Muller, S., Krawczak, M., Bassell, G.J., Beattie, C.E., and Wirth, B. (2008). Plastin 3 is a protective modifier of autosomal recessive spinal muscular atrophy. *Science* 320, 524-527.
- Owen, M.J., O'donovan, M.C., Thapar, A., and Craddock, N. (2011). Neurodevelopmental hypothesis of schizophrenia. *Br J Psychiatry* 198, 173-175.
- Palczewski, K., Subbaraya, I., Gorczyca, W.A., Helekar, B.S., Ruiz, C.C., Ohguro, H., Huang, J., Zhao, X., Crabb, J.W., Johnson, R.S., and Et Al. (1994). Molecular cloning and characterization of retinal photoreceptor guanylyl cyclase-activating protein. *Neuron* 13, 395-404.
- Pan, Y.W., Wang, W., and Xia, Z. (2013). Assessment of adult neurogenesis in mice. *Curr Protoc Toxicol* Chapter 12, Unit 12 20.
- Pekny, M., and Pekna, M. (2014). Astrocyte reactivity and reactive astrogliosis: costs and benefits. *Physiol Rev* 94, 1077-1098.
- Pekny, M., and Pekna, M. (2016). Reactive gliosis in the pathogenesis of CNS diseases. *Biochim Biophys Acta* 1862, 483-491.
- Pletnikov, M.V., Ayhan, Y., Xu, Y., Nikolskaia, O., Ovanesov, M., Huang, H., Mori, S., Moran, T.H., and Ross, C.A. (2008). Enlargement of the lateral ventricles in mutant DISC1 transgenic mice. *Mol Psychiatry* 13, 115.

- Porteros, A., Brinon, J.G., Crespo, C., Okazaki, K., Hidaka, H., Aijon, J., and Alonso, J.R. (1996). Neurocalcin immunoreactivity in the rat accessory olfactory bulb. *Brain Res* 729, 82-89.
- Power, P. (2015). Intervening early in bipolar disorder in young people: a review of the clinical staging model. *Ir J Psychol Med* 32, 31-43.
- Prior, T.W., Swoboda, K.J., Scott, H.D., and Hejmanowski, A.Q. (2004). Homozygous SMN1 deletions in unaffected family members and modification of the phenotype by SMN2. *Am J Med Genet* 130A, 307-310.
- Puthenveedu, M.A., Yudowski, G.A., and Von Zastrow, M. (2007). Endocytosis of neurotransmitter receptors: location matters. *Cell* 130, 988-989.
- Riessland, M., Ackermann, B., Forster, A., Jakubik, M., Hauke, J., Garbes, L., Fritzsche, I., Mende, Y., Blumcke, I., Hahnen, E., and Wirth, B. (2010). SAHA ameliorates the SMA phenotype in two mouse models for spinal muscular atrophy. *Hum Mol Genet* 19, 1492-1506.
- Riessland, M., Kaczmarek, A., Schneider, S., Swoboda, K.J., Lohr, H., Bradler, C., Grysko, V., Dimitriadi, M., Hosseinibarkoie, S., Torres-Benito, L., Peters, M., Upadhyay, A., Biglari, N., Krober, S., Holker, I., Garbes, L., Gilissen, C., Hoischen, A., Nurnberg, G., Nurnberg, P., Walter, M., Rigo, F., Bennett, C.F., Kye, M.J., Hart, A.C., Hammerschmidt, M., Kloppenburg, P., and Wirth, B. (2017). Neurocalcin Delta Suppression Protects against Spinal Muscular Atrophy in Humans and across Species by Restoring Impaired Endocytosis. *Am J Hum Genet* 100, 297-315.
- Rigo, F., Chun, S.J., Norris, D.A., Hung, G., Lee, S., Matson, J., Fey, R.A., Gaus, H., Hua, Y., Grundy, J.S., Krainer, A.R., Henry, S.P., and Bennett, C.F. (2014). Pharmacology of a central nervous system delivered 2'-O-methoxyethyl-modified survival of motor neuron splicing oligonucleotide in mice and non-human primates. *J Pharmacol Exp Ther*.
- Ripke, S., O'dushlaine, C., Chambert, K., Moran, J.L., Kahler, A.K., Akterin, S., Bergen, S.E., Collins, A.L., Crowley, J.J., Fromer, M., Kim, Y., Lee, S.H., Magnusson, P.K., Sanchez, N., Stahl, E.A., Williams, S., Wray, N.R., Xia, K., Bettella, F., Borglum, A.D., Bulik-Sullivan, B.K., Cormican, P., Craddock, N., De Leeuw, C., Durmishi, N., Gill, M., Golimbet, V., Hamshere, M.L., Holmans, P., Hougaard, D.M., Kendler, K.S., Lin, K., Morris, D.W., Mors, O., Mortensen, P.B., Neale, B.M., O'Neill, F.A., Owen, M.J., Milovancevic, M.P., Posthuma, D., Powell, J., Richards, A.L., Riley, B.P., Ruderfer, D., Rujescu, D., Sigurdsson, E., Silagadze, T., Smit, A.B., Stefansson, H., Steinberg, S., Suvisaari, J., Tosato, S., Verhage, M., Walters, J.T., Multicenter Genetic Studies of Schizophrenia, C., Levinson, D.F., Gejman, P.V., Kendler, K.S., Laurent, C., Mowry, B.J., O'donovan, M.C., Owen, M.J., Pulver, A.E., Riley, B.P., Schwab, S.G., Wildenauer, D.B., Dudbridge, F., Holmans, P., Shi, J., Albus, M., Alexander, M., Campion, D., Cohen, D., Dikeos, D., Duan, J., Eichhammer, P., Godard, S., Hansen, M., Lerer, F.B., Liang, K.Y., Maier, W., Mallet, J., Nertney, D.A., Nestadt, G., Norton, N., O'Neill, F.A., Papadimitriou, G.N., Ribble, R., Sanders, A.R., Silverman, J.M., Walsh, D., Williams, N.M., Wormley, B., Psychosis Endophenotypes International, C., Arranz, M.J., Bakker, S., Bender, S., Bramon, E., Collier, D., Crespo-Facorro, B., et al. (2013). Genome-wide association analysis identifies 13 new risk loci for schizophrenia. *Nat Genet* 45, 1150-1159.
- Rodrigues, N.R., Owen, N., Talbot, K., Ignatius, J., Dubowitz, V., and Davies, K.E. (1995). Deletions in the survival motor neuron gene on 5q13 in autosomal recessive spinal muscular atrophy. *Hum Mol Genet* 4, 631-634.
- Rosenzweig, S., and Wojtowicz, J.M. (2011). Analyzing dendritic growth in a population of immature neurons in the adult dentate gyrus using laminar quantification of disjointed dendrites. *Front Neurosci* 5, 34.
- Rossoll, W., Jablonka, S., Andreassi, C., Kroning, A.K., Karle, K., Monani, U.R., and Sendtner, M. (2003). Smn, the spinal muscular atrophy-determining gene product, modulates axon growth and localization of beta-actin mRNA in growth cones of motoneurons. *J Cell Biol* 163, 801-812.

- Sah, P. (1996). Ca²⁺-activated K⁺ currents in neurones: types, physiological roles and modulation. *Trends Neurosci* 19, 150-154.
- Salzer, J.L. (2015). Schwann cell myelination. *Cold Spring Harb Perspect Biol* 7, a020529.
- Sankaran, V.G., Lettre, G., Orkin, S.H., and Hirschhorn, J.N. (2010). Modifier genes in Mendelian disorders: the example of hemoglobin disorders. *Ann N Y Acad Sci* 1214, 47-56.
- Santarelli, L., Saxe, M., Gross, C., Surget, A., Battaglia, F., Dulawa, S., Weisstaub, N., Lee, J., Duman, R., Arancio, O., Belzung, C., and Hen, R. (2003). Requirement of hippocampal neurogenesis for the behavioral effects of antidepressants. *Science* 301, 805-809.
- Schaeffer, J., Tannahill, D., Cioni, J.M., Rowlands, D., and Keynes, R. (2018). Identification of the extracellular matrix protein Fibulin-2 as a regulator of spinal nerve organization. *Dev Biol* 442, 101-114.
- Schmid, E.M., and McMahon, H.T. (2007). Integrating molecular and network biology to decode endocytosis. *Nature* 448, 883-888.
- Scholzen, T., and Gerdes, J. (2000). The Ki-67 protein: from the known and the unknown. *J Cell Physiol* 182, 311-322.
- Shi, L., Fu, A.K., and Ip, N.Y. (2012). Molecular mechanisms underlying maturation and maintenance of the vertebrate neuromuscular junction. *Trends Neurosci* 35, 441-453.
- Shi, X., Ma, C., Zhu, Q., Yuan, D., Sun, M., Gu, X., Wu, G., Lv, T., and Song, Y. (2016). Upregulation of long intergenic noncoding RNA 00673 promotes tumor proliferation via LSD1 interaction and repression of NCALD in non-small-cell lung cancer. *Oncotarget* 7, 25558-25575.
- Shimohama, S., Chachin, M., Taniguchi, T., Hidaka, H., and Kimura, J. (1996). Changes of neurocalcin, a calcium-binding protein, in the brain of patients with Alzheimer's disease. *Brain Res* 716, 233-236.
- Shinozaki, G., and Potash, J.B. (2014). New developments in the genetics of bipolar disorder. *Curr Psychiatry Rep* 16, 493.
- Sim, K., Dewitt, I., Ditman, T., Zalesak, M., Greenhouse, I., Goff, D., Weiss, A.P., and Heckers, S. (2006). Hippocampal and parahippocampal volumes in schizophrenia: a structural MRI study. *Schizophr Bull* 32, 332-340.
- Simonnet, J., Eugene, E., Cohen, I., Miles, R., and Fricker, D. (2013). Cellular neuroanatomy of rat presubiculum. *Eur J Neurosci* 37, 583-597.
- Singh, N.K., Singh, N.N., Androphy, E.J., and Singh, R.N. (2006). Splicing of a critical exon of human survival motor neuron is regulated by a unique silencer element located in the last intron. *Mol Cell Biol* 26, 1333-1346.
- Smith, G.N., Thornton, A.E., Lang, D.J., Macewan, G.W., Ehmann, T.S., Kopala, L.C., Tee, K., Shiau, G., Voineskos, A.N., Kennedy, J.L., and Honer, W.G. (2012). Hippocampal volume and the brain-derived neurotrophic factor Val66Met polymorphism in first episode psychosis. *Schizophr Res* 134, 253-259.
- Snyder, J.S., Choe, J.S., Clifford, M.A., Jeurling, S.I., Hurley, P., Brown, A., Kamhi, J.F., and Cameron, H.A. (2009). Adult-born hippocampal neurons are more numerous, faster maturing, and more involved in behavior in rats than in mice. *J Neurosci* 29, 14484-14495.
- Somers, E., Riessland, M., Schreml, J., Wirth, B., Gillingwater, T.H., and Parson, S.H. (2013). Increasing SMN levels using the histone deacetylase inhibitor SAHA ameliorates defects in skeletal muscle microvasculature in a mouse model of severe spinal muscular atrophy. *Neurosci Lett* 544, 100-104.
- Sorrells, S.F., Paredes, M.F., Cebrian-Silla, A., Sandoval, K., Qi, D., Kelley, K.W., James, D., Mayer, S., Chang, J., Auguste, K.I., Chang, E.F., Gutierrez, A.J., Kriegstein, A.R., Mathern, G.W., Oldham, M.C., Huang, E.J., Garcia-Verdugo, J.M., Yang, Z., and Alvarez-Buylla, A. (2018). Human hippocampal neurogenesis drops sharply in children to undetectable levels in adults. *Nature* 555, 377-381.
- Spitzer, N.C. (2006). Electrical activity in early neuronal development. *Nature* 444, 707-712.
- Sumner, C.J., and Crawford, T.O. (2018). Two breakthrough gene-targeted treatments for spinal muscular atrophy: challenges remain. *J Clin Invest* 128, 3219-3227.

- Talbot, K., and Tizzano, E.F. (2017). The clinical landscape for SMA in a new therapeutic era. *Gene Ther* 24, 529-533.
- Tanapat, P., Galea, L.A., and Gould, E. (1998). Stress inhibits the proliferation of granule cell precursors in the developing dentate gyrus. *Int J Dev Neurosci* 16, 235-239.
- Terasawa, M., Nakano, A., Kobayashi, R., and Hidaka, H. (1992). Neurocalcin: a novel calcium-binding protein from bovine brain. *J Biol Chem* 267, 19596-19599.
- Toni, N., and Schinder, A.F. (2015). Maturation and Functional Integration of New Granule Cells into the Adult Hippocampus. *Cold Spring Harb Perspect Biol* 8, a018903.
- Toth, A.B., Shum, A.K., and Prakriya, M. (2016). Regulation of neurogenesis by calcium signaling. *Cell Calcium* 59, 124-134.
- Tripathi, A., Kar, S.K., and Shukla, R. (2018). Cognitive Deficits in Schizophrenia: Understanding the Biological Correlates and Remediation Strategies. *Clin Psychopharmacol Neurosci* 16, 7-17.
- Tzingounis, A.V., Kobayashi, M., Takamatsu, K., and Nicoll, R.A. (2007). Hippocalcin gates the calcium activation of the slow afterhyperpolarization in hippocampal pyramidal cells. *Neuron* 53, 487-493.
- Venkataraman, V., Duda, T., Ravichandran, S., and Sharma, R.K. (2008). Neurocalcin delta modulation of ROS-GC1, a new model of Ca(2+) signaling. *Biochemistry* 47, 6590-6601.
- Vercauteren, F.G., Flores, G., Ma, W., Chabot, J.G., Geenen, L., Clerens, S., Fazel, A., Bergeron, J.J., Srivastava, L.K., Arckens, L., and Quirion, R. (2007). An organelle proteomic method to study neurotransmission-related proteins, applied to a neurodevelopmental model of schizophrenia. *Proteomics* 7, 3569-3579.
- Villalobos, C., and Andrade, R. (2010). Visinin-like neuronal calcium sensor proteins regulate the slow calcium-activated afterhyperpolarizing current in the rat cerebral cortex. *J Neurosci* 30, 14361-14365.
- Viviano, J., Krishnan, A., Wu, H., and Venkataraman, V. (2016a). Data on the calcium-induced mobility shift of myristoylated and non-myristoylated forms of neurocalcin delta. *Data Brief* 7, 630-633.
- Viviano, J., Krishnan, A., Wu, H., and Venkataraman, V. (2016b). Electrophoretic mobility shift in native gels indicates calcium-dependent structural changes of neuronal calcium sensor proteins. *Anal Biochem* 494, 93-100.
- Voineskos, A.N., Winterburn, J.L., Felsky, D., Pipitone, J., Rajji, T.K., Mulsant, B.H., and Chakravarty, M.M. (2015). Hippocampal (subfield) volume and shape in relation to cognitive performance across the adult lifespan. *Hum Brain Mapp* 36, 3020-3037.
- Wake, H., Lee, P.R., and Fields, R.D. (2011). Control of local protein synthesis and initial events in myelination by action potentials. *Science* 333, 1647-1651.
- Wake, H., Ortiz, F.C., Woo, D.H., Lee, P.R., Angulo, M.C., and Fields, R.D. (2015). Nonsynaptic junctions on myelinating glia promote preferential myelination of electrically active axons. *Nat Commun* 6, 7844.
- Wang, J., Gu, B.J., Masters, C.L., and Wang, Y.J. (2017). A systemic view of Alzheimer disease - insights from amyloid-beta metabolism beyond the brain. *Nat Rev Neurol* 13, 703.
- Wang, W., Zhou, Z., Zhao, W., Huang, Y., Tang, R., Ying, K., Xie, Y., and Mao, Y. (2001). Molecular cloning, mapping and characterization of the human neurocalcin delta gene (NCALD). *Biochim Biophys Acta* 1518, 162-167.
- Whyatt, C.P., and Torres, E.B. (2018). Autism Research: An Objective Quantitative Review of Progress and Focus Between 1994 and 2015. *Front Psychol* 9, 1526.
- Wilson, C., and Terry, A.V., Jr. (2010). Neurodevelopmental animal models of schizophrenia: role in novel drug discovery and development. *Clin Schizophr Relat Psychoses* 4, 124-137.
- Wirth, B., Garbes, L., and Riessland, M. (2013). How genetic modifiers influence the phenotype of spinal muscular atrophy and suggest future therapeutic approaches. *Curr Opin Genet Dev* 23, 330-338.

- Wolman, M.A., Liu, Y., Tawarayama, H., Shoji, W., and Halloran, M.C. (2004). Repulsion and attraction of axons by semaphorin3D are mediated by different neuropilins in vivo. *J Neurosci* 24, 8428-8435.
- Woo, C.J., Maier, V.K., Davey, R., Brennan, J., Li, G., Brothers, J., 2nd, Schwartz, B., Gordo, S., Kasper, A., Okamoto, T.R., Johansson, H.E., Mandefro, B., Sareen, D., Bialek, P., Chau, B.N., Bhat, B., Bullough, D., and Barsoum, J. (2017). Gene activation of SMN by selective disruption of lncRNA-mediated recruitment of PRC2 for the treatment of spinal muscular atrophy. *Proc Natl Acad Sci U S A* 114, E1509-E1518.
- Xu, W., Cohen-Woods, S., Chen, Q., Noor, A., Knight, J., Hosang, G., Parikh, S.V., De Luca, V., Tozzi, F., Muglia, P., Forte, J., Mcquillin, A., Hu, P., Gurling, H.M., Kennedy, J.L., McGuffin, P., Farmer, A., Strauss, J., and Vincent, J.B. (2014). Genome-wide association study of bipolar disorder in Canadian and UK populations corroborates disease loci including SYNE1 and CSMD1. *BMC Med Genet* 15, 2.
- Yamatani, H., Kawasaki, T., Mita, S., Inagaki, N., and Hirata, T. (2010). Proteomics analysis of the temporal changes in axonal proteins during maturation. *Dev Neurobiol* 70, 523-537.
- Zareba-Koziol, M., Szwajda, A., Dadlez, M., Wyslouch-Cieszynska, A., and Lalowski, M. (2014). Global analysis of S-nitrosylation sites in the wild type (APP) transgenic mouse brain-clues for synaptic pathology. *Mol Cell Proteomics* 13, 2288-2305.
- Zelazo, P.D., Markant, J.C., and Thomas, K.M. (2013). "Postnatal Brain Development". Oxford University Press).
- Zilkova, M., Koson, P., and Zilka, N. (2006). The hunt for dying neurons: insight into the neuronal loss in Alzheimer's disease. *Bratisl Lek Listy* 107, 366-373.

7 Appendix

Appendix Table 5 List of potential binding partners of NCALD (comparison between wildtype IPs and control IPs)

Gene names	Protein names	Number of Peptides	Student's t-test q-value	Student's t-test
<i>Plcl2</i>	Inactive phospholipase C-like protein 2	63	0,037	-9,483
<i>Ppfia3</i>	Liprin-alpha-3	96	0,015	-8,234
<i>Hpca</i>	Neuron-specific calcium-binding protein hippocalcin	20	0,000	-7,987
<i>Mast4</i>	Microtubule-associated serine/threonine-protein kinase 4	94	0,000	-7,525
<i>Rasip1</i>	Ras-interacting protein 1	39	0,000	-6,974
<i>Plcl1</i>	Inactive phospholipase C-like protein 1	48	0,021	-6,892
<i>Ncald</i>	Neurocalcin-delta	15	0,000	-6,336
<i>Tubgcp2</i>	Gamma-tubulin complex component 2	34	0,019	-6,093
<i>Ogdhl</i>	Oxoglutarate dehydrogenase-like	35	0,017	-5,983
<i>Tubg2</i>	Tubulin gamma-2 chain	24	0,000	-5,982
<i>Golga2</i>	Golgin subfamily A member 2	41	0,023	-5,912
<i>Tubgcp3</i>	Gamma-tubulin complex component 3	45	0,009	-5,832
<i>Pawr</i>	PRKC apoptosis WT1 regulator protein	19	0,000	-5,542
<i>Slc4a10</i>	Anion exchange protein;Sodium-driven chloride bicarbonate exchanger	24	0,041	-5,209
<i>Map3k10</i>	Mitogen-activated protein kinase kinase kinase 10	28	0,017	-5,074
<i>Ogdh</i>	2-oxoglutarate dehydrogenase, mitochondrial	37	0,026	-4,939
<i>Kpna1</i>	Importin subunit alpha-5;Importin subunit alpha-5, N-terminally processed	19	0,025	-4,518
<i>Tubgcp6</i>	Gamma-tubulin complex component 6	25	0,020	-4,441
<i>Fnbp1l</i>	Formin-binding protein 1-like	28	0,019	-4,384
<i>Mrps36</i>	28S ribosomal protein S36, mitochondrial	4	0,012	-4,352
<i>Osbpl2</i>	Oxysterol-binding protein-related protein 2	19	0,016	-4,180
<i>Rnmt</i>	mRNA cap guanine-N7 methyltransferase	14	0,045	-4,026

<i>Prkar1a</i>	cAMP-dependent protein kinase type I-alpha regulatory subunit;cAMP-dependent protein kinase type I-alpha regulatory subunit, N-terminally processed	9	0,021	-3,889
<i>Eno1</i>	Alpha-enolase	16	0,045	-3,839
<i>Tubgcp4</i>	Gamma-tubulin complex component 4	16	0,036	-3,767
<i>Psmc3</i>	26S proteasome non-ATPase regulatory subunit 3	15	0,048	-3,706
<i>Mzt2</i>	Mitotic-spindle organizing protein 2	5	0,021	-3,690
<i>Vsnl1</i>	Visinin-like protein 1	12	0,000	-3,689
<i>Fam21</i>	WASH complex subunit FAM21	21	0,048	-3,550
<i>Vcp</i>	Transitional endoplasmic reticulum ATPase	19	0,046	-3,502
<i>Fmn2</i>	Formin-2	10	0,010	-3,488
<i>Uchl1</i>	Ubiquitin carboxyl-terminal hydrolase isozyme L1	10	0,021	-3,467
<i>Tubg1</i>	Tubulin gamma-1 chain	24	0,019	-3,445
<i>Crmp1</i>	Dihydropyrimidinase-related protein 1	24	0,014	-3,408
<i>Vps45</i>	Vacuolar protein sorting-associated protein 45	26	0,022	-3,305
<i>Igf2r</i>	Cation-independent mannose-6-phosphate receptor	30	0,012	-3,302
<i>Stxbp1</i>	Syntaxin-binding protein 1	38	0,035	-3,200
<i>Cttn</i>	Src substrate cortactin	21	0,025	-3,192
<i>Atp2b3</i>	Calcium-transporting ATPase	34	0,022	-3,154
<i>M6pr</i>	Cation-dependent mannose-6-phosphate receptor	5	0,009	-3,114
<i>Soga3</i>	Protein SOGA3	16	0,023	-3,096
<i>Stx1a</i>	Syntaxin-1A	12	0,045	-2,989
<i>Hpcal1</i>	Hippocalcin-like protein 1	18	0,013	-2,963
<i>Cltb</i>	Clathrin light chain B	5	0,045	-2,959
<i>Sv2b</i>	Synaptic vesicle glycoprotein 2B	10	0,022	-2,907
<i>Ppp2r1a</i>	Serine/threonine-protein phosphatase 2A 65 kDa regulatory subunit A alpha isoform	26	0,020	-2,890
<i>Ppp2ca;Ppp2cb</i>	Serine/threonine-protein phosphatase 2A catalytic subunit alpha isoform;Serine/threonine-protein phosphatase 2A catalytic subunit beta isoform	9	0,018	-2,844
<i>Hbbt1;Hbb-bs</i>	Beta-globin	9	0,014	-2,838
<i>Dnm1</i>	Dynamin-1	41	0,020	-2,835

<i>Sept7</i>	Septin-7	26	0,031	-2,833
<i>Psm11</i>	26S proteasome non-ATPase regulatory subunit 11	13	0,041	-2,768
<i>Dpysl5</i>	Dihydropyrimidinase-related protein 5	15	0,023	-2,767
<i>Hspa4</i>	Heat shock 70 kDa protein 4	17	0,012	-2,709
<i>Slc6a17</i>	Sodium-dependent neutral amino acid transporter SLC6A17	8	0,042	-2,633
<i>sept3</i>	Neuronal-specific septin-3	7	0,021	-2,612
<i>Syn1</i>	Synapsin-1	18	0,045	-2,612
<i>Cltc</i>	Clathrin heavy chain;Clathrin heavy chain 1	61	0,041	-2,607
<i>Dctn2</i>	Dynactin subunit 2	16	0,026	-2,576
<i>Lima1</i>	LIM domain and actin-binding protein 1	17	0,034	-2,565
<i>Gorasp2</i>	Golgi reassembly-stacking protein 2	6	0,022	-2,474
<i>Gfap</i>	Glial fibrillary acidic protein	63	0,020	-2,468
<i>Stx6</i>	Syntaxin-6	6	0,023	-2,463
<i>Prkacb</i>	cAMP-dependent protein kinase catalytic subunit beta	13	0,037	-2,426
<i>Phactr1</i>	Phosphatase and actin regulator 1;Phosphatase and actin regulator	17	0,010	-2,425
<i>Prickle2</i>	Prickle-like protein 2	16	0,036	-2,405
<i>Specc1</i>	Cytospin-B	37	0,024	-2,393
<i>Stx16</i>	Syntaxin-16	5	0,036	-2,370
<i>Src</i>	Neuronal proto-oncogene tyrosine-protein kinase Src	13	0,023	-2,357
<i>Sort1</i>	Sortilin	10	0,000	-2,357
<i>C2cd2l</i>	C2 domain-containing protein 2-like	15	0,035	-2,357
<i>Ruvbl2</i>	RuvB-like 2	11	0,051	-2,342
<i>Coro1b</i>	Coronin-1B	15	0,045	-2,337
<i>Prdx6</i>	Peroxiredoxin-6	8	0,044	-2,278
<i>Scamp3</i>	Secretory carrier-associated membrane protein 3	4	0,020	-2,228
<i>sept11</i>	Septin-11	16	0,015	-2,219
<i>Snap25</i>	Synaptosomal-associated protein 25	20	0,023	-2,194
<i>Gabra1</i>	Gamma-aminobutyric acid receptor subunit alpha-1	8	0,040	-2,157
<i>Hspa2</i>	Heat shock-related 70 kDa protein 2	25	0,046	-2,155

<i>Ndrp2</i>	Protein NDRG2	7	0,045	-2,154
<i>Stxbp5</i>	Syntaxin-binding protein 5	6	0,022	-2,104
<i>Twf1</i>	Twinfilin-1	11	0,050	-2,099
<i>Strn4</i>	Striatin-4	12	0,035	-2,073
<i>Etl4;Skt</i>	Sickle tail protein	24	0,050	-2,051
<i>Pfn2</i>	Profilin-2;Profilin	4	0,046	-2,016
<i>Hsph1</i>	Heat shock protein 105 kDa	26	0,008	-2,000
<i>Adcy5</i>	Adenylate cyclase type 5	12	0,033	-1,990
<i>Itpka</i>	Inositol-trisphosphate 3-kinase A	30	0,036	-1,980
<i>Pdia3</i>	Protein disulfide-isomerase A3	23	0,045	-1,978
<i>Rab3a</i>	Ras-related protein Rab-3A	12	0,026	-1,974
<i>Lancl1</i>	LanC-like protein 1	10	0,013	-1,963
<i>Sec22b</i>	Vesicle-trafficking protein SEC22b	12	0,025	-1,936
<i>Add3</i>	Gamma-adducin	23	0,050	-1,873
<i>Ppp3ca</i>	Serine/threonine-protein phosphatase 2B catalytic subunit alpha isoform	25	0,024	-1,867
<i>Ywhaz</i>	14-3-3 protein zeta/delta	23	0,045	-1,863
<i>Basp1</i>	Brain acid soluble protein 1	20	0,012	-1,863
<i>Rtn1</i>	Reticulon-1	12	0,021	-1,862
<i>Stx1b</i>	Syntaxin-1B	18	0,041	-1,796
<i>Hspa4l</i>	Heat shock 70 kDa protein 4L	15	0,024	-1,791
<i>Phyhip</i>	Phytanoyl-CoA hydroxylase-interacting protein	7	0,019	-1,775
<i>Eef1g</i>	Elongation factor 1-gamma	4	0,022	-1,742
<i>Tpi1</i>	Triosephosphate isomerase	17	0,019	-1,684
<i>Tpm1</i>	Triosephosphate isomerase	37	0,020	-1,682
<i>Ywhaq</i>	14-3-3 protein theta	18	0,041	-1,625
<i>Ppp1r9b</i>	Neurabin-2	56	0,034	-1,606
<i>Map9</i>	Microtubule-associated protein 9	9	0,016	-1,598
<i>Rtn4</i>	Reticulon-4	17	0,025	-1,587
<i>Ppp2r2a</i>	Serine/threonine-protein phosphatase 2A 55 kDa regulatory subunit B alpha isoform	19	0,011	-1,577

<i>Stx7</i>	Syntaxin-7	7	0,037	-1,566
<i>Map6</i>	Microtubule-associated protein 6	64	0,024	-1,549
<i>Mapt</i>	Microtubule-associated protein;Microtubule-associated protein tau	19	0,045	-1,499
<i>Cep170</i>	Centrosomal protein of 170 kDa	22	0,009	-1,499
<i>Glul</i>	Glutamine synthetase	16	0,044	-1,442
<i>Eef1a1</i>	Elongation factor 1-alpha 1	14	0,020	-1,412
<i>Rimbp2</i>	RIMS-binding protein 2	9	0,034	-1,389
<i>Zc3h11a</i>	Zinc finger CCCH domain-containing protein 11A	25	0,045	-1,331
<i>Mark1</i>	Serine/threonine-protein kinase MARK1	31	0,035	-1,316
<i>Ahcyl1</i>	Putative adenosylhomocysteinase 2	11	0,044	-1,315
<i>Cyfp2</i>	Cytoplasmic FMR1-interacting protein 2	22	0,035	-1,306
<i>Ywhah</i>	14-3-3 protein eta	20	0,000	-1,296
<i>Nhs12</i>	NHS-like protein 2	8	0,044	-1,266
<i>Farp1</i>	FERM, RhoGEF and pleckstrin domain-containing protein 1	13	0,037	-1,197
<i>Eif3l</i>	Eukaryotic translation initiation factor 3 subunit L	13	0,017	-1,191
<i>Ruvbl1</i>	RuvB-like 1	11	0,000	-1,182
<i>Map2</i>	Microtubule-associated protein 2	90	0,024	-1,158
<i>Numb1</i>	Numb-like protein	10	0,031	-1,091
<i>Eif4b</i>	Eukaryotic translation initiation factor 4B	12	0,046	-1,082
<i>Eif3d</i>	Eukaryotic translation initiation factor 3 subunit D	15	0,025	-1,077
<i>Ywhag</i>	14-3-3 protein gamma;14-3-3 protein gamma, N-terminally processed	19	0,038	-1,067
<i>Pin1</i>	Peptidyl-prolyl cis-trans isomerase NIMA-interacting 1	9	0,050	-1,058
<i>Vamp2</i>	Vesicle-associated membrane protein 2	11	0,036	-1,012
<i>Rps24</i>	40S ribosomal protein S24	10	0,045	-0,952
<i>Prpf4</i>	U4/U6 small nuclear ribonucleoprotein Prp4	26	0,041	-0,845
<i>Frmd4a</i>	FERM domain-containing protein 4A	9	0,042	-0,836
<i>Hspa8</i>	Heat shock cognate 71 kDa protein	51	0,033	-0,759
<i>Syt1</i>	Synaptotagmin-1	31	0,021	-0,745
<i>Rab11b;Rab11a</i>	Ras-related protein Rab-11A;Ras-related protein Rab-11B	11	0,048	-0,660

<i>Poldip3</i>	Polymerase delta-interacting protein 3	24	0,032	-0,618
<i>Hspa5</i>	78 kDa glucose-regulated protein	38	0,035	-0,580
<i>Rpsa</i>	40S ribosomal protein SA	19	0,046	-0,579
<i>Rpl24</i>	60S ribosomal protein L24	9	0,035	-0,419

Appendix Table 6 List of potential binding partners of NCALD (comparison between wildtype IPs and control IPs)

Gene names	Protein names	Number of Peptides	Student's t-test q-value	Student's t-test Difference
<i>Ncald</i>	Neurocalcin-delta	15	0	-7,31515
<i>Ogdh</i>	2-oxoglutarate dehydrogenase, mitochondrial	37	0,0327273	-6,41476
<i>Ogdhl</i>	Oxoglutarate dehydrogenase-like	35	0,0453333	-6,39871
<i>Map3k10</i>	Mitogen-activated protein kinase kinase kinase 10	28	0,034	-5,47567
<i>Mical3</i>	Protein-methionine sulfoxide oxidase MICAL3	26	0,034	-4,2531
<i>Map1lc3a</i>	Microtubule-associated proteins 1A/1B light chain 3A	2	0,0303415	-3,86627
<i>Mrps36</i>	28S ribosomal protein S36, mitochondrial	4	0,0334884	-3,64041
<i>Bcas1</i>	Breast carcinoma-amplified sequence 1 homolog	11	0,0272	-3,10259
<i>Cald1</i>	Caldesmon 1	9	0,0432184	-2,92907
<i>Mapre3</i>	Microtubule-associated protein RP/EB family member 3	8	0,0487103	-2,87439
<i>Cnksr2</i>	Connector enhancer of kinase suppressor of ras 2	18	0,0479208	-2,77992
<i>Coro1a</i>	Coronin-1A;Coronin	13	0,0391707	-2,76407
<i>Cttn</i>	Src substrate cortactin	21	0,0488403	-2,75635
<i>Fmn2</i>	Formin-2	10	0,0422222	-2,75019
<i>Bin1</i>	Myc box-dependent-interacting protein 1	11	0,0453333	-2,72064
<i>Prkar1b</i>	cAMP-dependent protein kinase type I-beta regulatory subunit	8	0,0407143	-2,53287
<i>Syn1</i>	Synapsin-1	18	0,0327536	-2,51268
<i>Et14;Skt</i>	Sickle tail protein	24	0,0340952	-2,49628

<i>Epb4.1;Epb41</i>	Protein 4.1	13	0,0181333	-2,48325
<i>Cfl2</i>	Cofilin-2	15	0,0386988	-2,25772
<i>Tom1</i>	Target of Myb protein 1	13	0,0295556	-2,25181
<i>Eef2</i>	Elongation factor 2	11	0,0394359	-2,19836
<i>Epb4.1l1;Epb41l1</i>	Band 4.1-like protein 1	33	0,0311	-2,15104
<i>Basp1</i>	Brain acid soluble protein 1	20	0,0388571	-1,99575
<i>Caskin1</i>	Caskin-1	30	0,0491698	-1,98887
<i>Ndrp2</i>	Protein NDRG2	7	0,0355429	-1,98361
<i>Prkar1a</i>	cAMP-dependent protein kinase type I-alpha regulatory subunit;cAMP-dependent protein kinase type I-alpha regulatory subunit, N-terminally processed	9	0,046955	-1,96419
<i>Twf1</i>	Twinfilin-1	11	0,0380392	-1,94299
<i>Dlg1</i>	Disks large homolog 1	20	0,0442353	-1,92518
<i>Ppp1r12a</i>	Protein phosphatase 1 regulatory subunit 12A	51	0,0480354	-1,89061
<i>Lmnb1</i>	Lamin-B1	45	0,0367742	-1,85116
<i>Igsf8</i>	Immunoglobulin superfamily member 8	14	0,0347692	-1,84031
<i>Lmna</i>	Prelamin-A/C;Lamin-A/C	19	0,043956	-1,83684
<i>Pfn2</i>	Profilin-2;Profilin	4	0,035625	-1,81664
<i>Tppp</i>	Tubulin polymerization-promoting protein	10	0,0337313	-1,79444
<i>Tpi1</i>	Triosephosphate isomerase	17	0,0318974	-1,76422
<i>Epb41l3</i>	Band 4.1-like protein 3;Band 4.1-like protein 3, N-terminally processed	44	0,0322857	-1,76238
<i>Dnaja1</i>	DnaJ homolog subfamily A member 1	2	0,0359259	-1,74732
<i>Hspa4</i>	Heat shock 70 kDa protein 4	17	0,0399481	-1,74243
<i>Ppp1r9b</i>	Neurabin-2	56	0,0482593	-1,71205
<i>Tcerg1</i>	Transcription elongation regulator 1	19	0	-1,70047
<i>Tpm3-rs7;Tpm3</i>		32	0,0354054	-1,69956
<i>Frmf4a</i>	FERM domain-containing protein 4A	9	0,0368571	-1,69703
<i>Tubb3</i>	Tubulin beta-3 chain	21	0,035873	-1,69387
<i>Dbn1</i>	Drebrin	49	0,0353125	-1,69138

<i>Nedd4l</i>	E3 ubiquitin-protein ligase NEDD4-like	37	0,0466383	-1,59188
<i>Vamp1</i>	Vesicle-associated membrane protein 1	7	0,0379733	-1,583
<i>Tpm1</i>	Tropomyosin 1	39	0,0427273	-1,54761
<i>Cplx1</i>	Complexin-1	3	0,0352727	-1,54463
<i>Map6</i>	Microtubule-associated protein 6	64	0,0393103	-1,50765
<i>Tubb5</i>	Tubulin beta-5 chain	31	0,0373077	-1,49033
<i>Rtn3</i>	Reticulon-3	19	0,0312941	-1,48975
<i>Lancl1</i>	LanC-like protein 1	10	0,0403077	-1,48794
<i>Map2</i>	Microtubule-associated protein 2	90	0,0365882	-1,45668
<i>Map1b</i>	Microtubule-associated protein 1B;MAP1B heavy chain;MAP1 light chain LC1	72	0,0498824	-1,43293
<i>Pip4k2b</i>	Phosphatidylinositol 5-phosphate 4-kinase type-2 beta	9	0,0343111	-1,40607
<i>Bsn</i>	Protein bassoon	97	0,0422472	-1,38531
<i>Crmp1</i>	Dihydropyrimidinase-related protein 1	24	0,0392632	-1,37971
<i>Rtn4</i>	Reticulon-4	17	0,0461474	-1,37676
<i>Mapt</i>	Microtubule-associated protein;Microtubule-associated protein tau	19	0,0226667	-1,36019
<i>Dnm1</i>	Dynamin-1	41	0,0209231	-1,31479
<i>Ppp2r1a</i>	Serine/threonine-protein phosphatase 2A 65 kDa regulatory subunit A alpha isoform	26	0,0342424	-1,30918
<i>Ywhah</i>	14-3-3 protein eta	20	0,0376842	-1,29483
<i>Nefm</i>	Neurofilament medium polypeptide	67	0,03776	-1,2486
<i>Dpysl2</i>	Dihydropyrimidinase-related protein 2	32	0,0478165	-1,23457
<i>Hsph1</i>	Heat shock protein 105 kDa	26	0,0370492	-1,23167
<i>Prkacb</i>	cAMP-dependent protein kinase catalytic subunit beta	13	0,0388	-1,22705
<i>Mark2</i>	Serine/threonine-protein kinase MARK2	23	0,0496752	-1,19705
<i>Prdx5</i>	Peroxiredoxin-5, mitochondrial	12	0,0471398	-1,18734
<i>Hspa8</i>	Heat shock cognate 71 kDa protein	51	0,0302222	-1,17909
<i>Eef1a1</i>	Elongation factor 1-alpha 1	14	0,029619	-1,17311
<i>Srcin1</i>	SRC kinase-signaling inhibitor 1	83	0,0298333	-1,15808

<i>Tufm</i>	Elongation factor Tu, mitochondrial	7	0,0451959	-1,09875
<i>Nono</i>	Non-POU domain-containing octamer-binding protein	18	0,0336216	-1,09511
<i>Palm</i>	Paralemmin-1	8	0,047614	-1,0621
<i>Ppp2r2a</i>	Serine/threonine-protein phosphatase 2A 55 kDa regulatory subunit B alpha isoform	19	0,038383	-1,04175
<i>Spon1</i>	Spondin-1	9	0,0332353	-1,02584
<i>Plcb1</i>	1-phosphatidylinositol 4,5-bisphosphate phosphodiesterase beta-1	28	0,0247273	-1,0144
<i>Nefl</i>	Neurofilament light polypeptide	52	0,0493981	-0,971658
<i>Camk2b</i>	Calcium/calmodulin-dependent protein kinase type II subunit beta	35	0,0364516	-0,959005
<i>Dctn2</i>	Dynactin subunit 2	16	0,0325455	-0,933247
<i>Gm9242;Gm6793</i>		34	0,0437209	-0,931716
<i>Elavl3</i>	ELAV-like protein	18	0,0489231	-0,912036
<i>Ywhag</i>	14-3-3 protein gamma;14-3-3 protein gamma, N-terminally processed	19	0,0358904	-0,901483
<i>Glul</i>	Glutamine synthetase	16	0,0484	-0,898485
<i>Prickle2</i>	Prickle-like protein 2	16	0,0395918	-0,894818
<i>Pdia3</i>	Protein disulfide-isomerase A3	23	0,0394762	-0,890786
<i>Pin1</i>	Peptidyl-prolyl cis-trans isomerase NIMA-interacting 1	9	0,0272	-0,881037
<i>Agap2</i>	Arf-GAP with GTPase, ANK repeat and PH domain-containing protein 2	33	0,0373793	-0,869799
<i>Hnrnpm</i>	Heterogeneous nuclear ribonucleoprotein M	36	0,03845	-0,860689
<i>Ik</i>	Protein Red	30	0,0346667	-0,85973
<i>Eif4b</i>	Eukaryotic translation initiation factor 4B	12	0,0456667	-0,843805
<i>Cep170</i>	Centrosomal protein of 170 kDa	22	0,038	-0,828345
<i>Apba2</i>	Amyloid beta A4 precursor protein-binding family A member 2	3	0,0488889	-0,795023
<i>Ccar1</i>	Cell division cycle and apoptosis regulator protein 1	27	0,0484571	-0,771659
<i>Rab11b;Rab11a</i>	Ras-related protein Rab-11A;Ras-related protein Rab-11B	11	0,0375833	-0,77088
<i>Sf3b3</i>	Splicing factor 3B subunit 3	81	0,0484643	-0,76327
<i>Matr3</i>	Matrin-3	51	0,0483826	-0,763242
<i>Hspa5</i>	78 kDa glucose-regulated protein	38	0,037697	-0,758642
<i>Ruvbl1</i>	RuvB-like 1	11	0,0417778	-0,751209

<i>Arhgef2</i>	Rho guanine nucleotide exchange factor 2	31	0,0383051	-0,7358
<i>Csde1</i>	Cold shock domain-containing protein E1	10	0,0311304	-0,710271
<i>Rpl12</i>	60S ribosomal protein L12	8	0,031831	-0,646967
<i>Cpeb3</i>	Cytoplasmic polyadenylation element-binding protein 3	22	0,0362105	-0,587071
<i>Syncrip</i>	Heterogeneous nuclear ribonucleoprotein Q	34	0,0473818	-0,574904
<i>Ap2m1</i>	AP-2 complex subunit mu	31	0,017	-0,51694
<i>Mark3</i>	MAP/microtubule affinity-regulating kinase 3	26	0,0376667	-0,447166

Appendix Table 7 List of genes with significant differential expression upon *Ncald* deletion and strongly correlated with *Ncald* gene expression (Hippocampus)

Gene	log2FoldChange	adjusted P-value	Chr	Description	Type of relationship	rho
<i>Lrp2</i>	-0,432	0,0358	2	low density lipoprotein receptor-related protein 2 [Source:MGI Symbol;Acc:MGI:95794]	anti-correlation with <i>Ncald</i>	-0,674
<i>Ubl3</i>	0,153	0,0081	5	ubiquitin-like 3 [Source:MGI Symbol;Acc:MGI:1344373]	correlation with <i>Ncald</i>	0,812
<i>Sema3c</i>	0,309	0,0002	5	sema domain, immunoglobulin domain (Ig), short basic domain, secreted, (semaphorin) 3C [Source:MGI Symbol;Acc:MGI:107557]	correlation with <i>Ncald</i>	0,839
<i>Bok</i>	0,331	0,0001	1	BCL2-related ovarian killer [Source:MGI Symbol;Acc:MGI:1858494]	correlation with <i>Ncald</i>	0,611
<i>Ncald</i>	2,674	0,0000	15	neurocalcin delta [Source:MGI Symbol;Acc:MGI:1196326]	correlation with <i>Ncald</i>	1,000

Appendix Table 8 List of genes with significant differential expression upon *Ncald* deletion and strongly correlated with *Ncald* gene expression (Cortex)

Gene	log2FoldChange	Adjusted P-value	Chr	Description	Type of relationship	rho
<i>Ms4a15</i>	-3,604	0,024	19	membrane-spanning 4-domains, subfamily A, member 15 [Source:MGI Symbol;Acc:MGI:3617853]	anti-correlation with <i>Ncald</i>	-0,771
<i>Lhx8</i>	-3,014	0,001	3	LIM homeobox protein 8 [Source:MGI Symbol;Acc:MGI:1096343]	anti-correlation with <i>Ncald</i>	-0,811
<i>Gbx1</i>	-2,884	0,001	5	gastrulation brain homeobox 1 [Source:MGI Symbol;Acc:MGI:95667]	anti-correlation with <i>Ncald</i>	-0,796
<i>Ntrk1</i>	-2,559	0,026	3	neurotrophic tyrosine kinase, receptor, type 1 [Source:MGI Symbol;Acc:MGI:97383]	anti-correlation with <i>Ncald</i>	-0,789
<i>Gpx6</i>	-2,527	0,010	13	glutathione peroxidase 6 [Source:MGI Symbol;Acc:MGI:1922762]	anti-correlation with <i>Ncald</i>	-0,796
<i>Slc10a4</i>	-2,422	0,006	5	solute carrier family 10 (sodium/bile acid cotransporter family), member 4 [Source:MGI Symbol;Acc:MGI:3606480]	anti-correlation with <i>Ncald</i>	-0,789
<i>Serpina9</i>	-2,343	0,030	12	serine (or cysteine) peptidase inhibitor, clade A (alpha-1 antiproteinase, antitrypsin), member 9 [Source:MGI Symbol;Acc:MGI:1919157]	anti-correlation with <i>Ncald</i>	-0,718
<i>Gpr149</i>	-2,329	0,000	3	G protein-coupled receptor 149 [Source:MGI Symbol;Acc:MGI:2443628]	anti-correlation with <i>Ncald</i>	-0,886
<i>Isl1</i>	-2,292	0,000	13	ISL1 transcription factor, LIM/homeodomain [Source:MGI Symbol;Acc:MGI:101791]	anti-correlation with <i>Ncald</i>	-0,889
<i>Gdnf</i>	-2,167	0,000	15	glial cell line derived neurotrophic factor [Source:MGI Symbol;Acc:MGI:107430]	anti-correlation with <i>Ncald</i>	-0,804
<i>Chat</i>	-2,102	0,006	14	choline acetyltransferase [Source:MGI Symbol;Acc:MGI:88392]	anti-correlation with <i>Ncald</i>	-0,857
<i>Olfir1393</i>	-2,044	0,003	11	olfactory receptor 1393 [Source:MGI Symbol;Acc:MGI:3031227]	anti-correlation with <i>Ncald</i>	-0,721

<i>Drd2</i>	-2,032	0,030	9	dopamine receptor D2 [Source:MGI Symbol;Acc:MGI:94924]	anti-correlation with Ncald	- 0,757
<i>Nkx2-1</i>	-2,024	0,008	12	NK2 homeobox 1 [Source:MGI Symbol;Acc:MGI:108067]	anti-correlation with Ncald	- 0,800
<i>Cd4</i>	-2,024	0,040	6	CD4 antigen [Source:MGI Symbol;Acc:MGI:88335]	anti-correlation with Ncald	- 0,714
<i>Htr1d</i>	-1,988	0,001	4	5-hydroxytryptamine (serotonin) receptor 1D [Source:MGI Symbol;Acc:MGI:96276]	anti-correlation with Ncald	- 0,868
<i>Adora2a</i>	-1,988	0,030	10	adenosine A2a receptor [Source:MGI Symbol;Acc:MGI:99402]	anti-correlation with Ncald	- 0,739
<i>Hist1h2bq</i>	-1,987	0,005	13	histone cluster 1, H2bq [Source:MGI Symbol;Acc:MGI:3702051]	anti-correlation with Ncald	- 0,614
<i>Gm136</i>	-1,954	0,030	4	predicted gene 136 [Source:MGI Symbol;Acc:MGI:2684982]	anti-correlation with Ncald	- 0,786
<i>Slc35d3</i>	-1,954	0,004	10	solute carrier family 35, member D3 [Source:MGI Symbol;Acc:MGI:1923407]	anti-correlation with Ncald	- 0,750
<i>Th</i>	-1,944	0,037	7	tyrosine hydroxylase [Source:MGI Symbol;Acc:MGI:98735]	anti-correlation with Ncald	- 0,693
<i>Epyc</i>	-1,902	0,016	10	epiphycan [Source:MGI Symbol;Acc:MGI:107942]	anti-correlation with Ncald	- 0,825
<i>Slc5a7</i>	-1,872	0,007	17	solute carrier family 5 (choline transporter), member 7 [Source:MGI Symbol;Acc:MGI:1927126]	anti-correlation with Ncald	- 0,832
<i>Scn4b</i>	-1,863	0,048	9	sodium channel, type IV, beta [Source:MGI Symbol;Acc:MGI:2687406]	anti-correlation with Ncald	- 0,711
<i>Ecel1</i>	-1,842	0,023	1	endothelin converting enzyme-like 1 [Source:MGI Symbol;Acc:MGI:1343461]	anti-correlation with Ncald	- 0,804
<i>Slc18a3</i>	-1,841	0,020	14	solute carrier family 18 (vesicular monoamine), member 3 [Source:MGI Symbol;Acc:MGI:1101061]	anti-correlation with Ncald	- 0,836
<i>Rgs9</i>	-1,815	0,023	11	regulator of G-protein signaling 9 [Source:MGI Symbol;Acc:MGI:1338824]	anti-correlation with Ncald	- 0,789
<i>Sh3rf2</i>	-1,800	0,030	18	SH3 domain containing ring finger 2 [Source:MGI Symbol;Acc:MGI:2444628]	anti-correlation with Ncald	- 0,746

<i>Rarb</i>	-1,679	0,009		14	retinoic acid receptor, beta [Source:MGI Symbol;Acc:MGI:97857]	anti-correlation with Ncald	- 0,786
<i>Syndig1l</i>	-1,677	0,040		12	synapse differentiation inducing 1 like [Source:MGI Symbol;Acc:MGI:2685107]	anti-correlation with Ncald	- 0,718
<i>Six3</i>	-1,676	0,030		17	sine oculis-related homeobox 3 [Source:MGI Symbol;Acc:MGI:102764]	anti-correlation with Ncald	- 0,843
<i>Drd1</i>	-1,655	0,021		13	dopamine receptor D1 [Source:MGI Symbol;Acc:MGI:99578]	anti-correlation with Ncald	- 0,736
<i>Penk</i>	-1,647	0,030		4	preproenkephalin [Source:MGI Symbol;Acc:MGI:104629]	anti-correlation with Ncald	- 0,746
<i>Ngfr</i>	-1,606	0,030		11	nerve growth factor receptor (TNFR superfamily, member 16) [Source:MGI Symbol;Acc:MGI:97323]	anti-correlation with Ncald	- 0,750
<i>Tac1</i>	-1,600	0,008		6	tachykinin 1 [Source:MGI Symbol;Acc:MGI:98474]	anti-correlation with Ncald	- 0,736
<i>Il20ra</i>	-1,555	0,001		10	interleukin 20 receptor, alpha [Source:MGI Symbol;Acc:MGI:3605069]	anti-correlation with Ncald	- 0,829
<i>Pde10a</i>	-1,489	0,021		17	phosphodiesterase 10A [Source:MGI Symbol;Acc:MGI:1345143]	anti-correlation with Ncald	- 0,779
<i>Stk26</i>	-1,487	0,026	X		serine/threonine kinase 26 [Source:MGI Symbol;Acc:MGI:1917665]	anti-correlation with Ncald	- 0,732
<i>Ccdc187</i>	-1,486	0,012		2	coiled-coil domain containing 187 [Source:MGI Symbol;Acc:MGI:3045295]	anti-correlation with Ncald	- 0,886
<i>Ptpn7</i>	-1,417	0,016		1	protein tyrosine phosphatase, non-receptor type 7 [Source:MGI Symbol;Acc:MGI:2156893]	anti-correlation with Ncald	- 0,746
<i>Gpr139</i>	-1,415	0,009		7	G protein-coupled receptor 139 [Source:MGI Symbol;Acc:MGI:2685341]	anti-correlation with Ncald	- 0,786
<i>Gpr6</i>	-1,381	0,025		10	G protein-coupled receptor 6 [Source:MGI Symbol;Acc:MGI:2155249]	anti-correlation with Ncald	- 0,707
<i>Oprk1</i>	-1,347	0,001		1	opioid receptor, kappa 1 [Source:MGI Symbol;Acc:MGI:97439]	anti-correlation with Ncald	- 0,743
<i>Pbx3</i>	-1,312	0,004		2	pre B cell leukemia homeobox 3 [Source:MGI Symbol;Acc:MGI:97496]	anti-correlation with Ncald	- 0,771

<i>Nexn</i>	-1,291	0,027		3	nexilin [Source:MGI Symbol;Acc:MGI:1916060]	anti-correlation with Ncald	- 0,793
<i>Rem2</i>	-1,284	0,001		14	rad and gem related GTP binding protein 2 [Source:MGI Symbol;Acc:MGI:2155260]	anti-correlation with Ncald	- 0,736
<i>Gng7</i>	-1,281	0,004		10	guanine nucleotide binding protein (G protein), gamma 7 [Source:MGI Symbol;Acc:MGI:95787]	anti-correlation with Ncald	- 0,786
<i>Myo3b</i>	-1,281	0,032		2	myosin IIIB [Source:MGI Symbol;Acc:MGI:2448580]	anti-correlation with Ncald	- 0,657
<i>Gprin3</i>	-1,214	0,043		6	GPRIN family member 3 [Source:MGI Symbol;Acc:MGI:1924785]	anti-correlation with Ncald	- 0,679
<i>Gpr88</i>	-1,214	0,030		3	G-protein coupled receptor 88 [Source:MGI Symbol;Acc:MGI:1927653]	anti-correlation with Ncald	- 0,707
<i>Abhd11os</i>	-1,195	0,033		5	abhydrolase domain containing 11, opposite strand [Source:MGI Symbol;Acc:MGI:1917062]	anti-correlation with Ncald	- 0,654
<i>Ankdd1a</i>	-1,189	0,001		9	ankyrin repeat and death domain containing 1A [Source:MGI Symbol;Acc:MGI:2686319]	anti-correlation with Ncald	- 0,875
<i>Kcna5</i>	-1,189	0,005		6	potassium voltage-gated channel, shaker-related subfamily, member 5 [Source:MGI Symbol;Acc:MGI:96662]	anti-correlation with Ncald	- 0,836
<i>Klhl13</i>	-1,184	0,003	X		kelch-like 13 [Source:MGI Symbol;Acc:MGI:1914705]	anti-correlation with Ncald	- 0,786
<i>Stk32a</i>	-1,180	0,007		18	serine/threonine kinase 32A [Source:MGI Symbol;Acc:MGI:2442403]	anti-correlation with Ncald	- 0,775
<i>Musk</i>	-1,175	0,004		4	muscle, skeletal, receptor tyrosine kinase [Source:MGI Symbol;Acc:MGI:103581]	anti-correlation with Ncald	- 0,768
<i>Kcnh8</i>	-1,173	0,008		17	potassium voltage-gated channel, subfamily H (eag-related), member 8 [Source:MGI Symbol;Acc:MGI:2445160]	anti-correlation with Ncald	- 0,896
<i>Mme</i>	-1,130	0,000		3	membrane metallo endopeptidase [Source:MGI Symbol;Acc:MGI:97004]	anti-correlation with Ncald	- 0,818
<i>Strip2</i>	-1,121	0,007		6	striatin interacting protein 2 [Source:MGI Symbol;Acc:MGI:2444363]	anti-correlation with Ncald	- 0,786
<i>Dlx6</i>	-1,105	0,004		6	distal-less homeobox 6 [Source:MGI Symbol;Acc:MGI:101927]	anti-correlation with Ncald	- 0,750

<i>Asic4</i>	-1,077	0,015		1	acid-sensing (proton-gated) ion channel family member 4 [Source:MGI Symbol;Acc:MGI:2652846]	anti-correlation with Ncald	- 0,746
<i>Pcp4l1</i>	-1,050	0,021		1	Purkinje cell protein 4-like 1 [Source:MGI Symbol;Acc:MGI:1913675]	anti-correlation with Ncald	- 0,761
<i>Gpr83</i>	-1,046	0,004		9	G protein-coupled receptor 83 [Source:MGI Symbol;Acc:MGI:95712]	anti-correlation with Ncald	- 0,721
<i>Prkch</i>	-1,043	0,028		12	protein kinase C, eta [Source:MGI Symbol;Acc:MGI:97600]	anti-correlation with Ncald	- 0,746
<i>Adcy5</i>	-1,039	0,008		16	adenylate cyclase 5 [Source:MGI Symbol;Acc:MGI:99673]	anti-correlation with Ncald	- 0,725
<i>Pou3f4</i>	-1,030	0,008	X		POU domain, class 3, transcription factor 4 [Source:MGI Symbol;Acc:MGI:101894]	anti-correlation with Ncald	- 0,793
<i>Htr1b</i>	-1,019	0,002		9	5-hydroxytryptamine (serotonin) receptor 1B [Source:MGI Symbol;Acc:MGI:96274]	anti-correlation with Ncald	- 0,786
<i>Zfp503</i>	-0,996	0,030		14	zinc finger protein 503 [Source:MGI Symbol;Acc:MGI:1353644]	anti-correlation with Ncald	- 0,775
<i>Adamts3</i>	-0,986	0,001		5	a disintegrin-like and metallopeptidase (reprolysin type) with thrombospondin type 1 motif, 3 [Source:MGI Symbol;Acc:MGI:3045353]	anti-correlation with Ncald	- 0,793
<i>Pde1b</i>	-0,966	0,015		15	phosphodiesterase 1B, Ca ²⁺ -calmodulin dependent [Source:MGI Symbol;Acc:MGI:97523]	anti-correlation with Ncald	- 0,764
<i>Pde7b</i>	-0,961	0,015		10	phosphodiesterase 7B [Source:MGI Symbol;Acc:MGI:1352752]	anti-correlation with Ncald	- 0,775
<i>Syt6</i>	-0,959	0,040		3	synaptotagmin VI [Source:MGI Symbol;Acc:MGI:1859544]	anti-correlation with Ncald	- 0,707
<i>Igf2bp2</i>	-0,958	0,030		16	insulin-like growth factor 2 mRNA binding protein 2 [Source:MGI Symbol;Acc:MGI:1890358]	anti-correlation with Ncald	- 0,861
<i>Sv2c</i>	-0,944	0,005		13	synaptic vesicle glycoprotein 2c [Source:MGI Symbol;Acc:MGI:1922459]	anti-correlation with Ncald	- 0,800
<i>Slco5a1</i>	-0,941	0,026		1	solute carrier organic anion transporter family, member 5A1 [Source:MGI Symbol;Acc:MGI:2443431]	anti-correlation with Ncald	- 0,825
<i>Sp9</i>	-0,938	0,013		2	trans-acting transcription factor 9 [Source:MGI Symbol;Acc:MGI:3574660]	anti-correlation with Ncald	- 0,775

<i>Dlx5</i>	-0,938	0,025	6	distal-less homeobox 5 [Source:MGI Symbol;Acc:MGI:101926]	anti-correlation with Ncald	- 0,725
<i>Sp7</i>	-0,927	0,043	15	Sp7 transcription factor 7 [Source:MGI Symbol;Acc:MGI:2153568]	anti-correlation with Ncald	- 0,696
<i>P2ry1</i>	-0,923	0,020	3	purinergic receptor P2Y, G-protein coupled 1 [Source:MGI Symbol;Acc:MGI:105049]	anti-correlation with Ncald	- 0,786
<i>Rerg</i>	-0,880	0,020	6	RAS-like, estrogen-regulated, growth-inhibitor [Source:MGI Symbol;Acc:MGI:2665139]	anti-correlation with Ncald	- 0,775
<i>Spata13</i>	-0,876	0,032	14	spermatogenesis associated 13 [Source:MGI Symbol;Acc:MGI:104838]	anti-correlation with Ncald	- 0,761
<i>Ankrd63</i>	-0,868	0,031	2	ankyrin repeat domain 63 [Source:MGI Symbol;Acc:MGI:2686183]	anti-correlation with Ncald	- 0,721
<i>Meis2</i>	-0,855	0,016	2	Meis homeobox 2 [Source:MGI Symbol;Acc:MGI:108564]	anti-correlation with Ncald	- 0,743
<i>Cyp2s1</i>	-0,854	0,006	7	cytochrome P450, family 2, subfamily s, polypeptide 1 [Source:MGI Symbol;Acc:MGI:1921384]	anti-correlation with Ncald	- 0,668
<i>Plppr1</i>	-0,849	0,016	4	phospholipid phosphatase related 1 [Source:MGI Symbol;Acc:MGI:2445015]	anti-correlation with Ncald	- 0,804
<i>Gnal</i>	-0,848	0,023	18	guanine nucleotide binding protein, alpha stimulating, olfactory type [Source:MGI Symbol;Acc:MGI:95774]	anti-correlation with Ncald	- 0,714
<i>Nmnat3</i>	-0,839	0,004	9	nicotinamide nucleotide adenyltransferase 3 [Source:MGI Symbol;Acc:MGI:1921330]	anti-correlation with Ncald	- 0,664
<i>Bcl11b</i>	-0,824	0,021	12	B cell leukemia/lymphoma 11B [Source:MGI Symbol;Acc:MGI:1929913]	anti-correlation with Ncald	- 0,668
<i>St8sia2</i>	-0,817	0,021	7	ST8 alpha-N-acetyl-neuraminide alpha-2,8-sialyltransferase 2 [Source:MGI Symbol;Acc:MGI:106020]	anti-correlation with Ncald	- 0,764
<i>Rasgrp2</i>	-0,801	0,033	CHR_MG4249_PATCH	RAS, guanyl releasing protein 2 [Source:MGI Symbol;Acc:MGI:1333849]	anti-correlation with Ncald	- 0,725
<i>Rasgrp2</i>	-0,801	0,033	19	RAS, guanyl releasing protein 2 [Source:MGI Symbol;Acc:MGI:1333849]	anti-correlation with Ncald	- 0,725
<i>Pdyn</i>	-0,801	0,014	2	prodynorphin [Source:MGI Symbol;Acc:MGI:97535]	anti-correlation with Ncald	- 0,793

<i>Mei4</i>	-0,800	0,032	9	meiotic double-stranded break formation protein 4 [Source:MGI Symbol;Acc:MGI:1922283]	anti-correlation with Ncald	- 0,868
<i>Klhl1</i>	-0,787	0,016	14	kelch-like 1 [Source:MGI Symbol;Acc:MGI:2136335]	anti-correlation with Ncald	- 0,714
<i>Pcsk9</i>	-0,782	0,039	4	proprotein convertase subtilisin/kexin type 9 [Source:MGI Symbol;Acc:MGI:2140260]	anti-correlation with Ncald	- 0,614
<i>Srgap1</i>	-0,766	0,030	10	SLIT-ROBO Rho GTPase activating protein 1 [Source:MGI Symbol;Acc:MGI:2152936]	anti-correlation with Ncald	- 0,829
<i>Tbc1d8</i>	-0,758	0,009	1	TBC1 domain family, member 8 [Source:MGI Symbol;Acc:MGI:1927225]	anti-correlation with Ncald	- 0,821
<i>Mctp1</i>	-0,752	0,026	13	multiple C2 domains, transmembrane 1 [Source:MGI Symbol;Acc:MGI:1926021]	anti-correlation with Ncald	- 0,746
<i>Ddx11</i>	-0,748	0,037	17	DEAD/H (Asp-Glu-Ala-Asp/His) box helicase 11 [Source:MGI Symbol;Acc:MGI:2443590]	anti-correlation with Ncald	- 0,879
<i>Tmem158</i>	-0,740	0,048	9	transmembrane protein 158 [Source:MGI Symbol;Acc:MGI:1919559]	anti-correlation with Ncald	- 0,654
<i>Klhl14</i>	-0,726	0,003	18	kelch-like 14 [Source:MGI Symbol;Acc:MGI:1921249]	anti-correlation with Ncald	- 0,871
<i>Slc17a8</i>	-0,721	0,011	10	solute carrier family 17 (sodium-dependent inorganic phosphate cotransporter), member 8 [Source:MGI Symbol;Acc:MGI:3039629]	anti-correlation with Ncald	- 0,818
<i>Entpd3</i>	-0,714	0,005	9	ectonucleoside triphosphate diphosphohydrolase 3 [Source:MGI Symbol;Acc:MGI:1321386]	anti-correlation with Ncald	- 0,814
<i>Shh</i>	-0,704	0,030	5	sonic hedgehog [Source:MGI Symbol;Acc:MGI:98297]	anti-correlation with Ncald	- 0,657
<i>Fras1</i>	-0,701	0,003	5	Fraser extracellular matrix complex subunit 1 [Source:MGI Symbol;Acc:MGI:2385368]	anti-correlation with Ncald	- 0,814
<i>Kcnab1</i>	-0,701	0,021	3	potassium voltage-gated channel, shaker-related subfamily, beta member 1 [Source:MGI Symbol;Acc:MGI:109155]	anti-correlation with Ncald	- 0,675
<i>Spock3</i>	-0,697	0,007	8	sparc/osteonectin, cwcv and kazal-like domains proteoglycan 3 [Source:MGI Symbol;Acc:MGI:1920152]	anti-correlation with Ncald	- 0,782
<i>Gad2</i>	-0,662	0,028	2	glutamic acid decarboxylase 2 [Source:MGI Symbol;Acc:MGI:95634]	anti-correlation with Ncald	- 0,811

<i>Cpne5</i>	-0,642	0,016		17	copine V [Source:MGI Symbol;Acc:MGI:2385908]	anti-correlation with Ncald	- 0,675
<i>Vrk1</i>	-0,641	0,027		12	vaccinia related kinase 1 [Source:MGI Symbol;Acc:MGI:1261847]	anti-correlation with Ncald	- 0,782
<i>B3gnt2</i>	-0,641	0,030		11	UDP-GlcNAc:betaGal beta-1,3-N-acetylglucosaminyltransferase 2 [Source:MGI Symbol;Acc:MGI:1889505]	anti-correlation with Ncald	- 0,632
<i>Fancb</i>	-0,628	0,032	X		Fanconi anemia, complementation group B [Source:MGI Symbol;Acc:MGI:2448558]	anti-correlation with Ncald	- 0,796
<i>Arhgap27</i>	-0,628	0,020		11	Rho GTPase activating protein 27 [Source:MGI Symbol;Acc:MGI:1916903]	anti-correlation with Ncald	- 0,761
<i>Slc32a1</i>	-0,606	0,045		2	solute carrier family 32 (GABA vesicular transporter), member 1 [Source:MGI Symbol;Acc:MGI:1194488]	anti-correlation with Ncald	- 0,775
<i>Ppp1r2</i>	-0,605	0,040		16	protein phosphatase 1, regulatory (inhibitor) subunit 2 [Source:MGI Symbol;Acc:MGI:1914099]	anti-correlation with Ncald	- 0,725
<i>Ebf1</i>	-0,599	0,048		11	early B cell factor 1 [Source:MGI Symbol;Acc:MGI:95275]	anti-correlation with Ncald	- 0,786
<i>Hs3st5</i>	-0,585	0,015		10	heparan sulfate (glucosamine) 3-O-sulfotransferase 5 [Source:MGI Symbol;Acc:MGI:2441996]	anti-correlation with Ncald	- 0,789
<i>Strn</i>	-0,571	0,030		17	striatin, calmodulin binding protein [Source:MGI Symbol;Acc:MGI:1333757]	anti-correlation with Ncald	- 0,829
<i>Rps6ka5</i>	-0,550	0,035		12	ribosomal protein S6 kinase, polypeptide 5 [Source:MGI Symbol;Acc:MGI:1920336]	anti-correlation with Ncald	- 0,796
<i>Zfp804a</i>	-0,543	0,034		2	zinc finger protein 804A [Source:MGI Symbol;Acc:MGI:2442949]	anti-correlation with Ncald	- 0,729
<i>Asb18</i>	-0,540	0,009		1	ankyrin repeat and SOCS box-containing 18 [Source:MGI Symbol;Acc:MGI:2655109]	anti-correlation with Ncald	- 0,832
<i>Dll1</i>	-0,539	0,033		17	delta like canonical Notch ligand 1 [Source:MGI Symbol;Acc:MGI:104659]	anti-correlation with Ncald	- 0,811
<i>Clip4</i>	-0,512	0,047		17	CAP-GLY domain containing linker protein family, member 4 [Source:MGI Symbol;Acc:MGI:1919100]	anti-correlation with Ncald	- 0,718
<i>Has3</i>	-0,463	0,050		8	hyaluronan synthase 3 [Source:MGI Symbol;Acc:MGI:109599]	anti-correlation with Ncald	- 0,789

<i>Rbms1</i>	-0,445	0,048	2	RNA binding motif, single stranded interacting protein 1 [Source:MGI Symbol;Acc:MGI:1861774]	anti-correlation with Ncald	- 0,875
<i>Mycbp</i>	-0,373	0,030	4	MYC binding protein [Source:MGI Symbol;Acc:MGI:1891750]	anti-correlation with Ncald	- 0,825
<i>Gm14418</i>	-0,351	0,020	2	predicted gene 14418 [Source:MGI Symbol;Acc:MGI:3702408]	anti-correlation with Ncald	- 0,732
<i>Mterf2</i>	-0,327	0,049	10	mitochondrial transcription termination factor 2 [Source:MGI Symbol;Acc:MGI:1921488]	anti-correlation with Ncald	- 0,818
<i>Stat5b</i>	-0,284	0,048	11	signal transducer and activator of transcription 5B [Source:MGI Symbol;Acc:MGI:103035]	anti-correlation with Ncald	- 0,796
<i>Tbc1d9b</i>	0,326	0,030	11	TBC1 domain family, member 9B [Source:MGI Symbol;Acc:MGI:1924045]	correlation with Ncald	0,846
<i>Cbln4</i>	0,845	0,030	2	cerebellin 4 precursor protein [Source:MGI Symbol;Acc:MGI:2154433]	correlation with Ncald	0,679
<i>Ncald</i>	2,849	0,000	15	neurocalcin delta [Source:MGI Symbol;Acc:MGI:1196326]	correlation with Ncald	1,000

Appendix Table 9 List of genes with significant differential expression upon *Ncald* deletion and strongly correlated with *Ncald* gene expression (Spinal Cord)

Gene	log2FoldChange	Adjusted P-value	Chr	Description	Type of relationship	rho
<i>Shh</i>	-0,538	0,045	5	sonic hedgehog [Source:MGI Symbol;Acc:MGI:98297]	anti-correlation with <i>Ncald</i>	-0,621
<i>Kctd9</i>	-0,363	0,019	14	potassium channel tetramerisation domain containing 9 [Source:MGI Symbol;Acc:MGI:2145579]	anti-correlation with <i>Ncald</i>	-0,756
<i>Rgs4</i>	-0,349	0,000	1	regulator of G-protein signaling 4 [Source:MGI Symbol;Acc:MGI:108409]	anti-correlation with <i>Ncald</i>	-0,735
<i>Tmem56</i>	-0,307	0,045	3	transmembrane protein 56 [Source:MGI Symbol;Acc:MGI:1923195]	anti-correlation with <i>Ncald</i>	-0,693
<i>Tiparp</i>	-0,291	0,021	3	TCDD-inducible poly(ADP-ribose) polymerase [Source:MGI Symbol;Acc:MGI:2159210]	anti-correlation with <i>Ncald</i>	-0,633
<i>Pdp1</i>	-0,261	0,033	4	pyruvate dehydrogenase phosphatase catalytic subunit 1 [Source:MGI Symbol;Acc:MGI:2685870]	anti-correlation with <i>Ncald</i>	-0,600
<i>Kif5c</i>	-0,254	0,020	2	kinesin family member 5C [Source:MGI Symbol;Acc:MGI:1098269]	anti-correlation with <i>Ncald</i>	-0,693
<i>Mapk6</i>	-0,202	0,019	9	mitogen-activated protein kinase 6 [Source:MGI Symbol;Acc:MGI:1354946]	anti-correlation with <i>Ncald</i>	-0,648
<i>Kbtbd2</i>	-0,164	0,044	6	kelch repeat and BTB (POZ) domain containing 2 [Source:MGI Symbol;Acc:MGI:2384811]	anti-correlation with <i>Ncald</i>	-0,660
<i>Ahcy1l</i>	-0,146	0,043	3	S-adenosylhomocysteine hydrolase-like 1 [Source:MGI Symbol;Acc:MGI:2385184]	anti-correlation with <i>Ncald</i>	-0,615
<i>Pld4</i>	0,286	0,014	12	phospholipase D family, member 4 [Source:MGI Symbol;Acc:MGI:2144765]	correlation with <i>Ncald</i>	0,666
<i>Fbln2</i>	0,434	0,003	6	fibulin 2 [Source:MGI Symbol;Acc:MGI:95488]	correlation with <i>Ncald</i>	0,795
<i>Ccnb2</i>	0,485	0,046	9	cyclin B2 [Source:MGI Symbol;Acc:MGI:88311]	correlation with <i>Ncald</i>	0,705
<i>Ckap2</i>	0,492	0,008	8	cytoskeleton associated protein 2 [Source:MGI	correlation with <i>Ncald</i>	0,650

				Symbol;Acc:MGI:1931797]		
<i>Mybpc1</i>	0,498	0,020	10	myosin binding protein C, slow-type [Source:MGI Symbol;Acc:MGI:1336213]	correlation with Ncald	0,689
<i>Cenpa</i>	0,607	0,045	5	centromere protein A [Source:MGI Symbol;Acc:MGI:88375]	correlation with Ncald	0,728
<i>Ogn</i>	0,790	0,014	13	osteoglycin [Source:MGI Symbol;Acc:MGI:109278]	correlation with Ncald	0,844
<i>Cdc25c</i>	0,797	0,019	18	cell division cycle 25C [Source:MGI Symbol;Acc:MGI:88350]	correlation with Ncald	0,663
<i>Rem1</i>	0,823	0,015	2	rad and gem related GTP binding protein 1 [Source:MGI Symbol;Acc:MGI:1097696]	correlation with Ncald	0,785
<i>Gsx1</i>	1,036	0,014	5	GS homeobox 1 [Source:MGI Symbol;Acc:MGI:95842]	correlation with Ncald	0,738
<i>Ncald</i>	2,376	0,000	15	neurocalcin delta [Source:MGI Symbol;Acc:MGI:1196326]	correlation with Ncald	1,000

8 Publications

Upadhyay, A., Hosseinibarkooie, S., Schneider, S., Kaczmarek, A., Torres-Benito, L., Mandoza-Ferreira, N., Grysko, V., Kye, M.J., Kononenko, N.L., and Wirth, B. (2018). Neurocalcin delta knockout impairs adult neurogenesis whereas half reduction is a safe therapeutic option for spinal muscular atrophy. (Under review in *Frontiers in Molecular Neuroscience*)

Riessland, M.*, Kaczmarek, A.*, Schneider, S.*, Swoboda, K.J., Löhr, H., Bradler, C., Grysko, V., Dimitriadi, M., Hosseinibarkooie, S., Torres-Benito, L., Peters, M., **Upadhyay, A.**, Biglari, N., Kröber, S., Hölker, I., Garbes, L., Gilissen, C., Hoischen, A., Nürnberg, G., Nürnberg, P., Walter, M., Rigo, F., Kye, M.J., Hart, A.C., Hammerschmidt, M., Kloppenburg, P., and Wirth, B. (2017). Neurocalcin Delta Suppression Protects against Spinal Muscular Atrophy in Humans and across Species by Restoring Impaired Endocytosis. *American Journal of Human Genetics* **100**(2): 297-315.

Acknowledgements

I am thankful to everyone who has helped me to successfully finish my PhD project. I may not be able to list each one of them maybe, but I try my best in following sentences.

First of all, I would like to thank RTG-Neuroscience graduate school and my supervisor Prof. Dr. Brunhilde Wirth for giving me an opportunity to pursue my PhD in her lab. She has been as supportive a supervisor can be and at the same time and as critical as required for my professional growth. Personally she has been an inspiration to look up to someone who is love with her work and very determined to give her best to everyone around her, with a cheerful smile on her face.

I would then like to thank my co-supervisor Dr. Natalia Kononenko, without whom this project would not have been as successful and as smooth as it has been. She also has been an inspiration in terms of her commitment and energy towards her work and building up a new working place.

I am also very thankful towards everyone in the Wirth lab for helping me whenever I was in a need or difficulty, scientifically and otherwise. To name a few, I am extremely thankful to Dr. Laura Torres-Benito for her care, support, supervision, guidance, friendship and smiles since my first day in the lab. I am also thankful to Dr. Svenja Schneider, Dr. Anna Kaczmarek and Vanessa Grysko for being excellent lab roommates with their supportive hands, ideas and laughter. I also would like to thank Anixa Muinos Bühl, Andrea Delle Vedove and Eike Strathmann for being very helpful with their scientific ideas, friendly support and laughter. Thank you also to Dr. Min Jeong Kye for great scientific advice, motivating conversations, and ideas. I would also like to thank you Natalia Mendoza Ferreira, for helping and encouraging me with writing my paper as well as thesis. I am also very thankful towards Dr. Mohsen Hosseini and Eike Starthmann for their technical and scientific help which has been a part of thesis. Additionally, I enjoyed my working time and space with Eva Janzen, Janine Milbradt, Ines do Carmo Gil Goncalves, Wiebke Rehorst, Max Thelen, Mert Karakaya, thanking all these people for nice working environment that I received. I also would like to thank our secretary Dr. Uwe Becker who always has been supportive on all administrative issues.

Dr. Isabell Witt, Kathy Joergens, and Dr. Katerina Vlantis have been a strong pillar of support in my professional as well as personal life in Germany, it being my first life away from home. I cannot thank enough to all these people. They have been helpful not only in administrative issues as well as for the travel grants and support, good organization of workshops and seminars but also beyond.

Outside the university, I would like to thank all my friends Vishal, Jass, Sandra, Anandhi, Dinesh, Ritika and Suman who have been not less than a family for me in a foreign land. Special thanks to Shivam for being my biggest support and critic out of his love. Lastly, I would like to thank my mother who is the reason of me being even capable of achieving all the things I achieved in life, including my doctoral thesis.

A silent and deep gratitude towards my guru.

CURRICULUM VITAE



Persönliche Daten

Name: Upadhyay
Vorname: Aaradhita
Geburtsdatum: 20.05.1992
Geburtsort: Raipur, Indien
Nationalität: Indisch

Schulbildung

2007 – 2009 Krishna public school, Bhilai, Indien, High school

Akademische Ausbildung

Aug. 2009 – May. 2014 Dr. D.Y. Patil Biotechnology and Bioinformatics Institute,

Dr. D.Y. Patil university

Master of Science (M.Sc.) im Fach "Biotechnologie"

Jan. 2015 – heute

Universität zu Köln

Promotionsstudium (Dr. rer. nat.) im Fach "Genetik"

Titel der Dissertation: „Neurocalcin delta knockout impairs adult neurogenesis whereas half reduction is a safe therapeutic option for spinal muscular atrophy“ angefertigt am Institut für Humangenetik unter der Anleitung von Frau Prof. Dr. Brunhilde Wirth

Korrespondenzanschrift

1108, Graeffstrasse 1

Neu Ehrenfeld

Köln 50823

Eidesstattliche Erklärung

Erklärung zur Dissertation

Ich versichere, dass ich die von mir vorgelegte Dissertation selbstständig angefertigt, die benutzten Quellen und Hilfsmittel vollständig angegeben und die Stellen der Arbeit einschließlich Tabellen, Karten und Abbildungen –, die anderen Werken im Wortlaut oder dem Sinn nach entnommen sind, in jedem Einzelfall als Entlehnung kenntlich gemacht habe, dass diese Dissertation noch keiner anderen Fakultät oder Universität zur Prüfung vorgelegen hat, dass sie – abgesehen von den angegebenen Teilpublikationen – noch nicht veröffentlicht worden ist sowie, dass ich eine solche Veröffentlichung vor Abschluss des Promotionsverfahrens nicht vornehmen werde. Die Bestimmungen dieser Promotionsordnung sind mir bekannt. Die von mir vorgelegte Dissertation ist von Prof. Dr. Brunhilde Wirth betreut worden.

Ich versichere, dass ich alle Angaben wahrheitsgemäß nach bestem Wissen und Gewissen gemacht habe und verpflichte mich, jedmögliche, die obigen Angaben betreffende Veränderungen dem Dekanat unverzüglich mitzuteilen.

.....

.....